Introduzione

Lo scopo di questa tesi è di sviluppare un confronto affidabile fra tre diversi metodi per la determinazione preliminare di orbite di asteroidi, al fine di testarne la validità e le caratteristiche su un campione di dati reali. Tali metodi hanno l'obiettivo di calcolare una prima approssimazione dell'orbita dell'oggetto, usata poi come stima iniziale per una più precisa determinazione orbitale tramite correzioni differenziali. Essi risultano di fondamentale importanza anche per il processo di identificazione, permettendo di associare varie osservazioni ottenute a distanza di tempo ad uno stesso oggetto.

I metodi per la determinazione preliminare di asteroidi analizzati si basano sull'elaborazione di tre osservazioni e, tramite procedure differenti, calcolano i vettori di stato eliocentrici dell'oggetto e ne derivano gli elementi orbitali. Le prove sono state effettuate su asteroidi appartenenti a famiglie o gruppi diversi al fine di fornire una buona statistica.

Nella prima parte di questo lavoro trattiamo il metodo classico di Gauss. Esso si basa su una procedura iterativa e sfrutta la particolare configurazione geometrica generata dalla posizione delle Terra, del Sole e dell'oggetto in esame. Il punto cruciale di questo metodo consiste nel calcolo del *sector-to-triangle ratio*, ovvero il rapporto tra l'area del settore orbitale costruito sui vettori eliocentrici e l'area del corrispondente triangolo. Questa quantità comprende informazioni di natura geometrica e dinamica, associate al moto Kepleriano.

Il metodo di Neutsch, anch'esso di stampo iterativo, appartiene ad una classe di metodi non Gaussiani. La procedura richiede la soluzione di un sistema lineare a partire da un'orbita generica. Questo metodo è stato rivisitato da Goffin, ed esteso all'utilizzo di orbite condizionate. Infine analizziamo un nuovo approccio al metodo di Gauss proposto da Casotto. Al contrario dei precedenti questo metodo è analitico e prevede la soluzione di un sistema non lineare di sei equazioni in sei variabili. L'innovazione apportata da questa nuova procedura consiste nell'esprimere tutte le equazioni coinvolte in funzione delle stesse variabili che consistono nelle tre distanze geocentriche e nei tre *sector-to-triangle ratios*.

La possibilità di ottenere soluzioni multiple al problema della determinazione preliminare venne analizzata da Charlier nel 1910. Egli definì

l'esistenza di alcune regioni, determinate dalla speciale configurazione formata dal Sole, dalla Terra e dall'asteroide, in cui fosse possibile trovare una o più orbite che soddisfano il problema. Questa teoria nacque come applicazione al metodo di Gauss e in questo lavoro è stata applicata al nuovo approccio di Casotto, provandone la validità.

Nella seconda parte della tesi sviluppiamo un confronto tra le orbite preliminari ottenute dai tre metodi e quelle finali e più accurate fornite dal JPL al fine di quantificare l'affidabilità della determinazione preliminare. Abbiamo creato un modello di propagazione basato sul Problema a tre corpi considerando le perturbazioni dovute a Giove. Dalle orbite così generate abbiamo calcolato gli elementi orbitali a varie epoche e li abbiamo confrontati con quelli previsti da JPL. Sono stati confrontati anche le componenti dei vettori posizione ottenendo un'accuratezza di 10^{-4} UA tra orbite preliminari ed effemeridi di JPL. Questo determina un buon accordo tra le due orbite e permette di utilizzare la determinazione preliminare per prevedere la posizione dell'oggetto.

Alla fine è stata calcolata una stima dell'errore negli elementi orbitali causato dall'incertezza nelle osservazioni. A tale scopo sono state generate tre distribuzioni di osservazioni sintetiche in prossimità di tre osservazioni iniziali, sono state poi scelte delle combinazioni casuali, selezionando un'osservazione per ogni gruppo. I risultati ottenuti dai metodi per la determinazione preliminare hanno fornito una distribuzione di elementi orbitali, dalla quale è stato possibile derivare l'errore associato all'incertezza.

Nel prossimo futuro le missioni spaziali, raggiungeranno precisioni astrometriche molto elevate. Gaia, per esempio, sarà in grado di effettuare misure con una precisione di 10^{-5} secondi d'arco, 100 volte più precise di quelle ottenute da Hipparcos. L'enorme mole di dati così ricavati favoriranno lo studio di asteroidi, comete, oggetti transnettuniani e corpi minori del Sistema Solare richiedendo l'utilizzo di algoritmi sempre più affidabili e aggiornati. Per questo motivo è di fondamentale importanza introdurre e sperimentare nuove procedure, sia per la determinazione orbitale che per quella preliminare.

Contents

Chapter 1

Introduction

The purpose of this thesis is to develop a reliable comparison among three methods for preliminary orbit determination in order to test their validity and peculiarities on a wide range of data. The aim of the preliminary orbit determination methods is to obtain the heliocentric position vectors of a Solar System object and to use them to compute the Keplerian elements.

In the first part of the work we treat the classical Gauss method, based on an iterative procedure, according to the Montenbruck version. Then we pass to the Neutsch approach, also based on an iterative procedure including the solution of a linear system referred to the problem geometry. This method was reviewed by Goffin, who extended it to conditioned orbits. Finally we analyze the Casotto method, an analytic process that solves a non-linear system of six dynamical equations derived from Gauss formulation. Moreover we test the validity of Charlier's theory on this method, obtaining a good agreement.

In the second part of the thesis we develop a comparison between the preliminary orbits obtained and the final one provided by JPL in order to quantify the reliability of the preliminary determination. In the end we consider the error problem and, producing a normal distribution of synthetic observations, we compute their effects on the orbital elements. The tests are made on several asteroids, belonging to different families or groups, in order to provide a strong statistic.

The large amount of data collected in contemporary epoch favors the studies of asteroids, comets, transneptunian objects and little bodies of Solar System, but preliminary orbit determination remains a fundamental tool, especially in those cases in which we dispose of only a narrow number of observations. It is the first step toward a more accurate orbit computation through differential corrections, and strictly connected with identification problem.

1.1 Historical background

The determination of the motion of the celestial bodies has been a subject of interest since antiquity. The first modern theories were developed in the 18th century through the studies of great scientists such as Newton, Laplace and Gauss.

The first method for the computation of the orbit of a Solar System body on the basis of only three observations was described by Newton in the *Principia* (1687). This method depended on a graphical construction which, by successive approximations, led to the orbital elements. Few years after the publication, in 1705, Edmund Halley applied that procedure for the computation and the prediction of some cometary orbits, among which Halley's comet. The first completely analytical method, suitable for parabolic orbits, was conceived by Euler in 1744 in his *Theoria Motuum Planetarum et Cometarum* [2]. Afterwards, Lambert in 1771, generalized the previous formulation to elliptic and hyperbolic orbits [13]. Contemporary to the last one was the theory proposed by Laplace, based on the estimation of the body velocity from the three observations.

The real change in orbit determination field was brought about by Carl Friedrich Gauss, a 24-year old German mathematician, in the first years of the 19th century. He applied his theory to the observation of Ceres asteroid, which had just been discovered by abbot Giuseppe Piazzi of Palermo, on New Year's day of 1801. His computation were so precise to allow the sighting of the same object one year later with only half degree error. This ingenious procedure was based on the determination of the object heliocentric position used in turn to solve Lambert's problem to finally obtain the orbital elements [13].

Nowadays the initial orbit determination is still an active area of research. Many papers have been published in the recent years among which we reference the works of Bucerius [7] in the 1950s, Montenbruck [6] who revisited the classical Gauss method, Neutsch (1981) [10] who invented a procedure independent from the Gauss equation, followed by Goffin (2000) [11] who extended Neutsch's work to conditioned orbits. We mention also the studies of Milani, Gronchi et al. [4], who have widely treated the subject with applications on NEOs and TNOs. Two of the latest contribution are the papers by T. Mirtorabi (2013) [12], who extended the Gauss method from three to N observations, and Casotto (2014) [9] who revised the Gauss problem in an analytic way. Moreover, we mention a new class of IOD methods, based on the use of the two-body integrals, has been developed by Taff et al. [28] and Gronchi et al. [27]. We focused our research on some of these methods and their applications.

1.2 The orbit determination problem

The preliminary orbit is a fundamental tool to predict an object apparent position over a period of time in order to track it. The main purpose of initial orbit determination (IOD) is to estimate set of orbital elements used as a first guess for the non-linear optimization procedure, through differential corrections, that identifies the nominal orbit using the method of the least squares [3].

When a new object is detected the amount of information is minimal, typically only its angular positions and its apparent magnitude, moreover an asteroid is typically observed only over a period of few hours or few weeks. In the moment of the next apparition the asteroid could be in a portion of sky larger than the field of view of the telescope and to became a lost asteroid. Therefore we can only collect a lot of observations without knowing which of them are referred to the same object.

It is clear now that the orbit determination is not possible with the discovery alone, but is connected with the identification problem, which consists in the association of those arcs of observations that belong to the same object among independent detections distant in times. In order to solve this problem it is necessary to select a small set of orbit arcs to examine. Since the strong non-linearity of the orbit determination problem, a first guess orbit is needed for each couple of observations. Then these preliminary orbits are used as input for differential correction procedure, which leads to a more realistic final orbit. The identification is confirmed if the observations can be fitted by the same orbit with acceptable residuals. Only when the object is identified is it possible to proceed, compiling a catalog containing the list of distinct objects, then orbits and other astrometric and physical information [3].

1.3 Asteroid groups and families

The asteroids are divided into groups and families. A family is a population of asteroids that share similar orbital elements, such as semi-major axis, eccentricity, and orbital inclination, as the result of collisions between asteroids. A group also involves minor planets that share similar orbits but they do not have the same formation history. The programs developed in this work were tested on various asteroids, belonging to different families and groups, in order to have a representative and consistent set of results to interpret. We introduce now the main families and groups of asteroids starting from the Earth to the Outer Solar System. The nearest group that we approach consist of the so-called NEOs, *i.e.* the Near Earth objects, that are those objects whose orbits brings them into proximity of the Earth. They include a few thousand Near-Earth asteroids (NEAs), Near-Earth comets,

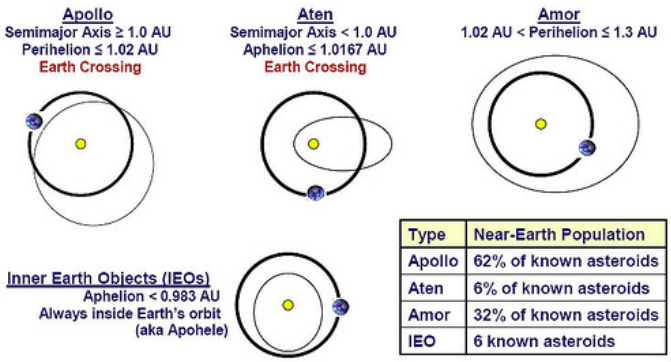

Figure 1.1: NEAs orbit types.

a number of solar-orbiting spacecraft, and meteoroids large enough to be tracked in space before striking the Earth. The NEAs are classified into four groups: Atiras, Aten, Amor, Apollo, as shown in Table 4.1 and in Figure 4.1.

Aten asteroids are defined by having a semi-major axes of less than one astronomical unit, Atiras or Inner Earth Objects also have semimajor axis less than one astronomical unit and aphelion less than 0.983 AU like Apophis. Apollo asteroids are Earth-crossing and have semi-major axis greater than 1 AU, but perihelion distances less than the Earth's aphelion distance ($q < 1.017$ AU). Some can get very close to the Earth, making them a potential threat to our planet. Amor asteroids approach the orbit of Earth from beyond, but do not cross it. Most Amors cross the orbit of Mars.

After this group we find the main belt, that lies between Mars and Jupiter at 2.06-3.27 UA and contains millions or more asteroids classified into 20-30 families. The name derives from the fact that the main belt contains approximately 93.4% of all numbered minor planets within the Solar System. Over 200 of them are known to be larger than 100 km. For what concerns the orbital distribution, it reaches a maximum at an eccentricity of around 0.07 and an inclination below 4 degrees.

The main belt is divided, according to the Kirkwood gaps, into three different regions, the Inner main belt before 3:1 resonance, the Middle main belt between the 3:1 and 5:2 and the Outer main belt between the 5:2 and 2:1 where lie Griqua asteroids. The families composing the main belt are shown in Table 1.2 while in Figure 1.2 we can see the distribution of the proper elements (a-e) from which clearly appears the division into families.

Proceeding outward we find the Near Jupiter asteroids. The Hildian asteroids are not a family, they are a dynamical group which are in 3:2 resonance with Jupiter. All the Hildas asteroids taken together form a particular

configuration called the "Hildas Triangle". At the vertices of the triangle, corresponding to the Lagrangian points L4 and L5 of Jupiter's orbit, the Hildas approach the Trojans. Each asteroid of this group librates around one of the two Jovian stable points, L4 and L5, that respectively lie 60 degrees ahead of and behind the planet in its orbit. The ones in L4 are called Greeks and the ones in L5 are named Trojans. Beyond Jupiter there are the Centaurus , these bodies have the features of both comets and asteroids, from this their name of an half human and half horse creature.

We pass now to the TNOs. A trans-Neptunian object is any minor planet in the Solar System that orbits the Sun at an average distance greater than Neptune. They are divided into different groups, summarized in Table 1.5. We find for example the Cubewanos, which are the classical Kuiper belt objects and are not controlled by any orbital resonance with Neptune. Their name derives from the first TNO discovered after Pluto, called 1992 QB1. On the other hand, Plutinos and Twotinos are in different resonances with Neptune. Haumea is the only known trans-neptunian collisional family. At the edge of the Solar System we find the extended scattered disk, populated by minor planet characterized by orbits with high eccentricity and high inclination, as Sedna, the most distant object ever seen in the Solar System [23]. It is at the center of a debate about its classification in fact some astronomers consider it as the first member of the Inner Oort cloud. Figure 1.3 illustrates the TNOs distribution in the Solar System.

Group	**Prototype**	**a (UA)**	**Q (UA)**	**q (UA)**	**n**	**Orbit**
Atiras	163693 Atira	< 1	< 0.983		6	Inner
Atens	2062 Aten	< 1	≤ 1.0167		640	Crossing
Apollos	1862 Apollo	> 1		<1.02	3800	Crossing
Amors	1221 Amor	1-1.524		1.02-1.3	3200	Approching

Table 1.1: Near Earth asteroids groups. n is the number of objects for each group, Q represents the aphelion an q the perihelion.

Group	**Prototype**	**a (UA)**	**e**	**i (°)**	**r**	**y**
Hungarias	434 Hungaria	1.78-2	< 0.18	16-34	9:2 J-3:2 M	1898
Phocaeas	25 Phocaea	2.25-2.5	> 0.1	18-32	4:1	1853

Table 1.2: Near Mars asteroids groups. r indicates the resonances with Jupiter and Mars.

Family	**Prototype**	**a (UA)**	**e**	**i (°)**	**n**	**y**
Vesta	4 Vesta	2.26-2.48	0.03-0.16	5-8.3	8620	1807
Flora	8 Flora	2.15-2.35	0.03-0.23	1.5-8.0	590	1847
Eunomia	15 Eunomia	2.53-2.72	0.08-0.22	11.1-15.8	7476	1851
Pallas	2 Pallas	2.72-2.79	0.13-0.37	30-38	41	1928
Koronis	158 Koronis	2.83-2.91	0-0.11	0-3.5	6130	1876
Eos	221 Eos	2.99-3.03	0.01-0.13	8-12	11593	1882
Hygiea	10 Hygiea	3.06-3.24	0.09-0.19	3.5-6.8	2615	1849
Themis	24 Themis	3.08-3.24	0.09-0.22	0-3	4329	1853
Griqua	1362 Griqua	3.1-3.27	0.3-0.5	24-41		1935

Table 1.3: Main belt asteroids families except for Griqua group.

Group	Prototype	a (UA)	e	i (°)	n	r	y
Cybele	65 Cybele	3.27-3.7	0.04-0.26	2-20		7:4	1861
Hilda	153 Hilda	3.7-4.2	< 0.3	< 20		3:2	1875
Troians	588 Achilles	5.05-5.35		> 40	4916	1:1	1906
Centaurs	2060 Chiron	5.2-30	0.1-0.6	7-24	44000	no	1977

Table 1.4: Near Jupiter asteroids groups

Group	Prototype	a (UA)	e	i (°)	r	y
Plutinos	134340 Pluto	39.401	0.20-0.25	10-25	2:3	1930
Cubewanos	1992 QB1	41-47	< 0.1	< 5	no	1992
Twotinos	1996TR66	47.731	0.1-0.3	< 15	1:2	1996
SDOs	136199 Eris	> 50	< 0.8	< 40	no	2005
Haumea	136108 Haumea	43	0.195	28	7:12	2004

Table 1.5: TNOs: transneptunian objects groups except for Haumea family.

1.4 Search programs

In this chapter we list the major centers and programs involved in the research and cataloging of minor planets. Nowadays the international efforts are involved to detect, track and characterize potentially hazardous asteroids and comets that could approach the Earth. The most considerable funds donated for this kind of researches come from NASA and United States military institutions; in fact, since 1998, NASA's Near-Earth Obser-

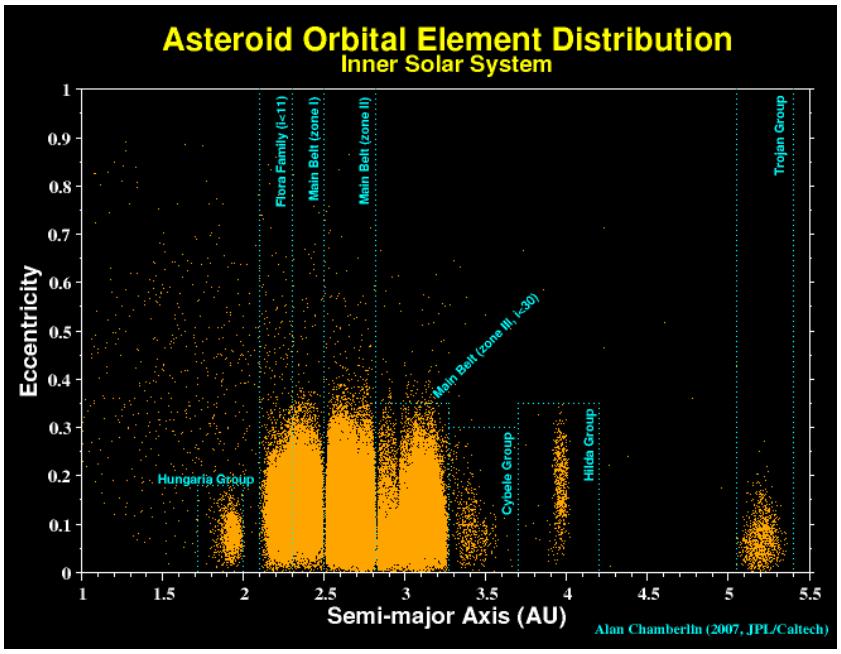

Figure 1.2: Proper elements of main belt families and other groups between Mars (1.5 AU) and Jupiter (5.2 AU). We note how the asteroids populate different regions of the elements space within some constraints.

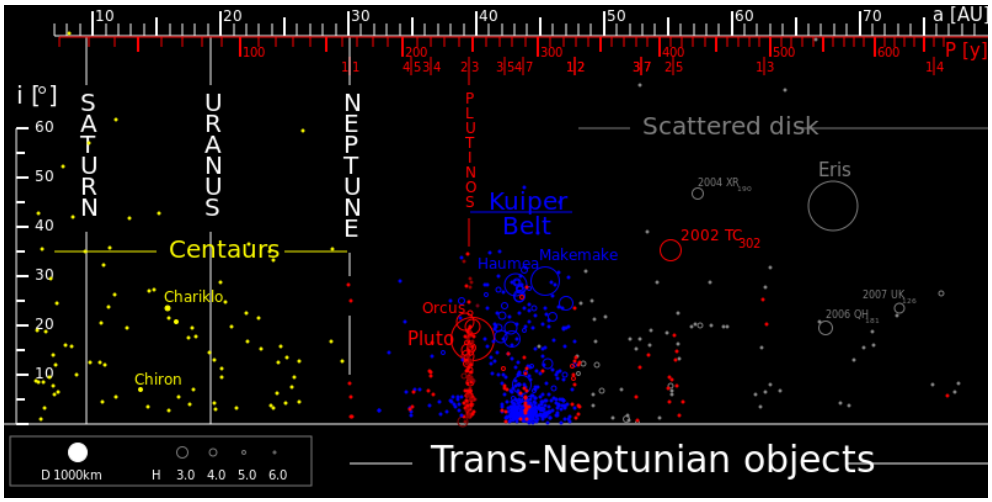

Figure 1.3: Distribution of the outer Solar System objects.

vation Search Program has been leading the search for potentially hazardous asteroids and it is responsible for the 98% of the discoveries to date.

The orbits of minor planets are nowadays made available through 3 web services: the MPC, the JPL and the AstDyS of Pisa.

Jet Propulsion Laboratory (JPL) at the California Institute of Technology is responsible of cataloging the asteroid population and provides the ephemeris of asteroids and minor planets..

The Minor Planet Center (MPC), in turn computes orbits and ephemerids of asteroids, comets and all types of minor planets. It works at the Smithsonian Astrophysical Observatory in Massachussets on behalf of the IAU (International Astronomical Union), supported by the NEO program funds.

The Asteroid Dynamical Site, or AstDyS, and the Near-Earth Objects Dynamical Site, NEODyS, sponsored by ESA, arise from a collaboration between Pisa and Belgrado Universities. The web site provides data on numbered and multiopposition asteroids, including orbital elements, their uncertainty, proper elements, ephemerids with uncertainty, and more. The orbits are computed with OrbFit free software every month or whenever the MPC releases a full update of the dataset.

We now turn to the observing centers among which we find the Catalina Sky Survay (CSS), a research program of the Lunar and Planetary Laboratory (LPL) at the Arizona University. The mission of CSS is to contribute to the inventory of the Near-Earth objects, or more specifically, the potentially hazardous asteroids (PHAs) that pose an impact risk to Earth and its inhabitants.

At LPL there is also the Spacewatch, a group founded in 1980, which primary goal is to explore the various populations of small objects in the Solar System, and to study the statistics of asteroids and comets in order to investigate the dynamical evolution of the Solar System.

Another important program funded by the United States Air Force and NASA is the Lincoln Near Earth Asteroid Research (LINEAR) of MIT. The goal of LINEAR is to demonstrate the application of technology originally developed for the surveillance of Earth orbiting satellites, to the problem of detecting and cataloging NEOs that threaten the Earth. The project uses a pair of Ground-based Electro-Optical Deep Space Surveillance (GEODSS) telescopes at Lincoln Laboratory's Experimental Test Site (ETS) at the White Sands Missile Range in Socorro, New Mexico.

Moreover we mention the Panoramic Survey Telescope and Rapid Response System (Pan-STARRS), an innovative design for a wide-field imaging facility developed at the University of Hawaii's Institute for Astronomy. A major goal of Pan-STARRS is to discover and characterize Earth-approaching objects, both asteroids and comets, that might pose a danger to our planet.

For what concern the space telescopes, the Wide-field Infrared Survey Explorer (WISE), a satellite carrying an infrared-sensitive telescope, will im-

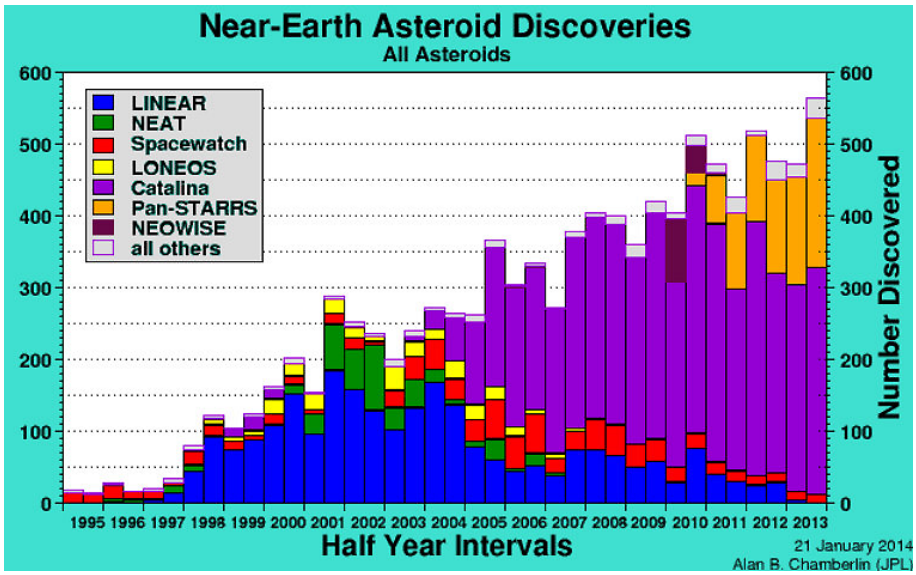

Figure 1.4: NEAs discovered until 2014. The legend shoes the surveys involved in the discovery of these asteroids.

age the entire sky and the Hubble telescope has provided consistent support for the studies of planets and asteroids. WISE was lunched in 2009, it will scan the entire sky in infrared light producing millions of images. The mission will uncover objects never seen before, including the coolest stars, the universe's most luminous galaxies and some of the darkest near-Earth asteroids and comets. Its vast catalogs will help answer fundamental questions about the origins of planets.

In Europe instead, a new ESA Center starts its work on 22 May 2013 and now celebrates its first year of activities: the NEO Coordination Centre (NEOCC) has regularly provided information and data on NEOs through its main services updated on a daily basis and have been organized several campaigns for astrometric and physical observations of NEAs.

To conclude the list we mention the Spaceguard Foundation, an association founded in 1996 in Rome with the aim of protect Earth from Solar System objects bombardment, and the informal association called EARN, European Asteroid Research Node, which has the aim to promote easy and fast communication, exchange of data and other information in both observational and theoretical research on asteroids.

Chapter 2

The Classical method of Gauss

The purpose of Gauss method for preliminary orbit determination is to obtain the heliocentric position vectors of a Solar System object and to use them to compute the Keplerian elements. The procedure requires, as input data, the coordinates of the object at three different observations and the intervals of time between them. Gauss developed a procedure based on the solution of the Two-Body Problem as a boundary value problem and supposed that the motion of the observer is known. It is important to note that determining the heliocentric vectors or the geocentric distances is equivalent, since the two sets are related through the knowledge of the observer's position at the observation times.

The technique used by Gauss exploited the particular geometric structure of the problem. In fact the gist of this method consists in the computation of the so-called *sector-to-triangle ratios* η_i, which incorporate relation between dynamical and geometric information associated with Keplerian motion. These quantities are defined as the ratios between the areas of the sectors bounded by the heliocentric vectors and the areas of the triangles formed by the same vectors. It gives rise to a set of highly non-linear, transcendental equations which must be solved with the aid of numerical methods. The quantities η_i are used to compute the geocentric distances and consequently the heliocentric vectors. The solution of the whole problem requires a two-level iterative scheme. At each step the non-linear system is solved and a better approximation of the geocentric distances is found. In the final step, by choosing two position vectors among the three computed, it is possible to obtain the initial velocity by solving a Lambert problem. Therefore the complete dynamical state obtained can easily be converted into a set of Keplerian elements. Gauss employed a particular geometrical process to obtain the same six elements directly from two position vectors.

It is possible to define two different classes of Gauss's methods: the

short methods, which provide a single orbit solution and the *comprehensive methods*, which provide three possible orbits based on the solution of the *Gauss-Lagrange equation*.

2.1 Geometrical conditions

In this section we introduce the fundamental geometrical equations on which the method is based. The objective here is to find a particular expression for the geocentric distances as functions of the *triangle area ratio* n_i. We start from the three observations which provide the directions of the object. The observations are:

$$(\alpha_1, \delta_1), (\alpha_2, \delta_2), (\alpha_3, \delta_3) \tag{2.1}$$

where α_i, δ_i with $i = 1, 2, 3$ are the equatorial coordinates of right ascension and declination at the three observation times t_i, $i = 1, 2, 3$. To find the $\hat{\mathbf{e}}_i$ unit vector components we use the direction cosines:

$$\hat{\mathbf{e}}_i = \begin{pmatrix} \cos\alpha_i \cos\delta_i \\ \sin\alpha_i \cos\delta_i \\ \sin\delta_i \end{pmatrix} \qquad i = 1, 2, 3.$$

Considering the heliocentric inertial reference system $\{\hat{\mathbf{i}}, \hat{\mathbf{j}}, \hat{\mathbf{k}}\}$ we obtain the direction of observation $\hat{\mathbf{e}}_i$:

$$\begin{aligned} \hat{\mathbf{e}}_1 &= \cos\alpha_1 \cos\delta_1 \hat{\mathbf{i}} + \sin\alpha_1 \cos\delta_1 \hat{\mathbf{j}} + \sin\delta_1 \hat{\mathbf{k}}, \\ \hat{\mathbf{e}}_2 &= \cos\alpha_2 \cos\delta_2 \hat{\mathbf{i}} + \sin\alpha_2 \cos\delta_2 \hat{\mathbf{j}} + \sin\delta_2 \hat{\mathbf{k}}, \\ \hat{\mathbf{e}}_3 &= \cos\alpha_3 \cos\delta_3 \hat{\mathbf{i}} + \sin\alpha_3 \cos\delta_3 \hat{\mathbf{j}} + \sin\delta_3 \hat{\mathbf{k}}. \end{aligned} \tag{2.2}$$

We now analyze the geometrical configuration formed by the Sun, the Earth and the target object. The next equation shows that we need to know only the geocentric distances to obtain the position vector of an object. In fact the observations already provide the directions $\hat{\mathbf{e}}_i$ and the Earth ephemeris are available from catalogs. So the heliocentric positions $\mathbf{r}_i$, $i = 1, 2, 3$, of the object can be written as:

$$\mathbf{r}_i = \rho_i \hat{\mathbf{e}}_i - \mathbf{R}_i \qquad i = 1, 2, 3. \tag{2.3}$$

in which $\hat{\mathbf{e}}_i$ are the vectors of unit length directed from the Earth towards the object, ρ_i are the distances of the object from the Earth and $\mathbf{R}_i$ are the Sun geocentric position vectors available from the appropriate tables. Recalling that, for unperturbed Keplerian motion, the orbit and the Sun lie on the same plane, we can write the object position vector as a linear combination of the other two:

$$n_2 \mathbf{r}_2 + n_1 \mathbf{r}_1 + n_1 \mathbf{r}_3 = \mathbf{0}. \tag{2.4}$$

The factors n_i, $i = 1, 2, 3$, depend on the positions of $\mathbf{r}_1$, $\mathbf{r}_2$ and $\mathbf{r}_3$. In what follows we assume that the observed arc of the orbit is rather small so both factors are positive. They are constants and one of them is redundant. We choose $n_2 = -1$ to make the treatment definite and we find the *equation of the orbital plane*:

$$\mathbf{r}_2 = n_1\mathbf{r}_1 + n_3\mathbf{r}_3. \tag{2.5}$$

In this way we reduce the number of coefficients to determine. So, substituting (2.3) in (2.5) we obtain the *fundamental equation* of the Gauss method:

$$n_1\rho_1\hat{\mathbf{e}}_1 - \rho_2\hat{\mathbf{e}}_2 + n_3\rho_3\hat{\mathbf{e}}_3 = n_1\mathbf{R}_1 - \mathbf{R}_2 + n_3\mathbf{R}_3. \tag{2.6}$$

By using the fundamental equation and the equation of the orbital plane we can reduce the number of unknowns from three (ρ_1, ρ_2, ρ_3) to two (n_1, n_3). For this reason we introduce the unit vectors $\hat{\mathbf{d}}_i, i = 1, 2, 3$ in terms of the observations $\hat{\mathbf{e}}_i$:

$$\begin{aligned} \hat{\mathbf{d}}_1 &= \hat{\mathbf{e}}_2 \times \hat{\mathbf{e}}_3, \\ \hat{\mathbf{d}}_2 &= \hat{\mathbf{e}}_3 \times \hat{\mathbf{e}}_1, \\ \hat{\mathbf{d}}_3 &= \hat{\mathbf{e}}_1 \times \hat{\mathbf{e}}_2. \end{aligned} \tag{2.7}$$

By the properties of the cross-product, each of them is perpendicular to the plane defined by the corresponding unit vectors. Now we can multiply (2.6) by the last three vectors obtaining a set of equations from which it is possible to get the distances:

$$\begin{aligned} n_1\rho_1(\hat{\mathbf{e}}_1 \cdot \hat{\mathbf{d}}_1) &= (n_1\mathbf{R}_1 - \mathbf{R}_2 + n_3\mathbf{R}_3) \cdot \hat{\mathbf{d}}_1, \\ -\rho_2(\hat{\mathbf{e}}_2 \cdot \hat{\mathbf{d}}_2) &= (n_1\mathbf{R}_1 - \mathbf{R}_2 + n_3\mathbf{R}_3) \cdot \hat{\mathbf{d}}_2, \\ n_3\rho_3(\hat{\mathbf{e}}_3 \cdot \hat{\mathbf{d}}_3) &= (n_1\mathbf{R}_1 - \mathbf{R}_2 + n_3\mathbf{R}_3) \cdot \hat{\mathbf{d}}_3. \end{aligned} \tag{2.8}$$

We introduce for convenience the following quantities:

$$\begin{aligned} D &= \hat{\mathbf{e}}_1 \cdot \hat{\mathbf{d}}_1 = \hat{\mathbf{e}}_2 \cdot \hat{\mathbf{d}}_2 = \hat{\mathbf{e}}_3 \cdot \hat{\mathbf{d}}_3, \\ D_{ij} &= \hat{\mathbf{d}}_i \cdot \mathbf{R}_j. \end{aligned} \tag{2.9}$$

Then, after simple substitutions, we obtain from (2.8) the three equations for the geocentric distances:

$$\begin{aligned} \rho_1 &= \frac{1}{n_1 D}(n_1 D_{11} - D_{12} + n_3 D_{13}), \\ \rho_2 &= -\frac{1}{D}(n_1 D_{21} - D_{22} + n_3 D_{23}), \\ \rho_3 &= \frac{1}{n_1 D}(n_1 D_{31} - D_{32} + n_3 D_{33}). \end{aligned} \tag{2.10}$$

The unknowns of the problem are the geocentric distances. If we know them the heliocentric vectors are determined from (2.3). With equations (2.10)

the unknowns are reduced from three to two: the n-coefficients. The factors D and D_{ij} follow directly from the observations.

In order to find expressions for n_1 and n_3 we consider the equation of the orbital plane (2.5). If we form the cross-product of both sides with $\mathbf{r}_1$ and $\mathbf{r}_3$, and recall that the cross-product of a vector with itself cancels out we obtain the expressions:

$$\begin{aligned} \mathbf{r}_2 \times \mathbf{r}_3 &= n_1(\mathbf{r}_1 \times \mathbf{r}_3), \\ \mathbf{r}_2 \times \mathbf{r}_1 &= n_3(\mathbf{r}_3 \times \mathbf{r}_1), \end{aligned} \tag{2.11}$$

from which follows:

$$\begin{aligned} n_1 &= \frac{\mid \mathbf{r}_2 \times \mathbf{r}_3 \mid}{\mid \mathbf{r}_1 \times \mathbf{r}_3 \mid}, \\ n_3 &= \frac{\mid \mathbf{r}_2 \times \mathbf{r}_1 \mid}{\mid \mathbf{r}_3 \times \mathbf{r}_1 \mid}. \end{aligned} \tag{2.12}$$

Recalling that the area Δ of a triangle bounded by two vectors $\mathbf{r}_a$ $\mathbf{r}_b$ is:

$$\Delta = \frac{1}{2} \mid \mathbf{r}_a \times \mathbf{r}_b \mid \tag{2.13}$$

it is possible to express equations (2.12) as the ratio between the areas of the triangles bounded by the heliocentric vectors. This means that the n-coefficients are defined as *triangle area ratios*:

$$\begin{aligned} n_1 &= \frac{\Delta_1}{\Delta_2}, \\ n_3 &= \frac{\Delta_3}{\Delta_2}, \end{aligned} \tag{2.14}$$

in which the triangle's areas are:

$$\Delta_1 = \frac{1}{2} \mid \mathbf{r}_2 \times \mathbf{r}_3 \mid \qquad \Delta_2 = \frac{1}{2} \mid \mathbf{r}_1 \times \mathbf{r}_3 \mid \qquad \Delta_3 = \frac{1}{2} \mid \mathbf{r}_1 \times \mathbf{r}_2 \mid \tag{2.15}$$

We notice that for small arcs of orbits the triangle area Δ is close to being equivalent to the corresponding sector area S, therefore we introduce a proportionality function η so that:

$$S_i = \eta_i \Delta_i, \qquad i = 1, 2, 3. \tag{2.16}$$

Recalling the second Kepler's law we note that S_i is proportional to the intervals τ_i defined as:

$$\tau_1 = \sqrt{GM_\odot}(t_3 - t_2), \qquad \tau_2 = \sqrt{GM_\odot}(t_3 - t_1), \qquad \tau_3 = \sqrt{GM_\odot}(t_2 - t_1), \tag{2.17}$$

where $GM_\odot$ is the gravitational parameter. Thus the n-coefficients become:

$$\begin{aligned} n_1 &= \frac{\eta_2}{\eta_1} \cdot \frac{\tau_1}{\tau_2}, \\ n_3 &= \frac{\eta_2}{\eta_3} \cdot \frac{\tau_3}{\tau_2}. \end{aligned} \tag{2.18}$$

These are exact equations which relate the triangle area ratios with the time intervals between observations. Another quantity appears, which is called *Sector-to-Triangle ratio* η. It represents the proportionality factor between the area of the sector bounded by the heliocentric vectors and the area of the triangle referred to the same vectors. For this reason it is always greater than one.

The fundamental contribution of Gauss was to notice that the computation of the n-coefficients could be exchanged with the computation of the η-functions. In turn, the sector-to-triangle ratios are determined from *Gauss's equation*.

2.2 Sector to triangle ratio and Gauss's equation

The core of the method consist in the solution of *Gauss's equation*. To derive this important equation we need first to define the *Sector-to-Triangle ratio* η as function of the orbital elements. The definition of η has in fact already been given in equation (2.16), which does not show the dependence on the elements. We know however that it is possible to express the triangle area depending on the true anomalies f_1 and f_2 associated with the radius vectors r_1 and r_2:

$$\Delta = \frac{1}{2} r_1 r_2 \sin(f_2 - f_1) \tag{2.19}$$

The sector's area $S(t)$ derives, in turn from the third of Kepler's law $n^2 a^3 = GM_\odot$ considering $n = \frac{2\pi}{T}$ with T the period of the orbit. It is the area swept by the radius vector in the interval $t - t_0$, where t_0 is the time of perihelion passage and can be expressed as:

$$S(t) = \frac{1}{2} \sqrt{GM_\odot} \sqrt{a(1-e^2)} (t - t_0). \tag{2.20}$$

In this case, calling the semi-latus rectum $p = a(1 - e^2)$, we can simplify in this way:

$$S = \frac{1}{2} \sqrt{p} \cdot \tau, \tag{2.21}$$

with $\tau = \sqrt{GM_\odot}(t - t_0) = \sqrt{\mu}(t - t_0)$.

A new expression for the *sector to triangle ratio* can then be formed as:

$$\eta = \frac{S}{\Delta} = \frac{\sqrt{p} \cdot \tau}{r_1 r_2 \sin \Delta f}. \tag{2.22}$$

If we try to eliminate p by using the known relations for the Two-Body Problem we find that it is no longer possible to express η as a solvable algebraic equation, but we obtain a transcendental equation. The first step to derive it requires the use of the Lagrangian coefficients [9] express as function of the true anomaly f:

$$\begin{aligned} F &= 1 - \frac{r}{p}(1 - \cos\Delta f), \\ \dot{F} &= \sqrt{\frac{\mu}{p}}\frac{1-\cos\Delta f}{\sin\Delta f}\left(\frac{1-\cos\Delta f}{p} - \frac{1}{r_0} - \frac{1}{r}\right), \\ G &= \frac{r r_0}{\sqrt{\mu p}}\sin\Delta f, \\ \dot{G} &= 1 - \frac{r_0}{p}(1 - \cos\Delta f), \end{aligned} \tag{2.23}$$

and of the eccentric anomaly E:

$$\begin{aligned} F &= 1 - \frac{a}{r_0}(1 - \cos\Delta E), \\ \dot{F} &= -\frac{n a^2}{r_1 r_2}\sin\Delta E, \\ G &= \Delta t - \frac{1}{n}(\Delta E - \sin\Delta E), \\ \dot{G} &= 1 - \frac{a}{r}(1 - \cos\Delta E). \end{aligned} \tag{2.24}$$

From the two expressions of F and using the bisection rule $2\sin^2\frac{x}{2} = 1 - \cos x$, we obtain:

$$\sin\frac{\Delta f}{2} = \sqrt{\frac{pa}{r_1 r_2}}\sin\frac{\Delta E}{2}. \tag{2.25}$$

Considering now the two expressions for $\dot{F}$ and using the relation $\mu = n^2 a^3$ and the identity $\sin\theta/\sqrt{1-\cos\theta} = \sqrt{2}\cos(\theta/2)$ we can write a new expression for the semi-latus rectum p:

$$p = \frac{(1 - \cos\Delta f) r_1 r_2}{r_1 + r_2 - 2\sqrt{r_1 r_2}\cos\frac{\Delta E}{2}\cos\frac{\Delta f}{2}}. \tag{2.26}$$

Recalling moreover the STT ratio derived in (2.22) we can get the *first equation of Gauss*:

$$\eta^2 = \frac{m}{l + \sin^2\frac{\Delta E}{4}}, \tag{2.27}$$

which relates the sector to triangle ratio with the eccentric anomaly. The introduced auxiliary variables are:

$$\begin{aligned} m &= \frac{\mu(\Delta t)^2}{2^{\frac{3}{2}}(r_1 r_2 + \mathbf{r}_1 \cdot \mathbf{r}_2)^{\frac{3}{2}}}, \\ l &= \frac{r_1 + r_2}{2^{\frac{3}{2}}\sqrt{r_1 r_2 + \mathbf{r}_1 \cdot \mathbf{r}_2}} - \frac{1}{2}. \end{aligned} \tag{2.28}$$

They depend on the heliocentric vectors and on the known time intervals. If we calculate them for the three observations we will obtain three sets of auxiliary variables, one for each pair of observations.

If we compare now the expression of G as function of true anomaly with the STT ratio derived in (2.22), we obtain a new relation for G as follows:

$$G\eta = \Delta t. \tag{2.29}$$

Consequently, equating the previous one and, this time, the Lagrange expression for G as function of eccentric anomaly we obtain:

$$\frac{1}{\eta} = 1 - \frac{1}{n\Delta t}\sqrt{\frac{a^3}{\mu}}(\Delta E - \sin \Delta E). \tag{2.30}$$

To eliminate the semimajor axis a from the previous we use (2.22) and (2.25) getting a new expression for the STT :

$$\eta = \frac{\sqrt{\mu}\Delta t}{2\sqrt{ar_1r_2}\sin\frac{\Delta E}{2}\frac{\Delta f}{2}}. \tag{2.31}$$

Taking the cube of each member and multiplying memberwise with (2.30) yields:

$$\eta^3 - \eta^2 = \frac{\mu(\Delta t)^2}{8(r_1r_2)^{\frac{3}{2}}\cos^3\frac{\Delta f}{2}}\frac{\Delta E - \sin \Delta E}{\sin^3\frac{\Delta E}{2}}. \tag{2.32}$$

Noting that the first factor on the right hand side of the equation is identical to the m variable we can rewrite a simpler version of the *second equation of Gauss*:

$$\eta^2(\eta - 1) = m\frac{(\Delta E - \sin \Delta E)}{\sin^3\frac{\Delta E}{2}}. \tag{2.33}$$

Starting from the two equations of Gauss (2.27) and (2.33), it is possible to calculate a new combined equation. It was exactly in this derivation that Gauss developed his *hypergeometric function* as we know it today. We briefly review this important procedure. The crucial point of the method is to express the function

$$w = \frac{(\Delta E - \sin \Delta E)}{\sin^3\frac{\Delta E}{2}}, \tag{2.34}$$

appearing in the second Gauss's equation in terms of the variable:

$$x = \sin^2\frac{\Delta E}{4}, \tag{2.35}$$

which appears in the first one. To do so, we derive w with respect to x to obtain:

$$\frac{dw}{dx} = \frac{dw}{dE}\frac{dE}{dx}. \tag{2.36}$$

Calculating first:

$$\begin{aligned} \frac{dx}{dE} &= \frac{1}{4}\sin\frac{\Delta E}{2}, \\ \frac{dw}{dE} &= \frac{2}{\sin\frac{\Delta E}{2}} - \frac{3}{2}w\frac{\cos\Delta E/2}{\sin\Delta E/2}, \end{aligned} \tag{2.37}$$

we can finally write:

$$\sin^2\frac{\Delta E}{2}\frac{dw}{dx} = 8 - 6w\cos\frac{\Delta E}{2}. \tag{2.38}$$

From (2.34) we can easily obtain two expression:

$$\begin{aligned} \cos\frac{\Delta E}{2} &= 1 - 2x \\ \sin^2\frac{\Delta E}{2} &= 4x(1-x) \end{aligned} \tag{2.39}$$

which substitute into (2.38) yield the differential equation:

$$2x(1-x)\frac{dw}{dx} + 3(1-2x)w - 4 = 0. \tag{2.40}$$

It is possible to recognize here a special form of the Gauss hypergeometric equation for $w(x)$ with parameters $\alpha = 3$, $\beta = 1$, and $\gamma = 5/2$. The solution is easily written in terms of the hypergeometric function $F(\alpha, \beta; \gamma; x)$ as:

$$w(x) = \frac{4}{3}F(3, 1; \frac{5}{2}; x), \tag{2.41}$$

where $\frac{4}{3}$ is a normalization factor. If we substitute the expression of x obtained from the first equation:

$$x = \frac{m}{\eta^2} - l, \tag{2.42}$$

we can define a new function in terms of the variables η, m and l:

$$W(\eta, l, m) = \frac{4}{3}F(3, 1; \frac{5}{2}; \frac{m}{\eta^2} - l). \tag{2.43}$$

The *combined equation of Gauss* results finally from (2.33):

$$\eta^2(\eta - 1) = mW(\eta, l, m). \tag{2.44}$$

This equation provides the STT ratio directly from two heliocentric position vectors which appear through the l and m auxiliary variables. Moreover it is valid not only for elliptic orbit but also for the parabolic and hyperbolic ones.

The method requires the computation of three combined equations of Gauss, one for each pair of observations. The results are entered in (2.18) and the n-coefficients determined. Then the triangle area ratios are used to calculate the geocentric distances from (2.10) which, in turn provide the heliocentric vectors from (2.3). At this point we restart the procedure, calculating the new three pairs of auxiliary variables, which allow to solve the three combined equations of Gauss.

2.3 Initialization

In this section we want to define two different expression for triangle area ratios n_1 and n_3. In fact, to start the procedure and determine a first approximation of geocentric distances we need to define some initial values for the triangle to area ratios. Both of these sets depend on the approximation chosen for the Lagrangian coefficients F and G as function of time. This leads to two different approximations: if we choose a first-order approximation for F and G we will obtain a zeroth-order, or Bouguer, approximation for n_1 and n_3. On the other hand, if we choose a second-order for the coefficients, we will find a first-order, or Encke approximation, for n_1 and n_3 [9]. We start expressing the first and the third heliocentric positions in terms of the state at the time of the second observation:

$$\begin{aligned} \mathbf{r}_1 &= F(t_1,t_2)\mathbf{r}_2 + F(t_1,t_2)\dot{\mathbf{r}}_2, \\ \mathbf{r}_3 &= F(t_3,t_2)\mathbf{r}_2 + F(t_3,t_2)\dot{\mathbf{r}}_2. \end{aligned} \tag{2.45}$$

We introduce the auxiliary variables:

$$u = \frac{\mu}{r_j^3} \qquad s = \frac{\mathbf{r}_j \cdot \dot{\mathbf{r}}_j}{r_j^2} \qquad w = \frac{\dot{\mathbf{r}}_j \cdot \dot{\mathbf{r}}_j}{r_j^2} \tag{2.46}$$

so the Lagrange coefficients can be expressed as series in power of the time interval $\Delta t_{ij} = t_i - t_j$

$$\begin{aligned} F(t_i,t_j) &= 1 - \frac{1}{2}u\Delta t^2 + \frac{1}{2}us\Delta t^3 + \frac{1}{2u}u(3w - 2u - 15s^2)\Delta t^4 + ..., \\ G(t_i,t_j) &= \Delta t - \frac{1}{6}u\Delta t^3 + \frac{1}{4}us\Delta t^4 + ... \end{aligned} \tag{2.47}$$

Now we substitute (2.45) into (2.12) obtaining:

$$\begin{aligned} n_1 &= \frac{G_3}{F_1G_3 - G_1F_3}, \\ n_3 &= \frac{G_1}{F_3G_1 - G_3F_1}. \end{aligned} \tag{2.48}$$

If we consider a first order approximation of Lagrange coefficients as following:

$$\begin{aligned} F_{10} &= F_{30} \cong 1, \\ G_{10} &= \Delta t_{21}, \\ G_{30} &= \Delta t_{23}, \end{aligned} \tag{2.49}$$

we obtain a zeroth-order, or Bouguer approximation for n_1 and n_3:

$$\begin{aligned} n_{10} &= \frac{\Delta t_{23}}{\Delta t_{13}}, \\ n_{30} &= -\frac{\Delta t_{21}}{\Delta t_{13}}. \end{aligned} \tag{2.50}$$

On the other hand if we use more precise expressions, considering a second-order approximation for F and G :

$$\begin{aligned} F_{11} &= 1 - \frac{1}{2} u_2 \Delta t_{21}^2, \\ F_{31} &= 1 - \frac{1}{2} u_2 \Delta t_{23}^2, \\ G_{11} &= \Delta t_{21} - \frac{1}{6} u_2 \Delta t_{21}^2, \\ G_{31} &= \Delta t_{23} - \frac{1}{6} u_2 \Delta t_{23}^2, \end{aligned} \tag{2.51}$$

we have a first-order, or Encke approximation, for n_1 and n_3:

$$\begin{aligned} n_{11} &= \frac{\Delta t_{23}}{\Delta t_{13}} - \frac{1}{6} u_2 \Delta t_{21} \Delta t_{23} \left(1 + \frac{\Delta t_{23}}{\Delta t_{13}} \right), \\ n_{31} &= -\frac{\Delta t_{21}}{\Delta t_{13}} - \frac{1}{6} u_2 \Delta t_{21} \Delta t_{23} \left(1 - \frac{\Delta t_{21}}{\Delta t_{13}} \right). \end{aligned} \tag{2.52}$$

2.4 The comprehensive Gauss method

The three observations used in the Gauss method can be fitted by various orbits arcs. As a matter of fact there are several pairs of r and ρ values that satisfy the problem, the number of which can be analyzed in terms of the Charlier's theory [8]. The improvement carried by the comprehensive approach consists in the introduction of the *Gauss-Lagrange equation*: an eighth order equation that enables us to discriminate among the possible solutions [6]. Generally there are three solutions in the proximity of conjunction and two near opposition. One of these is always represented by the Earth orbit so it is automatically discarded.

To analyze the problem we use the Encke approximation for the triangle area ratios already defined in (2.52). We rearrange them in terms of the

intervals of time defined in (2.17):

$$\Delta t_{21} = -\tau_3, \qquad \Delta t_{13} = \tau_2, \qquad \Delta t_{23} = \tau_1, \tag{2.53}$$

and we obtain:

$$\begin{aligned} n_1 &= \frac{\tau_1}{\tau_2} + \frac{1}{6}\tau_1\tau_3(1+\frac{\tau_1}{\tau_2})\frac{1}{r_2^3}, \\ n_3 &= \frac{\tau_3}{\tau_2} + \frac{1}{6}\tau_1\tau_3(1+\frac{\tau_3}{\tau_2})\frac{1}{r_2^3}. \end{aligned} \tag{2.54}$$

We can rewrite them divided into two coefficients as follows:

$$\begin{aligned} n_{10} &= \frac{\tau_1}{\tau_2}, \qquad \mu_1 = \frac{1}{6}\tau_1\tau_3(1+\frac{\tau_1}{\tau_2}), \\ n_{30} &= \frac{\tau_3}{\tau_2}, \qquad \mu_3 = \frac{1}{6}\tau_1\tau_3(1+\frac{\tau_3}{\tau_2}), \end{aligned} \tag{2.55}$$

so that:

$$\begin{aligned} n_1 &= n_{10} + \mu_1, \\ n_3 &= n_{30} + \mu_3. \end{aligned} \tag{2.56}$$

Moreover, directly from (2.10) we can write:

$$\begin{aligned} \rho_0 &= -\frac{1}{D}(n_{10}D_{21} - D_{22} + n_{30}D_{23}), \\ \sigma &= \frac{1}{D}(\mu_1 D_{21} + \mu_3 D_{23}). \end{aligned} \tag{2.57}$$

Therefore, using the expressions for the geocentric distances in (2.10) we obtain the simple relationship:

$$\rho_2 = \rho_0 - \frac{\sigma}{r_2^3}, \tag{2.58}$$

where ρ_0 and σ are calculated from the observations, while ρ_2 and r_2 are unknowns. Thus, in order to solve the previous equation we need another equation. We use the (2.3) expressed for the second observation:

$$\mathbf{r}_2 = \rho_2\hat{\mathbf{e}}_2 - \mathbf{R}_2, \tag{2.59}$$

that squared becomes:

$$r_2^2 = \rho_2^2 + R^2 - 2\rho_2\hat{\mathbf{e}}_2 \cdot \mathbf{R}_2. \tag{2.60}$$

Defining $\gamma = \hat{\mathbf{e}}_2 \cdot \hat{\mathbf{R}}_2$ we obtain:

$$r_2 = \sqrt{(\rho_2 - \gamma R_2)^2 + R_2^2(1-\gamma^2)}. \tag{2.61}$$

It's possible to define $\gamma = \cos\alpha$ as the cosine of the α angle between the line of sight $\hat{\mathbf{e}}$ and Sun's direction $\hat{\mathbf{R}}$. The object is in conjunction when $\gamma = +1$ and $\alpha = 0^\circ$ while it's in opposition if $\gamma = -1$ and $\alpha = 180^\circ$.

Equations (2.61) and (2.58) form a system of two equations with two unknowns so it is possible to solve it by replacing the last into the first. The relation obtained in this way are the *Gauss-Lagrange equation*

$$\sqrt[3]{\frac{\sigma}{\rho_0 - \rho_2}} = \sqrt{(\rho_2 - \gamma R_2)^2 + R_2^2(1-\gamma^2)} \tag{2.62}$$

that is a third degree equation in ρ_2. The solutions will be up to three therefore it will possible to consider three different (ρ_2, r_2) pairs which in turn will lead to three different possible orbits.

To simplify the resolution we employ in the algorithm a different but equivalent form of the equation, the eighth order following polynomial:

$$r_2^8 - (\rho_0^2 - 2\gamma\rho_0 R_2 + R_2^2) r_2^6 + 2\sigma(\rho_0 - \gamma R_2) r_2^2 - \sigma^2 = 0 \tag{2.63}$$

this is obtained substituting the value of ρ_2 from equation (2.61) into (2.62).

2.5 Orbital elements

The final step consist in the computation of Keplerian elements. It is possible to derive them directly from two heliocentric position vectors with a special procedure instead of solving a Lambert problem [6].

We define the unit vectors $\hat{\mathbf{e}}_a$ and $\hat{\mathbf{e}}_0$ lying on the orbit plane. The first one points on the position vector $\mathbf{r}_a$ direction and the second one is perpendicular to it. The unit vector $\hat{\mathbf{R}}$ is perpendicular to the orbit plane

$$\begin{aligned} \hat{\mathbf{e}}_a &= \frac{\mathbf{r}_a}{|\,\mathbf{r}_a\,|}, \\ \hat{\mathbf{e}}_0 &= \frac{\mathbf{r}_0}{|\,\mathbf{r}_0\,|}, \\ \hat{\mathbf{R}} &= \hat{\mathbf{e}}_a \times \hat{\mathbf{e}}_0, \end{aligned} \tag{2.64}$$

with $\mathbf{r}_0 = \mathbf{r}_b - (\mathbf{r}_b \cdot \hat{\mathbf{e}}_a)\hat{\mathbf{e}}_a$. The unit vector $\hat{\mathbf{R}}$ is defined using ecliptic coordinates longitude l and latitude b. Its components can be write depending on the inclination angle i and on the longitude of ascending node Ω.:

$$\begin{aligned} l &= \Omega - 90 \\ b &= 90 - i \end{aligned} \tag{2.65}$$

$$\hat{\mathbf{R}} = \begin{pmatrix} \cos b \cos l \\ \cos b \sin l \\ \sin b \end{pmatrix} = \begin{pmatrix} \sin i \sin \Omega \\ -\sin i \cos \Omega \\ \cos i \end{pmatrix}$$

from which we obtain:

$$\begin{aligned} i &= 90 - \arcsin R_z = \arccos R_z, \\ \Omega &= 90 + \arctan(\frac{R_y}{R_x}) = \arctan(\frac{-R_x}{R_y}). \end{aligned} \tag{2.66}$$

We pass now to the argument of latitude u_a required to calculate the argument of perihelion ω:

$$\begin{aligned} \cos u_a &= \hat{\mathbf{e}}_a \cdot \hat{\mathbf{e}}_\Omega = x_a \cdot \cos\Omega + y_a \cdot \sin\Omega, \\ \cos(u_a + 90) &= \hat{\mathbf{e}}_0 \cdot \hat{\mathbf{e}}_\Omega = x_0 \cdot \cos\Omega + y_0 \cdot \sin\Omega. \end{aligned} \tag{2.67}$$

The unit vector along the line of sight is:

$$\hat{\mathbf{e}}_\Omega = \begin{pmatrix} \cos\Omega \\ \sin\Omega \\ 0 \end{pmatrix}$$

therefore we have, for the argument of latitude:

$$\begin{aligned} u_a &= \arctan(\frac{-x_0\cos\Omega - y_0\sin\Omega}{x_a\cos\Omega + y_a\sin\Omega}) \\ &= \arctan(\frac{x_0R_y - y_0R_x}{-x_aR_y + y_aR_x}). \end{aligned} \tag{2.68}$$

All the other orbital elements are measured starting from the sector to triangle ratio η. For the semi-latus rectum we find:

$$p = (\frac{2\Delta\eta}{\tau})^2 \tag{2.69}$$

with $\Delta = \frac{1}{2}r_a r_b \sin(\nu_b - \nu_a) = \frac{1}{2}r_a r_0$. Starting from the equation of a conic section:

$$r = \frac{p}{1 + e\cos\nu}, \tag{2.70}$$

we can derive the eccentricity e through the expressions:

$$\begin{aligned} e\cos\nu_a &= \frac{p}{r_a} - 1, \\ e\cos\nu_b &= \frac{p}{r_b} - 1. \end{aligned} \tag{2.71}$$

Recalling the relation:

$$\begin{aligned} \cos\nu_b &= \cos\nu_a\cos(\nu_b - \nu_a) - \sin\nu_a\sin(\nu_b - \nu_a) \\ &= \cos\nu_a(\frac{\mathbf{r}_b \cdot \hat{\mathbf{e}}_a}{r_b}) - \sin\nu_a(\frac{r_0}{r_b}), \end{aligned} \tag{2.72}$$

we obtain:

$$\begin{aligned} e\cos\nu_a &= \frac{p}{r_a} - 1, \\ e\sin\nu_a &= [(\frac{p}{r_a} - 1)(\frac{\mathbf{r}_b \cdot \hat{\mathbf{e}}_a}{r_b}) - (\frac{p}{r_b} - 1)]/\frac{r_0}{r_b}, \end{aligned} \tag{2.73}$$

and finally we can compute the eccentricity e and the true anomaly ν_a:

$$e = \sqrt{(e\cos\nu_a)^2 + (e\sin\nu_a)^2}, \tag{2.74}$$

$$\nu_a = \arctan(\frac{e\sin\nu_a}{e\cos\nu_a}). \tag{2.75}$$

At this point it is possible to determine which type of orbit has been found: for $e < 1$ we have an ellipse, on the other hand for $e > 1$ we find an hyperbole. The argument of perihelion is:

$$\omega = u_a - \nu_a, \tag{2.76}$$

while the longitude of pericenter results:

$$\bar{\omega} = u_a - \nu_a + \Omega. \tag{2.77}$$

The semi-major axis is:

$$a = \frac{p}{1 - e^2}, \tag{2.78}$$

and the perihelion distance became:

$$q = \frac{p}{1 + e}. \tag{2.79}$$

At the end we define the time of perihelion passage t_0. For elliptic orbits we need to calculate first the eccentric anomaly E:

$$\begin{aligned} \cos E_a &= \frac{\cos\nu_a + e}{1 + e\cos\nu_a}, \\ \sin E_a &= \frac{\sqrt{1 - e^2}\sin\nu_a}{1 + e\cos\nu_a}, \end{aligned} \tag{2.80}$$

and the mean anomaly M from Kepler's equation:

$$M_a = E_a - e\sin E_a. \tag{2.81}$$

Recalling that the mean anomaly in an orbital period T varies following the third Kepler's law we obtain:

$$\begin{aligned} n &= \frac{2\pi}{T} = \sqrt{\frac{GM}{a^3}}, \\ M &= 2\pi\frac{t - t_0}{T} = (t - t_0)n, \\ t_0 &= t_a - \frac{M_a}{\sqrt{\frac{GM}{a^3}}}. \end{aligned} \tag{2.82}$$

Finally we have calculated all the six orbital elements: the angular ones i Ω and ω and the phoronomic ones e a and t_0. The nature of the orbit is so completely determined.

Chapter 3

New initial orbit determination methods

Several variants of the fundamental methods of Gauss and Laplace have been developed over the years, as well as new approaches. In this Chapter we introduce one new method, developed by Neutsch [10] which is not based on the classical methods, and a recent revisitation of the method of Gauss by Casotto [9]. We close the chapter with a brief introduction to the classical methods used to determine the orbits of binary stars, transneptunian objects and those of exoplanets.

3.1 The Neutsch method

A new approach to initial orbit determination was developed by Neutsch in 1982 [10]. Neutsch's method belongs to a different class of methods, which have nothing in common with the method of Gauss or Laplace. This is an example of non-Gaussian and non-Laplacian method. Goffin resumed Neutsch's work and expanded it for the computation of conditioned orbit [11]. These are the cases in which we have less then three observations and we need to reduce the unknowns of the problem by imposing additional conditions. We treat here the non-conditioned problem. The purpose is to write a set of equations which includes both geometrical and dynamical equations in the form of a linear system. The implementation of the method requires an iterative procedure which starts from a generic orbit, solves the linear system which provides the dynamical state of the object and finally converts it to Keplerian elements. At this point the process restarts, using the orbital elements as new input and so on until convergence. In order to derive the equations involved in the problem we define, at first, the heliocentric position of the object as a function of the six orbital elements which are unknown, and of the time of observation:

$$\mathbf{r}_i = f(t_i, a, e, M_0, i, \omega, \Omega) \qquad i = 1, 2, 3. \tag{3.1}$$

The same heliocentric state vector can be expressed also as a function of the position $\mathbf{r}_0$ and the velocity $\dot{\mathbf{r}}_0$ at epoch t_0:

$$\mathbf{r}_i = f(t_i, x_0, y_0, z_0, \dot{x}_0, \dot{y}_0, \dot{z}_0) \qquad i = 1, 2, 3. \tag{3.2}$$

Thus the initial state vector will be the unknown to be determined. In order to do this we write the position vector of the object at time t_i in two different ways. The first one yields:

$$\begin{aligned} x_i &= a_i\rho_i + X_i, \\ y_i &= b_i\rho_i + Y_i, \qquad i = 1, 2, 3, \\ z_i &= c_i\rho_i + Z_i, \end{aligned} \tag{3.3}$$

with ρ_i the geocentric distances of the object, X_i, Y_i, Z_i the components of the Earth heliocentric position vector and a_i, b_i, c_i corresponds to the direction cosines of the geocentric position of the object both obtained from the observations. The second way to define $\mathbf{r}_i$ is with the aid of the F and G functions, or Lagrangian coefficients in this way:

$$\begin{aligned} x_i &= F_i x_0 + G_i \dot{x}_0, \\ y_i &= F_i y_0 + G_i \dot{y}_0, \qquad i = 1, 2, 3. \\ z_i &= F_i z_0 + G_i \dot{z}_0. \end{aligned} \tag{3.4}$$

The Lagrangian coefficients F and G can be expressed as functions of the eccentric anomaly [26] as:

$$\begin{aligned} F_i &= 1 + \frac{\cos E_i - E_0 - 1}{1 - e\cos E_0}, \\ G_i &= t_i - t_0 + \frac{\sin E_i - E_0 - (E_i - E_0)}{n}. \end{aligned} \tag{3.5}$$

If the last two set of equations (3.3) and (3.4) are combined, the following basic equations are obtained:

$$\begin{aligned} F_i x_0 + G_i \dot{x}_0 - a_i\rho_i &= X_i, \\ F_i y_0 + G_i \dot{y}_0 - b_i\rho_i &= Y_i, \qquad i = 1, 2, 3. \\ F_i z_0 + G_i \dot{z}_0 - c_i\rho_i &= Z_i. \end{aligned} \tag{3.6}$$

Therefore it is possible to solve the linear system of equations derived from (3.6). Written explicitly in matrix form it becomes:

$$\begin{pmatrix} F_1 & 0 & 0 & G_1 & 0 & 0 & -a_1 & 0 & 0 \\ 0 & F_1 & 0 & 0 & G_1 & 0 & -b_1 & 0 & 0 \\ 0 & 0 & F_1 & 0 & 0 & G_1 & -c_1 & 0 & 0 \\ F_2 & 0 & 0 & G_2 & 0 & 0 & 0 & -a_2 & 0 \\ 0 & F_2 & 0 & 0 & G_2 & 0 & 0 & -b_2 & 0 \\ 0 & 0 & F_2 & 0 & 0 & G_2 & 0 & -c_2 & 0 \\ F_3 & 0 & 0 & G_3 & 0 & 0 & 0 & 0 & -a_3 \\ 0 & F_3 & 0 & 0 & G_3 & 0 & 0 & 0 & -b_3 \\ 0 & 0 & F_3 & 0 & 0 & G_3 & 0 & 0 & -c_3 \end{pmatrix} \begin{pmatrix} x_0 \\ y_0 \\ z_0 \\ \dot{x}_0 \\ \dot{y}_0 \\ \dot{z}_0 \\ \rho_1 \\ \rho_2 \\ \rho_3 \end{pmatrix} = \begin{pmatrix} X_1 \\ Y_1 \\ Z_1 \\ X_2 \\ Y_2 \\ Z_2 \\ X_3 \\ Y_3 \\ Z_3 \end{pmatrix} \tag{3.7}$$

When the initial state vector is found it is necessary to convert the Cartesian elements into Keplerian elements and to restart the process, using this new set as initial orbit approximation. First of all, to convert the elements, we must transform the equatorial coordinates into ecliptic ones:

$$\begin{aligned} x_e &= x, \\ y_e &= z \sin\epsilon + y \cos\epsilon, \\ z_e &= z \cos\epsilon - y \sin\epsilon, \end{aligned} \tag{3.8}$$

and the same for the velocity. After that it's possible to calculate the angular momentum $\mathbf{h} = \mathbf{r} \times \mathbf{v}$. The elements derive from this quantities as follows:

$$a = \frac{r\mu}{2\mu - r\dot{r}^2}, \tag{3.9}$$

for the semi-major axis. The eccentricity in turn becomes:

$$e^2 = 1 - \frac{h^2}{\mu a}, \tag{3.10}$$

the inclination is:

$$\tan i = \frac{\sqrt{h_x^2 + h_y^2}}{h_z}, \tag{3.11}$$

and the ascending node:

$$\tan\Omega = \frac{h_x}{-h_y}. \tag{3.12}$$

For the mean anomaly we use the Kepler equation, defining before the eccentric anomaly E :

$$\begin{aligned} \tan E &= \frac{r\dot{r}}{a - r}\sqrt{\frac{a}{\mu}}, \\ M &= E - e \sin E. \end{aligned} \tag{3.13}$$

The true anomaly in turn becomes:

$$\tan\frac{f}{2} = \sqrt{\frac{1+e}{1-e}}\tan\frac{E}{2}, \tag{3.14}$$

the argument of latitude:

$$\tan u = \frac{z_e h}{y_e h_x - x_e h_y}, \tag{3.15}$$

and in the end the argument of perihelion:

$$\omega = u - f. \tag{3.16}$$

The six orbital elements are so determined. This method has the disadvantage of necessitating of an approximate initial orbit: if it is very different from the real one it is possible that the method gives a solution of the system (3.7) which leads to a wrong orbit.

3.2 The Gauss-Casotto method

This method is based on the same equations solved by Gauss, but does not require an iterative process. The core of the method consists of a system of six non-linear equations: three of them derive from the geometry of the system explained in section 2.1.1 and the other three from the *Gauss combined equation* derived in Section 2.2. The innovation carried by this method consists in expressing all the fundamental equations involved as function of the same unknowns which are the three geocentric distances and the three STT ratios. To explain the first set of equations we start by recalling the configuration formed by the Sun, the Earth and the object:

$$\mathbf{r}_i = \rho_i \hat{\mathbf{e}}_i + \mathbf{R}_i, \qquad i = 1, 2, 3. \tag{3.17}$$

valid for the three observations. $\mathbf{R}_i$ are the Earth heliocentric position vectors, $\mathbf{r}_i$ the object heliocentric position vectors, $\hat{\mathbf{e}}_i$ the unit vector position vectors and ρ_i the object geocentric distances from the Earth. As in the Gauss method we consider the heliocentric vectors to lie on the same plane so the coplanarity condition leads to linear dependence. We can then write:

$$n_1\mathbf{r}_1 + n_2\mathbf{r}_2 + n_3\mathbf{r}_3 = \mathbf{0}. \tag{3.18}$$

Substituting (3.17) equation into (3.18) we find :

$$n_1\rho_1\hat{\mathbf{e}}_1 + \rho_2\hat{\mathbf{e}}_2 + n_3\rho_3\hat{\mathbf{e}}_3 = -n_1\mathbf{R}_1 - \mathbf{R}_2 - n_3\mathbf{R}_3, \tag{3.19}$$

which is the *fundamental equation* of the Gauss method. The three geocentric distances can be isolated. For example to isolate ρ_1 we can multiplying

scalarly by a vector perpendicular to both the $\hat{\mathbf{e}}_2$ and $\hat{\mathbf{e}}_3$. Such a vector can be determined, recalling the vector products defined in (2.7) and (2.9), as $\xi_i = \frac{d_i}{D}$. Therefore we obtain:

$$\begin{aligned} n_1\rho_1 + (n_1\mathbf{R}_1 + n_2\mathbf{R}_2 + n_3\mathbf{R}_3)\cdot\xi_1 &= 0, \\ n_2\rho_2 + (n_2\mathbf{R}_2 + n_3\mathbf{R}_3 + n_1\mathbf{R}_1)\cdot\xi_2 &= 0, \\ n_3\rho_3 + (n_3\mathbf{R}_3 + n_1\mathbf{R}_1 + n_2\mathbf{R}_2)\cdot\xi_3 &= 0. \end{aligned} \tag{3.20}$$

In order to rewrite the set in a more useful manner we can express the n-coefficients in terms of the STT ratios:

$$n_1 = \frac{\eta_2}{\eta_1}\frac{\tau_3}{\tau_2}, \qquad n_2 = -1, \qquad n_3 = -\frac{\eta_2}{\eta_3}\frac{\tau_1}{\tau_2}, \tag{3.21}$$

and of the observation time intervals:

$$\begin{aligned} \tau_1 &= t_1 - t_2 < 0, \\ \tau_2 &= t_3 - t_1 > 0, \\ \tau_3 &= t_3 - t_2 < 0. \end{aligned} \tag{3.22}$$

Moreover, if we write for convenience the coefficients $a_{ij} = \xi_i \cdot \mathbf{R}_j$ with $i = 1, 2, 3$ and $j = 1, 2, 3$, finally we can determine the three geometrical equations. Using the same notation as in the Gauss method, the same coefficients can be defined as $a_{ij} = \frac{D_{ij}}{D}$.

We now turn to the second set of equations. The auxiliary variables are introduced:

$$\begin{aligned} m_{ij} &= \frac{\mu(\Delta t_{ij})^2}{2^{\frac{3}{2}}(r_i r_j + \mathbf{r}_i\cdot\mathbf{r}_j)^{\frac{3}{2}}}, \\ l_{ij} &= \frac{r_i + r_j}{2^{\frac{3}{2}}\sqrt{r_i r_j + \mathbf{r}_i\cdot\mathbf{r}_j}} - \frac{1}{2}. \end{aligned} \tag{3.23}$$

two for each interval of time between the observations. For example we find m_1 depending on τ_1 and on the two vectors $\mathbf{r}_1$ and $\mathbf{r}_2$, and so on for the other. The *Gauss combined equations* defined as in (2.44):

$$\eta_i^2(\eta_i - 1) = m_i W(\eta_i, l_i, m_i), \qquad i = 1, 2, 3. \tag{3.24}$$

represent the three dynamical equations.

At this point we can write the system of six non-linear, partly transcendental equations:

$$\begin{cases} (\rho_1 + a_{11})\eta_1\eta_2\tau_3 - a_{12}\eta_1\eta_3\tau_2 - \eta_2\eta_3\tau_1 a_{13} = 0 \\ a_{21}\eta_1\eta_2\tau_3 - (\rho_2 + a_{22})\eta_1\eta_3\tau_2 - \eta_2\eta_3\tau_1 a_{23} = 0 \\ a_{31}\eta_1\eta_2\tau_3 - a_{32}\eta_1\eta_3\tau_2 - (\rho_3 + a_{33})\eta_2\eta_3\tau_1 = 0 \\ \eta_1^2(\eta_1 - 1) - m_1(\rho_1,\rho_2)W[\eta_1, l_1(\rho_1,\rho_2), m_1(\rho_1,\rho_2)] = 0 \\ \eta_2^2(\eta_2 - 1) - m_2(\rho_1,\rho_3)W[\eta_2, l_2(\rho_1,\rho_2), m_2(\rho_1,\rho_3)] = 0 \\ \eta_3^2(\eta_3 - 1) - m_3(\rho_2,\rho_3)W[\eta_3, l_3(\rho_1,\rho_2), m_3(\rho_2,\rho_3)] = 0 \end{cases} \tag{3.25}$$

One of the last three equations is redundant therefore the system is reducible to only five equations. In spite of this it is preferable to consider all the six equations because in this way it results symmetric and more robust.
As we can notice the auxiliary variables are functions of $\mathbf{r}_i$, $i = 1, 2, 3$ which, in turn depend on ρ_i as shown by relation (3.17). As a consequence the unknowns are six, the three geocentric distances and the STT ratios: $\rho_1, \rho_2, \rho_3, \eta_1, \eta_2, \eta_3$.

3.2.1 Initial conditions

To solve the system it is possible to use the Newton-Raphson method. It is necessary to define an initial conditions vector $\mathbf{z_0}$:

$$\mathbf{z_0} = (\rho_1\, \rho_2\, \rho_3\, \eta_1\, \eta_2\, \eta_3). \tag{3.26}$$

Recalling the n-coefficients derivation in the last chapter we have, for the zeroth-order, or Bouguer guess:

$$\begin{aligned} n_{10} &= \frac{\tau_3}{\tau_2}, \\ n_{30} &= -\frac{\tau_1}{\tau_2}, \end{aligned} \tag{3.27}$$

and the geocentric distances are simply calculated as:

$$\begin{aligned} \rho_{10} &= \frac{\tau_2 a_{12} + \tau_1 a_{13}}{\tau_3} - a_{11}, \\ \rho_{20} &= \frac{\tau_3 a_{21} - \tau_1 a_{23}}{\tau_2} - a_{22}, \\ \rho_{30} &= \frac{\tau_3 a_{31} - \tau_2 a_{32}}{\tau_1} - a_{33}. \end{aligned} \tag{3.28}$$

At this point we need to know the three expressions of STT ratios, one for each pair of observations. They are derived through the *first equation of Gauss*:

$$\eta_{i0} = \sqrt{\frac{m_{i0}}{l_{i0} + \sin^2 \frac{\Delta E_{i0}}{4}}} \qquad i = 1, 2, 3. \tag{3.29}$$

The six values found, three geocentric distances and three sector-to-triangle ratios, are used as input value to solve the system (3.25). Finally the zeroth-order position vectors become:

$$\mathbf{r}_{i0} = \rho_{i0}\hat{\mathbf{e}}_i + \mathbf{R}_i \qquad i = 1, 2, 3. \tag{3.30}$$

If we choose instead the first-order, or Encke approximation, the n-coefficients become:

$$\begin{aligned} n_{11} &= n_{10}\left[1 - \frac{1}{6}\frac{\mu}{r_2^3}\tau_1(\tau_2 + \tau_3)\right], \\ n_{31} &= n_{30}\left[1 + \frac{1}{6}\frac{\mu}{r_2^3}\tau_3(\tau_2 - \tau_1)\right], \end{aligned} \tag{3.31}$$

but for calculating them it is necessary to know initial value for the heliocentric vector r_2, so with the aid of the *Gauss-Lagrange equation* we obtain the heliocentric distance corresponding to the second observation:

$$r_2^8 - Ar_2^6 + Br_2^3 - C = 0. \tag{3.32}$$

The coefficients are given by

$$\begin{aligned} A &= [A_2 + 2(\hat{\mathbf{e}}_2 \cdot \mathbf{R}_2)]A_2 + R_2^2, \\ B &= [2A_2 + 2(\hat{\mathbf{e}}_2 \cdot \mathbf{R}_2)]B_2, \\ C &= B_2^2, \end{aligned} \tag{3.33}$$

where:

$$\begin{aligned} A_2 &= \frac{1}{\tau_2}(\tau_3 a_{21} - \tau_1 a_{23}) - a_{22}, \\ B_2 &= \frac{\mu}{2}(\tau_3 a_{21} - \tau_1 a_{23})\frac{\tau_1 \tau_3}{\tau_2} \end{aligned} \tag{3.34}$$

From these we can calculate the geocentric distances:

$$\begin{aligned} \rho_{11} &= \frac{a_{12}}{n_{11}} - \frac{n_{31}}{n_{11}} a_{13} - a_{11}, \\ \rho_{21} &= n_{11} a_{21} - a_{22} + n_{31} a_{23}, \\ \rho_{31} &= \frac{a_{32}}{n_{31}} - \frac{n_{11}}{n_{31}} a_{31} - a_{33}, \end{aligned} \tag{3.35}$$

and using (3.30) we obtain the first order heliocentric vectors. We then solve the six equations of system (3.25) and we get the three heliocentric vectors:

$$\begin{aligned} \mathbf{r}_{11} &= \rho_{11}\hat{\mathbf{e}}_1 + \mathbf{R}_1, \\ \mathbf{r}_{21} &= \rho_{21}\hat{\mathbf{e}}_2 + \mathbf{R}_2, \\ \mathbf{r}_{31} &= \rho_{31}\hat{\mathbf{e}}_3 + \mathbf{R}_3. \end{aligned} \tag{3.36}$$

3.3 Analysis of multiple solutions

Determining orbits from only three observations can be ambiguous. This particularly occurs when we treat with small arcs of orbit. The fact is that the three observations can be fitted by different curves providing different solutions to the initial orbit determination problem. The multiplicity of these solutions was examined by Charlier in 1910 [8], who identified four regions in space bounded by the Earth's orbit and a drop-shaped curve in which is possible to find more orbits fitting the observations. The objective here is to prove the validity of Charlier's theory also on the method developed by Casotto.

3.3.1 Charlier's theory

The Charlier's studies allow to identify regions in space in which is possible to find two or three different orbits that fit the observations. Recalling the Gauss method we can show that each orbit corresponds to a solution of the *Gauss-Lagrange equation*.
In order to explain the Charlier procedure we start from the usual relation between position vectors:

$$\mathbf{r} = \mathbf{R} + \rho\hat{\mathbf{e}} \tag{3.37}$$

and square it, placing $u = \frac{\rho}{R}$ and $v = \frac{r}{R}$ we have :

$$v^2 = 1 + u^2 + 2nu \tag{3.38}$$

where $n = -\cos\phi$ with ϕ the angle between the object geocentric position vector and the Sun geocentric position vector, or elongation.

Lagrange, in 1778, [8] showed the existence of the relation:

$$u = \lambda(1 - \frac{1}{v^3}) \tag{3.39}$$

with the λ constant obtained from the observations. Substituting this expression for u into (3.38) we get an eighth-order equation in v:

$$v^8 - v^6[1 - n^2 + (n+\lambda)^2] + 2\lambda(n+\lambda)v^3 - \lambda^2 = 0. \tag{3.40}$$

The quantity $\lambda(n+\lambda)$ is always positive [8]. It depends on the combined values of λ and n. They result both positive in case of observations of external Earth orbit object. On the other hand, they result both negative if we observe an inner Earth orbit object. This equation provides eight different solutions and with the help of the theorem of Cartesius about the equations roots, the following results can be proved :
• two real positive roots,
• one real negative root,
• one root equal to unit (Earth solution),
• four imaginary roots.
Only two of them need to be considered: the real positive ones.
The condition for finding two solutions is the following:

$$1 - 3n\lambda > 0, \tag{3.41}$$

according to (3.38) and (3.39) it's possible to obtain the expressions for n and λ:

$$\begin{aligned} n &= \frac{v^2 - 1 - u^2}{2u}, \\ \lambda &= \frac{u}{1 - \frac{1}{v^3}}. \end{aligned} \tag{3.42}$$

Substituting these values into (3.41) , the inequality condition becomes:

$$1 > \frac{v^2 - 1 - u^2}{2} \cdot \frac{3}{1 - \frac{1}{v^3}}. \tag{3.43}$$

This last relation divides the space of the solutions into different regions bounded by two surfaces, a sphere and a curve:

$$\begin{aligned} u &= 1, \\ u^2 &= v^2 + \frac{2}{3v^3} - \frac{5}{3}, \end{aligned} \tag{3.44}$$

which are surfaces of revolution with the radius Earth-Sun as axis of symmetry. Figure 3.1 gives an idea of these areas and the relative positions of Sun, Earth and object. The possibility to find more than one solution does not depend on the Earth's position only but on the complete configuration. In B and D regions we find only one solution (except the Earth's one), while in A and C regions there are double solutions therefore it's necessary to choose the correct one in order to define a proper orbit. This theory doesn't work if we do not assume geocentric observations. Milani, Gronchi et al. [4] developed a theory for this situation and found that the number of preliminary orbit solutions can be larger than in Charlier's theory. Recalling the form of the *Gauss-Lagrange equation* we can easily apply this theory to the Gauss problem of orbit determination and find one or two solutions depending on the configuration of the bodies.

3.3.2 Search for multiple solutions

In order to prove the validity of Charlier's theory also on Casotto's method we tested our data on a numerical grid. Each node of the grid corresponds to a six-dimensional vector formed by three geocentric distances and three sector-to-triangle ratios as (3.26). The idea was to use these vectors as input to solve the non-linear system (3.25). The technique used to analyze the problem is the following.

First we generated artificial data in order to produce observations both in conjunction and opposition configurations and hence to work in a controlled environment. In real situations in fact it is obvious to get observations only when the bodies are in proximity of opposition. We used also conjunction data in order to prove the validity of the theory in its entirety. This observations were entered to solve the non-linear system and a first solution was found. After that six loops one inside the other were generated, each referred to a system variable. The variation intervals for the unknowns were chosen in a reasonable way in order to neglect unsuitable values. We substituted the vector thus created in the system and we selected the ones for which the system was verified or was close to be. Those vectors were finally used as

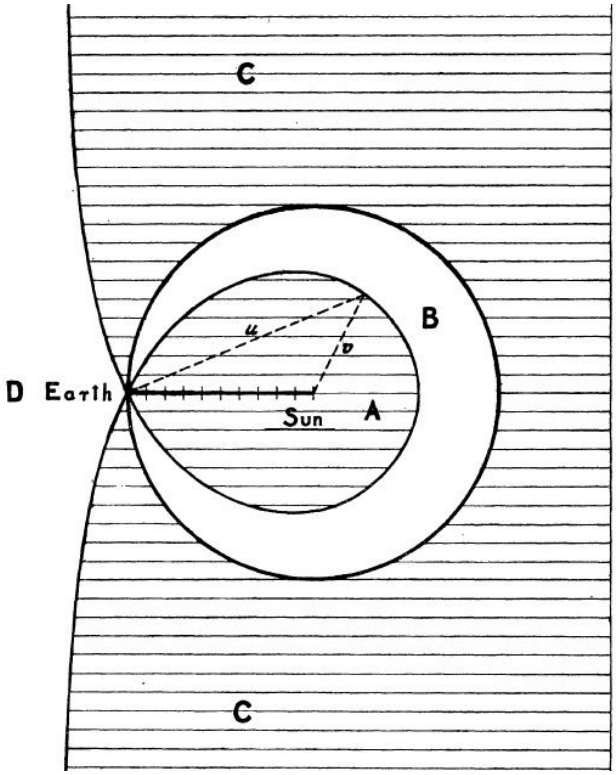

Figure 3.1: The multiplicity of the solutions depends on the relative positions of the Earth, the Sun and the object. The letters A and C mark the areas in which is possible to find two different solutions of the problem which lead to two different orbits. The letters B and D on the other hand mark the regions in which one unique solution is found [8].

input to solve the non-linear system. In this way we avoid the possibility of non convergence of numerical methods and reduced the running time of the program, restricting the use of the Matlab routine `fsolve` to those cases in which the input vector is rather near to a solution. In fact the method requires an initial value close to the solution to converge. At last we found all the possible solutions of the non-linear system. For the tests we used a sample of asteroids that included Earth inner orbits and Earth outer orbits in different configurations.

As we can see from the table 3.1 the results confirm Charlier's theory: we found two or three solutions depending on the configurations expected from the theory. Moreover we notice that one solution corresponds to the Earth orbit.

The selection intervals

In order to optimize the algorithm we chose the smallest possible interval for each unknown. The six variables are: the three geocentric distances ρ_1, ρ_2, ρ_3 and the three sector to triangle ratios η_1, η_2, η_3. Clearly the geocentric distances could not be greater than the object heliocentric distance plus one astronomical unit as in conjunction. So the values for ρ_i for $i = 1, 2, 3$, ranged between zero and 3 AU.

The selection of STT ratio interval of values required a more detailed reasoning. The expression for STT ratio is:

$$\eta = \frac{\sqrt{a(1-e^2)}\tau}{r_a r_b \sin f_a - f_b}, \tag{3.45}$$

so we could calculate the variation of η with respect to eccentricity as :

$$\frac{d\eta}{de} = -\frac{ae\tau}{\sqrt{a(1-e^2)}r_a r_b \sin(f_a - f_b)}. \tag{3.46}$$

Entering reasonable interval of values for eccentricity and semi-major axis we obtained a appropriate range for η_i with $i = 1, 2, 3$. We chose $0.07 < e < 0.55$ with lower limit referred to Ceres and upper to a NEO of Amor family, and for semi-major axis $1 < a < 3$ AU. For a time interval between observations of about ten days the STT ratio varied from 0.07 for Ceres to 0.8 for Alinda. We noticed that η increased when the semi-major axis a decreased or the eccentricity e increased, so we set up the following limits for our investigation: $1 < \eta < 1.8$ for bodies with high eccentricity such as NEO and $1 < \eta < 1.1$ for main belt asteroids. The lower limit was one because the sector area could not be less than the triangle area.

Object	**Conf.**	N^o **sol**	ρ_1	ρ_2	ρ_3	η_1	η_2	η_3
Ceres	C	1^o	3.4550	3.3760	3.1985	1.0031	1.0127	1.0032
		2^o	-0.0000	-0.0000	0.0000	1.0442	1.1971	1.0452
		3^o	2.3232	2.3624	2.1509	1.0173	1.0682	1.0161
Ceres	O	1^o	1.7027	1.5819	1.7100	1.0026	1.0105	1.0026
		2^o	-0.0000	-0.0000	-0.0000	1.0475	1.2116	1.0478
Eos	C	1^o	3.6621	3.5659	3.4274	1.0009	1.0039	1.0009
		2^o	0.0000	-0.0000	0.0000	1.0196	1.0809	1.0192
		3^o	2.1488	2.1421	2.0139	1.0095	1.0353	1.0079
Eos	O	1^o	1.7783	1.7466	1.8204	1.0009	1.0038	1.0009
		2^o	-0.0000	-0.0000	0.0000	1.0193	1.0814	1.0197
Aten	C	1^o	1.6913	1.6502	1.6005	1.0057	1.0243	1.0063
		2^o	-0.0000	-0.0000	-0.0000	1.0044	1.0181	1.0044

Table 3.1: Different number of solutions depending on the system configuration. The test was performed for different objects in opposition or conjunction (O or C). The solutions with $\rho = 0$ correspond to the Earth orbit.

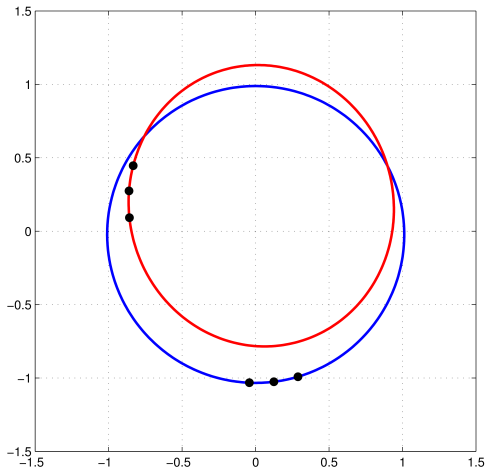

Figure 3.2: In this figure are represented the orbits of the NEO Aten, the red one, and of the Earth, the blue one. The black points are the three synthetic observations chosen in the proximity of conjunction. The x-y plane is the ecliptic plane measured in AU.

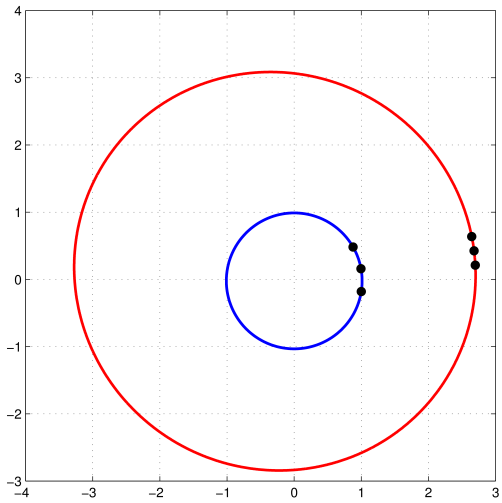

Figure 3.3: In this figure are represented the orbits of the main belt asteroid Eos, the red one, and of the Earth, the blue one. The black points are the three synthetic observations chosen in the proximity of opposition.

3.4 Orbit determination techniques

We present hereafter some examples with the purpose of giving a more extensive look at the problem of the orbit determination. We first consider the case of binary stars, then that of transneptunian objects and finally the case of exoplanets. We will focus especially on those techniques which use astrometric methods to solve the problem and to determine the orbit of the object.

3.4.1 Binary stars

It has long been known that a great part of the stars has a companion and form a binary system. Sometimes it is possible to observe stars accidentally aligned along the line of sight but not physically bounded, which are called *optical* binaries, but they have not any physical interest.

We are concerned with the *physical* binaries which are divided among: *visuals*, when it is possible to optically resolve the two companions, *spectroscopics*, when their double nature is revealed from the study of the relative velocity derived from their emission spectrum, and *photometrics* when the inclination of the system is about 90° and consequently it is possible to measure the variation of luminosity due to the transit of the bodies one in front of the other. It is important to recall some problems that affect the procedure before proceeding with their explanation. The first concerns the

convergences of mathematical methods used to solve non-linear systems or transcendental equations as *Kepler's equation*. Another is about the observational errors which prevent the generation of a well-conditioned system to calculate the orbital parameters especially when the arc is too short [15].

A widely adopted method for the orbit determination of binary stars is the *Kowalskij method*, a geometry based technique [14]. The observation of a binary system offers its projection on the plane tangent to the celestial sphere in the point that is the barycenter of the system itself. This projection has the shape of an ellipse of equation:

$$Ax^2 + 2Bxy + Cy^2 + 2Dx + 2Ey = 1, \tag{3.47}$$

where x and y refer to a coordinates system whose origin is coincident to the primary star and they are oriented respectively toward North and East. If we use polar coordinates we can write:

$$\begin{aligned} x &= \rho\cos\theta, \\ y &= \rho\sin\theta, \end{aligned} \tag{3.48}$$

with ρ distance between the stars and θ the position angle.

In order to compute the five parameters A, B, C, D, E, F in (3.47) and obtain the orbit, five observations are required, each at a different instant of time and then the least square method is applied. We proceed with a change of coordinates passing to the orbital plane with Z axis perpendicular to it and X axis pointing toward the node Ω:

$$\begin{aligned} x &= X\cos\Omega - Y\sin\Omega\cos i + Z\sin\Omega\sin i, \\ y &= X\sin\Omega + Y\cos\Omega\cos i - Z\sin\Omega\cos i, \\ z &= Y\sin i + Z\cos i. \end{aligned} \tag{3.49}$$

Substituting (3.49) into (3.47) we obtain the equation of an ellipse as a function of X, Y, Z. With the same procedure we find another equation for the ellipse this time starting from another reference system lying on the orbital plane and with ξ axis pointing toward pericenter:

$$\begin{aligned} \xi &= X\cos\omega - Y\sin\omega, \\ \eta &= X\sin\omega + Y\cos\omega. \end{aligned} \tag{3.50}$$

We substitute (3.50) into the standard form for the ellipse referred to the center instead of to a focus:

$$\frac{(\xi + ae)^2}{a^2} + \frac{\eta^2}{a^2(1-e^2)} = 1. \tag{3.51}$$

At this point we equate the two different expressions obtained and since they are referred to the same system of coordinates they must coincide identically.

This fact put some constraints which allow to calculate the orbital elements using the parameters previous computed. At the end we have:

$$\begin{aligned}
\tan 2\Omega &= \left[\frac{2(B+DE)}{A-C+D^2-E^2}\right], \\
\tan^2 i &= p^2\frac{-2(B+DE)}{\sin 2\Omega}, \\
\tan^2 i &= p^2(A+C+D^2+E^2)-2, \\
e\cos\omega &= p(D\cos\Omega+E\sin\Omega), \\
e\sin\omega &= p(-D\sin\Omega+E\cos\Omega)\cos i. \qquad (3.52)
\end{aligned}$$

From the first it is straightforward to obtain the longitude of the ascending node Ω, from the second and the third we can get the inclination i and the semi latus-rectum p, and the last two provide the eccentricity e and the pericenter longitude ω. In the end it is simple to calculate the semi-major axis a remembering the relation $p = a(1-e^2)$. The time elements as the revolution period P and the perihelion passage T are determined next.

Recalling the geometry of the system it is simple to define the following relation between angles:

$$\tan(\theta-\Omega) = \tan(\omega+\nu)\cos i. \qquad (3.53)$$

Therefore, knowing the value of θ which is the longitude of the secondary star in the orbital coordinate system, we can easily obtain the true anomaly f. This is necessary to determine the eccentric anomaly E:

$$E = 2\tan^{-1}\left[\sqrt{\frac{1-e}{1+e}}\tan(\frac{f}{2})\right], \qquad (3.54)$$

and the main anomaly M from Kepler's equation:

$$M = E - e\sin E. \qquad (3.55)$$

We know that the mean anomaly is related with the period and the time perihelion passage T by the equation:

$$M = \frac{2\pi}{P}(t-T), \qquad (3.56)$$

which is solvable with the aid of the relation below that requires values from two different observations:

$$T = \frac{M_1 t_2 - M_2 t_1}{M_1 - M_2}. \qquad (3.57)$$

In this way the period P and the perihelion passage time T are determined.

Starting from the same assumptions, Asada et al. [17] obtain the apparent parameters of (3.47) with the least square method and then apply two transformations, one rotation and one translation:

$$\begin{pmatrix} x \\ y \end{pmatrix} = \begin{pmatrix} \cos\Omega & \sin\Omega \\ -\sin\Omega & \cos\Omega \end{pmatrix} \begin{pmatrix} \bar{x}+\rho \\ \bar{y}+\sigma \end{pmatrix},$$

instead of the two rotation used in the previous procedure. The barred variables correspond to the equatorial coordinates and the new parameters appearing are defined by:

$$\begin{pmatrix} \rho \\ \sigma \end{pmatrix} = \begin{pmatrix} A & B \\ B & C \end{pmatrix}^{-1} \begin{pmatrix} D \\ E \end{pmatrix}.$$

After the appropriate transformation we find the expressions for orbital elements.

An improvement of the Kowalskij method is presented by Olevic and Cvetkovic [16] who named their algorithm KOVOLE just in honor of the inventor. The change consists in the possibility to consider short arcs and to solve the orbital problem with success because the errors result quite small.

As we have previously anticipated, there are other important methods to compute the orbits of binary stars, for completeness we give an idea of these methods without examining the procedure in the details, providing the fundamental references. Spectroscopy is a powerful tool to study binary systems, in fact it allows to calculate the relative velocity of a star with respect to the other by the Doppler effect. A limit is imposed by the geometry of the observation. In fact we are able to see only the projection of the motion on the plane tangent to the line of sight, therefore it is impossible to determine both inclination and semi-major axis independently. The result will always be connected in terms of the product $a \sin i$.

If the spectra of both stars are are available we get information also about the mass ratio, through the following relation:

$$\frac{a_1}{a_2} = \frac{\mu_2}{\mu_1} = \frac{v_1}{v_2}. \tag{3.58}$$

If we are in the particular case in which the inclination of the binary system is close to 90° a different method is applicable. The study of the star eclipses is a suitable technique because of it gives the possibility to study also faint stars and requires smaller telescope than those used for spectroscopy, therefore the cost is reduced. Depending on the type of light curve a different star configuration is defined, for example a total eclipse or a partial eclipse. Also this time there is a limit imposed by the geometry that connects two elements, the node longitude Ω and the argument of pericenter ω which remain undetermined.

3.4.2 Transneptunian objects

The orbit determination methods applied to the TNOs are different from those used for the main belt asteroids or other small bodies of the Solar System. Nowadays the researches and the increasing discoveries of Kuiper belt objects require new techniques to analyze and predict their orbits.

The fact is that TNOs are so distant from the Earth that their motions appear approximately linear. This makes the classical methods unable to operate, because they are based on the measure of the curvature of the orbit that is impossible to detect in this case. Transneptunian objects pose particular problems also because they are faint and recovery observations are quite costly, requiring the investment of 2-4 meters telescopes.

To obtain images of TNOs, typically 3-5 frames are taken in 2 hours between the first and the last observation, this sequence is called *Very Short Arc*. The arcs too short for a full orbit determination are called *Too Short Arc* (TSA). In these cases the computational algorithm based on the Gauss method fails because, as we know, the smaller is the curvature, the less accurate is the orbit. On the other hand, if the survey were to use longer intervals between the observations, the curvature of the observed arc would be significant and this would complicate the algorithm to detect from one frame to another the moving images of the same object because it could escape from the field of view [5].

In order to avoid this problem the methods for orbit determination are based on a wide statistics of the observation uncertainties. In fact, the problem of uncertainties becomes particularly important if we treat short arcs and it is closely linked to the recovery and the tracking of these distant objects. Generally we can say that a short arc will lead to huge errors and that a long arc will have high accuracy, but it is necessary to compute the errors to be sure about the precision of the orbit. The MPC, for example, does not provide uncertainties on positions and orbital elements. Its approach to short arcs is to select the simplest orbit that fits the data assuming that it is most likely to resemble those of known objects. In this way it removes the degeneracies but it causes a bias against objects that actually are on unusual orbits and their dynamical classification [20].

There are several ways of computing ephemeris uncertainties. The *JPL Horizon system* uses a covariance matrix method that works beautifully for small and medium uncertainties. Both the *OrbFit* [1] software of the University of Pisa and *FindOrb* by Project Pluto [2] use the Monte Carlo method.

These software create synthetic observations at specific dates by adding gaussian deviations to the true positions (a sort of "noise"). Then an orbit is fitted to the synthetic observations. This process creates a so-called "virtual

[1] hamilton.dm.unipi.it/astdys/
[2] www.projectpluto.com/

asteroid" which represents a possible orbit that fits the synthetic observations. If the process is repeated, at the end we will have a lot of virtual

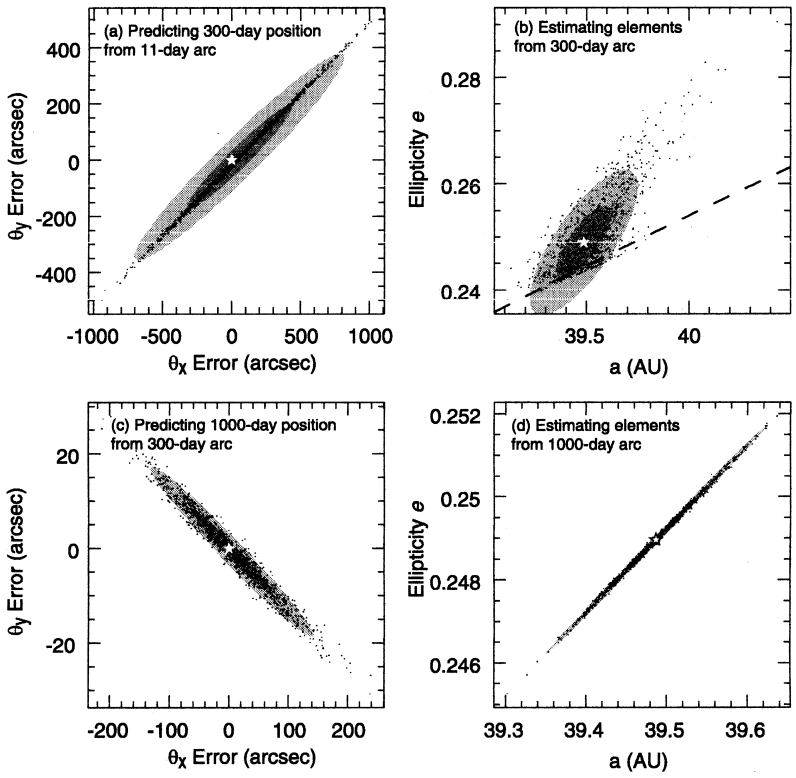

Figure 3.4: Demonstration of propagation of errors in positions and orbital elements for Pluto.(a) Position errors for a 300 days prediction obtained from 4 observations chosen among a 11 days arc. The two ellipse shaded corresponds to 1 σ and 3 σ uncertainty regions. (b) Uncertainties on "a-e" plane obtained from 1000 observations of a 300 days arc. (c) Position errors resulting for a 1000 days prediction from 300 days arc. (d) The same as (b) but for 6 observations from 1000 days arc. [20]

asteroids that illustrate the region in which the real asteroid might actually be. This region has the form of an ellipse, instead the virtual asteroids seem to form a sort of globular cluster. As shown in figure 3.4 by Bernstein and Khushalani [20] the orbit prediction results much more accurate if the arc considered is long both in terms of positions and orbital elements.

Another method proposed by Virtanen et al. is the "Statistical orbital Ranging". It can be used even if only two observations and it is has proven to be a very powerful computational tool for sparsely observed objects and very short arcs. A deviation in right ascension (R.A.) and declination (Dec.) are introduced and the corresponding topocentric distances are assumed. At the

end a trial orbit is computed and compared to all observations. If the orbit fits the observations to some predefined accuracy it is added to a sample of possible orbits. The a priori probability density function (PDF) is mapped with a large set of sample orbits each associated with a weight proportional to R.A. and Dec. residuals. Figure 3.5 shows an example of probability

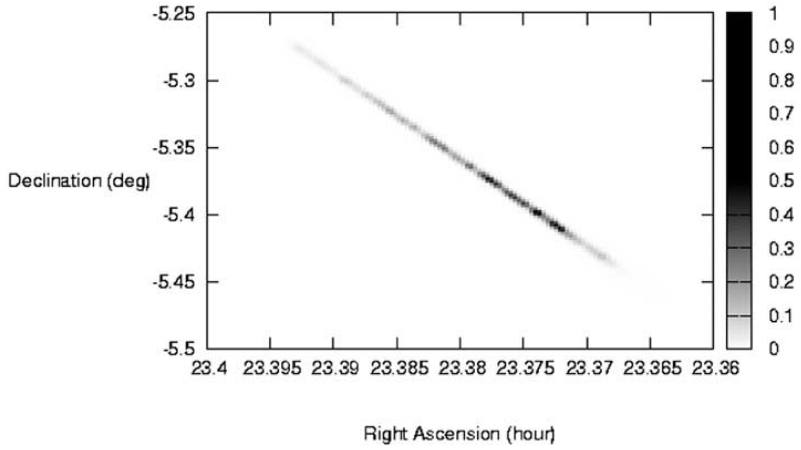

Figure 3.5: Ephemeris probability density function for 2001 QE_{298}. The object was observed in the area where the probability peaks. [22]

density function for $2001QE_{298}$. Moreover, noting that semi-major axis, eccentricity and inclination are highly correlated with positions it is possible to impose reasonable limits to these orbital elements and thus to reduce the research region. This method is used by TNOEPH: transneptunian object ephemeris service [22]. It is a web service for ephemeris uncertainties predictions and dynamical classification of short arc TNOs. A constraint on the observing schedule is that the positional uncertainty must not be larger than the field of view. In the near future the service will offer rigorous solutions also for long arc objects [21].

The method of Virtanen et al. differs from the one proposed by Milani et al., in fact they assume the observation of two angles and two angular rates at the same time, instead of assuming the observation of two angles at two different epochs. In this technique a TSA is represented by a reference time, two average angular coordinates and two corresponding angular rates for the reference time. These information about a too short arc are collected into a vector called attributable. Then an admissible region is selected, defined by the values of geocentric range r and the range-rate $\dot{r}$ which are respectively the distance between the object and the Earth and the time derivative of the distance between the object and the Earth, measured by the Doppler shift. Each point of this region corresponds to a full set of six initial conditions for the asteroid orbit that is finally calculated using a triangulation [5].

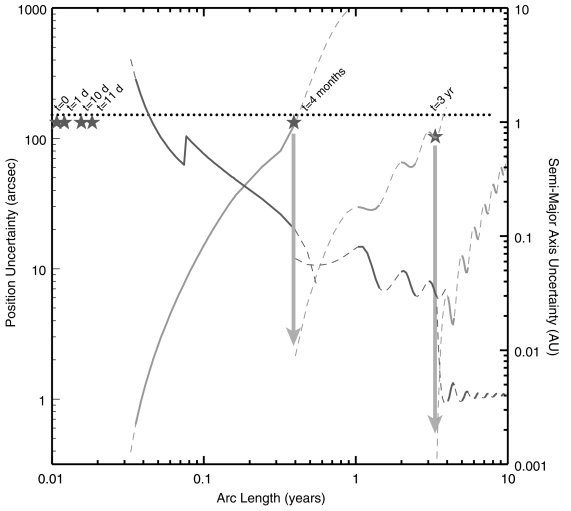

Figure 3.6: Observation optimization. The upward-sloping lines depict the uncertainty in position while the downward-sloping lines show the uncertainty on a.The stars are the observations. [20]

Another important improvement in this area consists in how to maximize some measures of the accuracy of TNOs orbit while minimizing the number of recovery observations required. Concerning this, Bernstein and Khushalani have applied a study proposed in Figure 3.6. It is clear that if a new observation is made before an appropriate interval of time the uncertainty on the semi-major axis will decrease.

As an example of TNOs research and studies we introduce the Nasa's New Horizons mission. The spacecraft was lunched in 2006 and is intended to approach Pluto in July 2015. Its main goals are the study of Pluto's atmosphere and surface: the planetary science community want to know the composition and the behavior of its atmosphere and its geological structure. After the flyby of the dwarf planet New Horizon will visit one or more Kuiper Belt Objects. The Hubble Space Telescope will scan an area of sky in the direction of the constellation Sagittarius to identify any object orbiting within the Kuiper Belt. To search for a suitable candidate the Hubble telescope will need a lot of observing time and to discriminate between a foreground KBO and the background stars. The spacecraft will turn at the predicted rate that KBOs are moving against the background stars. In the resulting images, the stars will be streaked, but any KBOs should appear as pinpoint objects. If New Horizon is able to select a suitable target it will be the first mission to approach an Outer Solar System object. This is just one example of the importance of orbit determination, in fact only an accurate examination of the object trajectory can make possible this fascinating goal.

3.4.3 Exoplanetary systems

The methods used to detect extrasolar planets are, in principle the same used to detect binary stars. They are based on the measurement of the radial velocity through spectroscopic techniques, on the transit photometry, on the astrometric measures, or on other special techniques. Unfortunately, if the methods adopted for extrasolar planets and binary stars can be considered to be qualitatively the same, a boundary is imposed by some quantitative features. In fact, the extrasolar planets are faint objects with respect to their stars, moreover they are very far from the Earth and their angular distances from the stars is too small to be easily revealed with the actual instrumentations. In order to avoid these problems, the use of the highest resolution instrumentation is required. Since the last years the method of radial velocity was responsible of the greater number of discoveries, but nowadays the method of transits has become the most efficient technique, discovering about 800 exo-planets in 2014 [24].

All these methods lead to the determination of orbital parameters of the planets in different ways and with different constraints. For example, the fundamental expression of the radial velocity method is:

$$K = \frac{m_p \sin i}{(m_s + m_p)^{2/3}} \sqrt{\frac{2\pi G}{P}} \frac{1}{\sqrt{1-e^2}}, \tag{3.59}$$

where K is the semi-amplitude of the radial velocity variation, P is the orbital period, e the eccentricity and m_s the mass of the star. All these quantities are known from the observations or through independent measurements, as for the mass of the star, so it is possible to derive $m_p \sin i$ which provides a lower limit at the value of the mass of the planet but cannot provide the precise value. This is a very efficient method in the case of planets in short-period orbits close to the stars [24]. Balan and Lahav in 2008 [25] developed a software called ExoFit which is able to estimate the orbital parameters of extra-solar planets using a Bayesian Markov Chain Monte Carlo (MCMC) method to fit a Keplerian radial velocity curve onto the radial velocity data.

The method of transit photometry is based on the decreasing of the luminosity of a star when a planet transit in front of it on the light of sight. In this way it is possible to obtain the planet radius r_p, the period P, the semi-major axis a from the third Kepler's law and the inclination i that must be about 90°. If this technique is combined with the previous, it is possible to compute also the mass of the planet m_p using the inclination thus obtained.

The astrometric technique, which measures the change of the projected position of the star in the plane of the sky. The amplitude of this angular shift is:

$$\Delta\theta = \frac{a}{d}, \tag{3.60}$$

where a is the semi-major axis and d the distance of the star from the Earth. Since the astrometric method measures two components of the star's motion, it has the potential of determining all parameters and the mass of the planet [24]. Nevertheless the quantity $\Delta\theta$ is so small that a precision of the order of μas are required. In the near future the new interferometric instrumentation and the astrometric space missions will enable to carry out astrometric measurements accurate enough to detect extrasolar planets and to determine all their parameters [24].

Chapter 4

Application to asteroid and TNO observations

In this chapter we focus on the applications of three methods for initial orbit determination to real observations: the Gauss method, the Neutsch method and the Casotto method. These methods were tested on real observations referred to several objects among asteroids, near Earth objects and transneptunian objects chosen in order to have a significant sample.

A great part of the work concerned the implementation of the algorithms of the three techniques. Each method required the same input, three visual observations and through different procedures provided object's dynamical state both in terms of Cartesian components and orbital elements The results allowed to compute a first prediction of the object's motion, the computed ephemeris depending on the propagation model adopted. In order to obtain a more realistic propagation we used a Three-Body Problem model considering the perturbations generated by Jupiter, the planet that more affects the Solar System objects' motions. We neglected the Mars perturbations because they are too small to be revealed in the observations given the accuracies of the telescopes.

The preliminary orbits thus obtained were compared with the final orbits provided by JPL. The differences between the two were strictly linked with the errors due to the observations. Therefore, to estimate the variation of the orbital elements due to these observational errors we associated to the three initial observations a population of synthetic, normally distributed observations. Next we applied the preliminary orbit determination methods to all the possible sets of three observations, one for each epoch. Then, the orbits obtained were compared with that determined from the real observations. Finally, to prove the possibility to recover the same object night after night we calculated the mean motion with respect to Earth. In the end we produced several plots in order to illustrate the behavior of some asteroids among the many selected for the tests.

4.1 Implementation of the algorithms

The algorithms were developed in the Matlab programming language. The reliability of the programs was first tested on fictitious, or synthetically generated data, then we proceeded with the application to real data, provided by the *Minor Planet Center* database.

All methods accept the same three sets of input data:

- geocentric equatorial coordinates of the three observations, right ascension and declination: (α_i, δ_i), $i = 1, 2, 3$,
- instants of time at which the observations are carried out: t_1, t_2, t_3,
- the Earth positions at the same times: $\mathbf{R}_1, \mathbf{R}_2, \mathbf{R}_3$ provided by catalogs,

and provide the same output:

- three position vectors $\mathbf{r}_i$, $i = 1, 2, 3$, corresponding to the three observations,
- the orbital elements $a, e, i, \omega, \Omega, M(t_i)$ of the object.

A brief comparison of the methods shows that the first one is the most complicated. It consists in an iterative procedure and includes the use of two fundamental equations: the eighth-order Gauss-Lagrange equation and the Gauss equation.

The Neutsch method is also iterative. To initialize the problem an initial orbit guess is necessary, which is in generally enough to take as a circular orbit with a reasonable semi-major axis and the program generally converges.

At last Gauss method as modified by Casotto is non-iterative and suggests a more straightforward process. It solves a non-linear system of six equations in six unknowns derived from the study of Gauss equations already defined in chapter 2.

In the following we provide the detailed procedures and the flow charts of the three methods.

4.1.1 The Gauss-Montenbruck algorithm

The first algorithm is the Montenbruck's version of the Gauss method based on the works of Bucerius in the 1950s [7] [6]. It is based on the following scheme, described in the flow chart in Figure 4.1:

1. Compute the object geocentric unit vectors (2.2) starting from the observation and the Earth position vector.
2. Set the initial values for μ_{10}, μ_{30}, n_{30} and n_{30} introduced in Section 2.3, (they will change every iteration).

3. Repeat the steps (a)...(f) until the value of the geocentric distance of the object ρ does not change significantly anymore.
   (a) Compute the initial value of ρ_0 and σ and then solve the Gauss-Lagrangian equation (2.63).
   (b) Use the value r_2 just obtained to calculate improved triangle-areas ratio values n_1 and n_3 introduced in (2.54).
   (c) Compute the new geocentric distances ρ_i for the object and with them the geocentric position vectors $\mathbf{r}_i$ defined in (2.10).
   (d) Compute the sector-to-triangle ratios η_i, $i = 1, 2, 3$, from (2.44).
   (e) Use μ_i to compute improved values μ_1 e μ_3.
   (f) Update ρ_0 as by setting it equal to ρ_2.
4. Compute the orbital elements from the last value of $\mathbf{r}_1$ and $\mathbf{r}_3$.

4.1.2 The Neutsch algorithm

Using the same starting data of the previous section, proceed to the following computational steps that are illustrate in Table 4.2:

1. Define an initial orbit with reliable values (a circular orbit is in generally sufficient).
2. Repeat the next steps until convergence:
   (a) Compute the Lagrange coefficients F e G with (3.5).
   (b) Solve the linear system (3.7) with initial state vector $\mathbf{x} = (x_0 \;\; y_0 \;\; z_0 \;\; \dot{x}_0 \;\; \dot{y}_0 \;\; \dot{z}_0)$.
   (c) Compute the Keplerian elements from the cartesian elements.

4.1.3 The Gauss-Casotto algorithm

Referring to the flow chart in Table 4.3, the procedure consist in the following steps:

1. Define initial geocentric distance ρ_{0i} and initial heliocentric distance of the object r_{0i}.
2. Compute the auxiliary variables m_i and l_i, $i = 1, 2, 3$, with the expressions in (3.23).
3. Define initial approximation for STT ratio with the *first equation of Gauss* (2.27).
4. Solve the non-linear system (3.25).

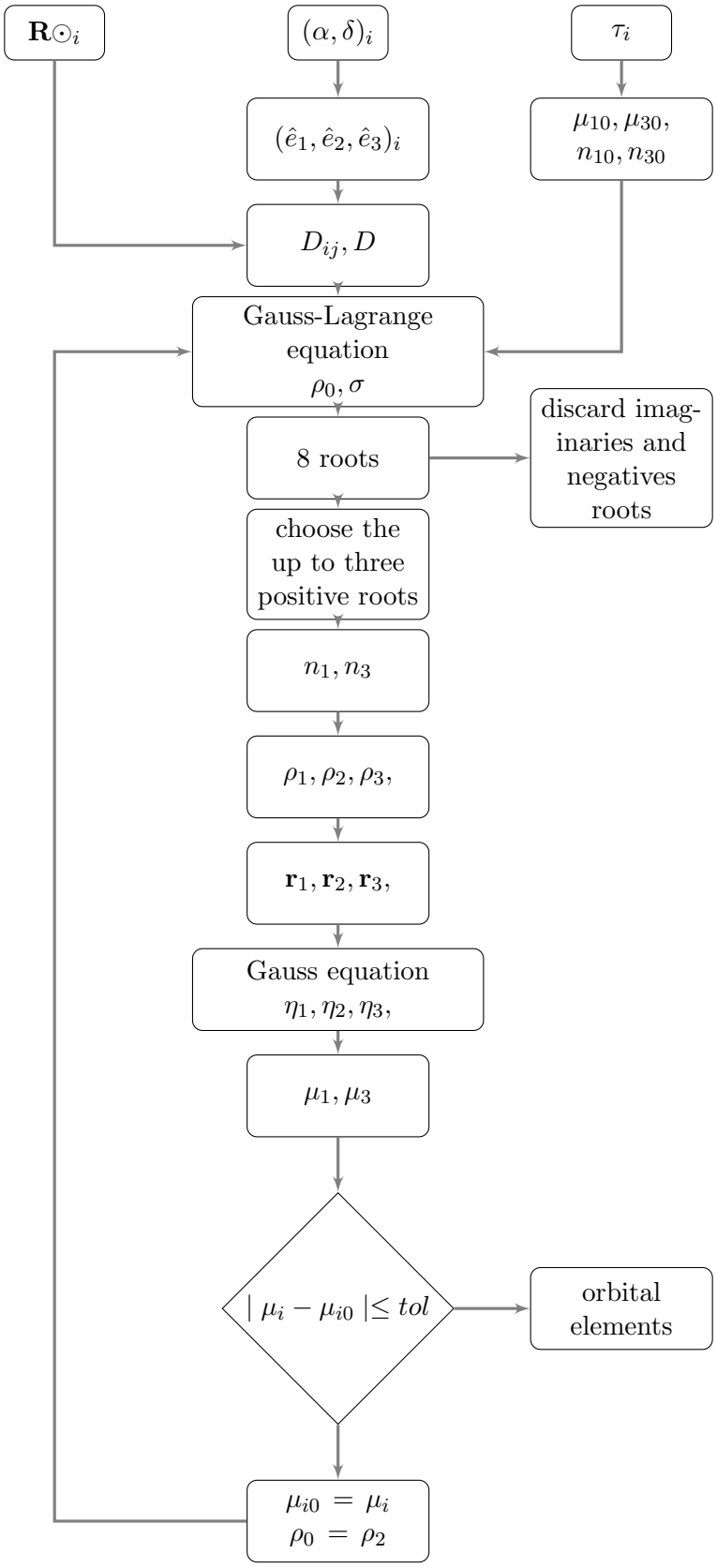

Table 4.1: Flow chart of the Gauss-Montenbruck algorithm.

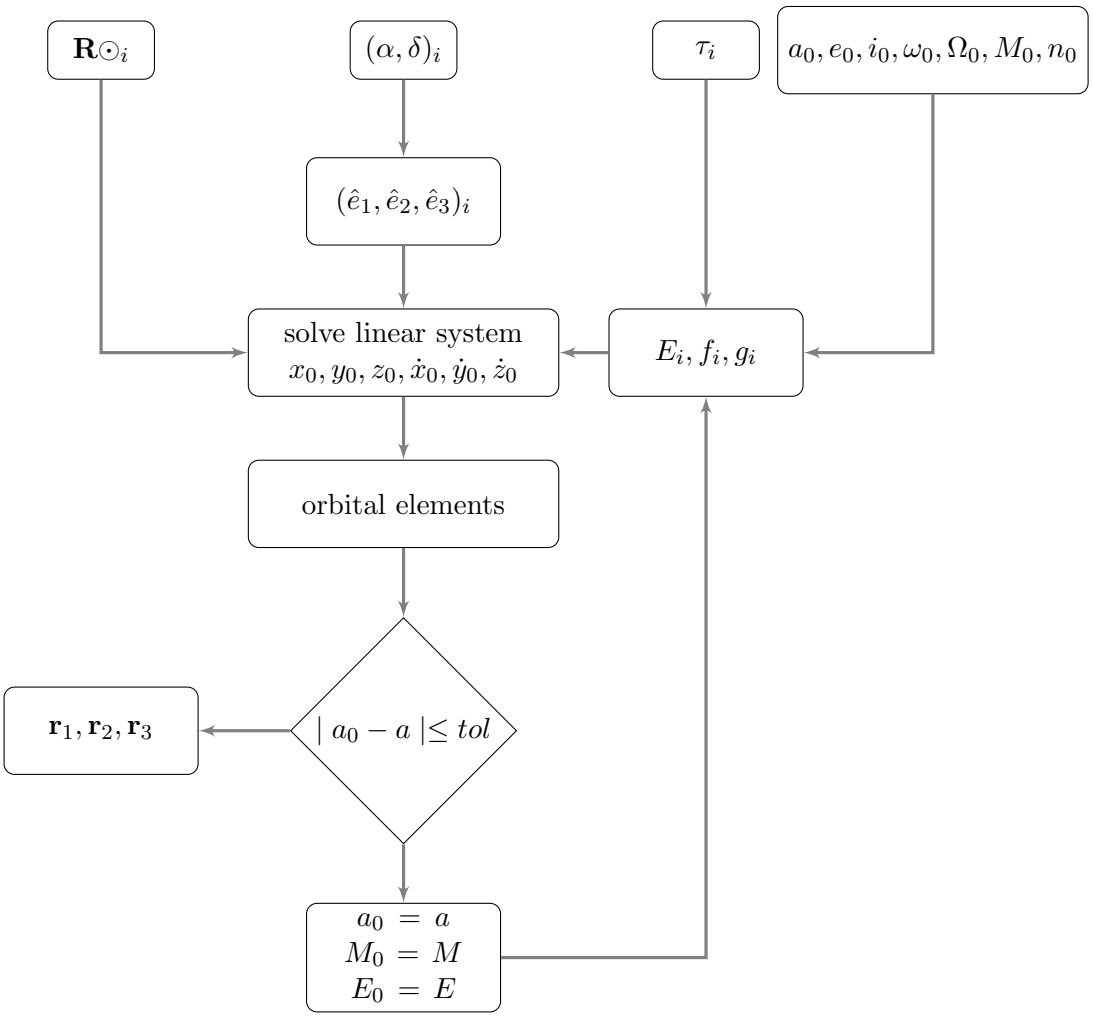

Table 4.2: Flow chart of the Neutsch algorithm.

5. Derive the position vectors $\mathbf{r_1}, \mathbf{r_2}, \mathbf{r_3}$.

6. Compute the orbital elements.

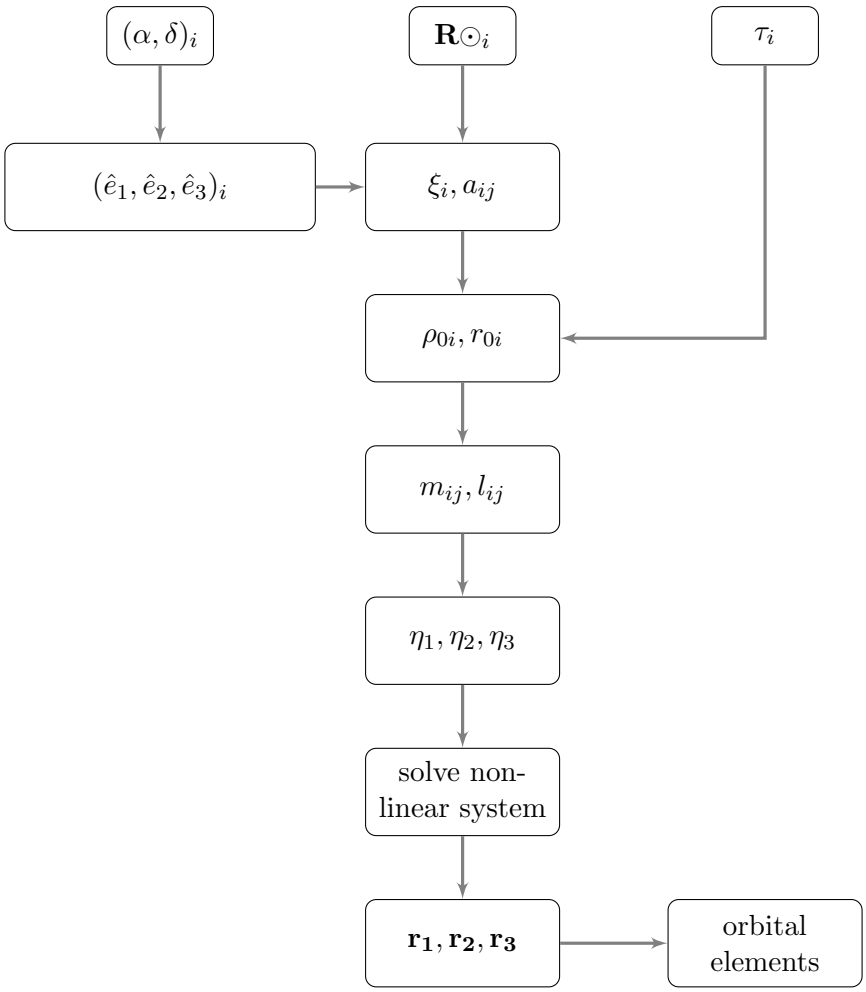

Table 4.3: Flow chart of the Gauss-Casotto algorithm.

4.1.4 Code development

We provide a list of the principal programs developed for the solution of the initial orbit determination problem. Some of them are used in different main programs.

- `Gauss Method`. The program solves the initial orbit determination problem with the Gauss method. The input and output are described in section 4.1.1.

- `Neutsch_Method`. The program solves the initial orbit determination problem with the Neutsch method.
- `Casotto Method`. The program solves the initial orbit determination problem with the Casotto method.
- `Gauss_Lagrange_equation`. A function that solves the Gauss-Lagrange equation required in the comprehensive Gauss method.
  - *Input*: the geocentric distance ρ_0 of the object at the time of the second observation. The parameters σ and γ.
  - *Output*: the value of the heliocentric distance r_2 of the object at the time of the second observation.
- `Gauss_equation`. A function that solves the Gauss equation.
  - *Input*: the three heliocentric position vectors $\mathbf{r}_1$, $\mathbf{r}_2$, $\mathbf{r}_3$.
  - *Output*: the three *Sector-to-triangle ratios* η_1, η_2, η_3.
- `elements_from_two_positions`. A function that determines the orbital elements starting from two position vectors.
  - *Input*: two heliocentric position vectors $\mathbf{r}_i$, $i = 1, 2$.
  - *Output*: the six orbital elements.
- `elements_from_state_vector`. A function that determines the orbital elements starting from the state vector of an object.
  - *Input*: one state vectors $\mathbf{x} = (\mathbf{r}, \mathbf{v})$.
  - *Output*: the six orbital elements.
- `orbit_plot`. The program generates the plots of the orbit propagation of the Earth and the object.
  - *Input*: The state vector $\mathbf{r}$ corresponding to the first observation, the state vector of the Earth $\mathbf{R}$ and of Jupiter at the same date.
  - *Output*: Plot of Earth and object orbits.
- `Keplerian_motion_3D`. The equation of Two-Body motion perturbed by Jupiter required for the orbit integration.
  - *Input*: The initial state vector $\mathbf{r}$ of the object and the initial state vector of Jupiter at the date required.
  - *Output*: State vectors at each instant in the period of integration .

- `mean_motion`. The function computes the mean motion of the object with respect to Earth.
  - *Input*: Position vector **r** and velocity **v** of the object and the ones of the Earth.
  - *Output*: Mean motion n with respect to Earth.
- `error_angles`. The function computes the angular distance seen from Earth between the preliminary orbit and the real one day by day.
  - *Input*: Position of the Earth and position of the object.
  - *Output*: Angular error θ at intervals of 10 days.
- `Main_errors`. A program to generate the synthetic observations starting from a normal distribution of errors and to evaluate the variation in orbital elements due to them.
  - *Input*: The three observations and the error deviation in right ascension σ_α and declination σ_δ.
  - *Output*: The errors in orbital elements.
- `Plot`. A program to generate plots.
  - *Input*: The three observations, the state vector of Jupiter, the state vector of the Earth and the true orbital elements of the object.
  - *Output*: The plots of comparison between true and preliminary orbital elements, the plots of the residuals of the Cartesian state and the plots of the mean motion with respect to Earth.

4.1.5 Algorithm running times

To compare the efficiency of the three methods we computed their running time. We selected the central part of the algorithms, that included their computational core excluding the input-output operations. The initial conditions are the same for the three algorithms. For Gauss-Montenbruck and Gauss-Casotto we used the zeroth order, i.e the Bouguer formulas to initialize the problem. To increase the timing accuracy, the process was rerun over 1000 cycles. The resulting execution times are displayed in Table 4.4.

Clearly the difference in running time between the methods is of about one order of magnitude. The Gauss-Montenbruck method is the slowest as expected because of its complexity. The fastest one is the Neutsch method, but it depends on the initial orbit choice. In fact it is not always possible to suppose an orbit close to the real one and to ensure the method's

Method	Ceres	Apophis	393136	393309	263013	Quaoar
Gauss-Montenbruck	0.26846	0.89379	0.48164	0.29343	0.22132	0.06851
Neutsch	0.00664	0.02373	0.01033	0.00762	0.00552	0.00276
Gauss-Casotto	0.03545	0.14994	0.04903	0.03986	0.04085	0.03624

Table 4.4: Running times in seconds for different objects.

convergence. The last is the best compromise between running time and robustness. The great part of the time is used to solve the non-linear system with the Matlab routine `fsolve`. In principle the running time of initial orbit determination is not a problem because of the power of modern computers.

4.2 Computation of preliminary orbits

4.2.1 Pre-processing

The observational data we used as input to solve the initial orbit determination problem were obtained from the *Minor Planet Center*[1] in the form of equatorial coordinates in the Earth-centered reference system J2000 at the standard epoch J2000.0 (12:00 UT on 1 January 2000). This coordinate frame is defined with the $x-y$ plane lying on the celestial equator with the x-axis aligned with the mean equinox of J2000.0 and the z-axis pointing the North Pole. These data are available already corrected for various geometrical and physical effects according to standard procedures [18]. The observations of a Solar System body, in fact, refer to the object as seen from the Earth, thus affected by atmosphere's refraction, Earth's motion and other effects. It is necessary to clean these effects in order to obtain available *geometrical observations*.

The ephemeris predictions used to compare preliminary orbits with the final orbit are provided by the JPL on-line service *HORIZONS*[2]. They are available in the form of osculating orbital elements, or Cartesian vectors, which consist of position, velocity and acceleration. The most recent and highly accurate set of ephemeris is the DE430 generated in April 2013.They are created by fitting numerically integrated orbits of the Moon and planets to observations and they include the perturbations generated by 343 asteroids which represent 90% of the total mass of the main belt [19].

[1] www.minorplanetcenter.net
[2] ssd.jpl.nasa.gov

4.2.2 IOD computations: the case of Ceres

In this section we explain the actual results of this work. First of all we present the preliminary orbits obtained and a comparison with the more accurate ones provided by JPL.

We tested the algorithms on several asteroids belonging to different families or groups in order to have a wide sample on which to base the evaluation of the methods. The results of the algorithms are the heliocentric positions vectors which lead to an approximation of the orbital elements. The position vectors are compatible within a precision of 10^{-12} AU. In Table 4.6 we exhibit an example of preliminary orbital elements at different dates for Ceres while Table 4.7 shows the state vectors at the same epochs. The observations which they refer are shown in Table 4.5. The table containing all the examined asteroids is located at the end of the chapter.

Asteroid	**Date (UT)**	$\alpha(h)$	$\delta(^\circ)$
	1999 01 06.17747	03 51 31.230	+18 37 42.80
	1999 01 25.80330	03 50 03.710	+19 44 50.80
	1999 02 01.10758	03 51 53.232	+20 10 39.23
	2003 09 20.49289	07 00 39.031	+23 08 40.55
Ceres	2003 09 29.45717	07 12 05.950	+23 14 24.30
	2003 10 22.54200	07 36 27.706	+23 38 46.82
	2005 06 03.23041	14 51 41.242	-08 51 06.86
	2005 06 15.19336	14 45 29.496	-09 25 07.67
	2005 06 30.15039	14 42 36.537	-10 27 52.33

Table 4.5: The table shows the observations for Ceres and their corresponding date in UT.

Asteroid	**Date (UT)**	$a(AU)$	e	$i(^\circ)$
		$\omega(^\circ)$	$\Omega(^\circ)$	$M(^\circ)$
		2.7698	0.0807	10.6592
	1999 01 06.17747	75.9422	78.1987	-70.4435
		2.7816	0.0802	10.6619
Ceres	2003 09 20.49289	73.0283	78.2013	-59.8802
		2.7653	0.0800	10.6690
	2005 06 03.23041	75.4892	78.1033	70.9582

Table 4.6: The table shows the orbital elements derived from the observations using the three methods.

Date (UT)	x	y	z
	$\dot{x}$	$\dot{y}$	$\dot{z}$
1999 01 06.17747	0.7121487149867	2.6160801305031	-0.0428239512416
	-0.0101916088009	0.0019530097432	0.0019433003433
2003 09 20.49289	0.3303118469692	2.6633416389899	0.0290962790406
	-0.0104933076408	0.0005036419901	0.0019504465289
2005 06 03.23041	-1.5935977176754	-2.1803041082254	0.2193330018642
	0.0078153594519	-0.0068968532716	-0.0016757752997

Table 4.7: The table shows the state vectors derived from the observations using the three methods.

4.2.3 Propagation of the orbit within the Three-Body Problem framework

Using the state vector defined by positions and velocities as initial conditions it was possible to calculate the propagation of the orbit by integrating the equations of motions within the framework of the Three-Body Problem. The propagated orbit are shown Figure 4.1. In the Solar System the Sun is the main center of attraction while all the other bodies can be considered as perturbing bodies. The equations of motion that we adopt are:

$$\ddot{\mathbf{r}}_i + G(m_S + m_i)\frac{\mathbf{r}_i}{r_i^3} = \frac{\partial R_i}{\partial \mathbf{r}_i}, \qquad i = 1, 2, \tag{4.1}$$

where the perturbing function R_i is given by:

$$R_i = G\sum_{j=1}^{N-1} m_j\left(\frac{1}{r_{ij}} - \frac{\mathbf{r}_i \cdot \mathbf{r}_j}{r_j^3}\right), \qquad i = 1, 2, \tag{4.2}$$

where N are the number of perturbing bodies. In our case we consider just one perturbing object, Jupiter, so we can write explicitly the equation of motion in the form:

$$\ddot{\mathbf{r}}_A + G(m_S + m_A)\frac{\mathbf{r}_A}{r_A^3} = Gm_J\left(\frac{\mathbf{r}_J - \mathbf{r}_A}{r_{JA}^3} - \frac{\mathbf{r}_J}{r_J^3}\right), \tag{4.3}$$

$$\ddot{\mathbf{r}}_J + G(m_S + m_J)\frac{\mathbf{r}_J}{r_J^3} = Gm_J\left(\frac{\mathbf{r}_A - \mathbf{r}_J}{r_{JA}^3} - \frac{\mathbf{r}_A}{r_A^3}\right), \tag{4.4}$$

where $\mathbf{r}_A$ is the position vector of the asteroid, $\mathbf{r}_J$ is the position vector of Jupiter and m_S, m_A and m_J are respectively the mass of the Sun, the asteroid and Jupiter. The last are the equations of motions of an asteroid and Jupiter in heliocentric coordinates perturbed by each other. In the implemented programs the asteroid mass m_A was neglected.

We considered Jupiter, which causes a perturbation of about 10^{-4} AU on the position vector that corresponds to a detectable variation in the

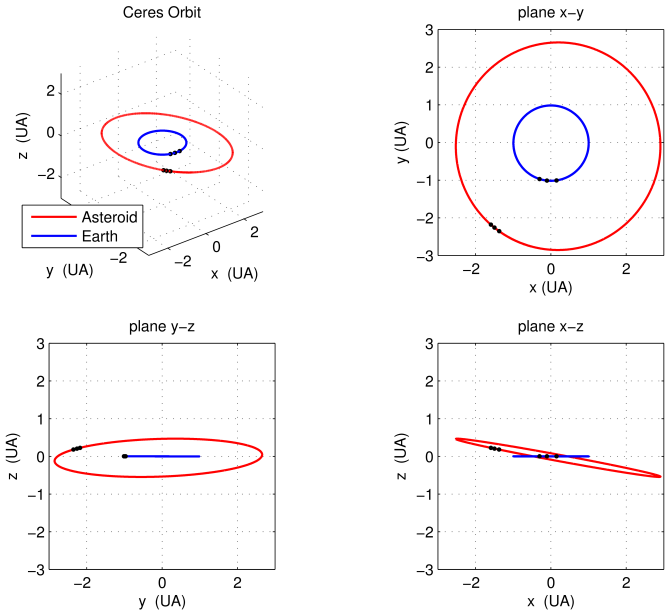

Figure 4.1: Preliminary orbit of Ceres obtained integrating the equation of motion of the Three-Body Problem considering the perturbation of Jupiter.

observations of about $1''$ (for a main belt asteroid). We considered also the perturbations caused by Mars, given its proximity with the main belt asteroids, but its effects on the observations were too small to be detected with a telescope. The variation in the position vector was in fact of the order of 10^{-7} AU.

4.3 Preliminary orbits vs final orbits

In this section we illustrate the comparison between the preliminary orbits obtained in the present analysis and the final orbits provided by the JPL *HORIZONS* system. Several tests were developed in order to evaluate the reliability of the preliminary orbits obtained from three observations with respect to the more accurate JPL orbits. It is important to notice that the IOD results cannot coincide with the more precise of JPL because of several reasons. In the first place we computed the position of the Earth on the basis on ephemeris DE405, while the truth values were obtained from the web service which is based on the DE430 set of ephemeris, which translates in a difference in the state vector of the Earth of about 10^{-4} AU. Another cause of differences is the fact that the JPL ephemeris are computed starting from all the available observations with much more realistic integration models, rather than from only three observations using a Two-Body problem as in

our IOD case. Keeping in mind these important facts we proceeded with the tests. First of all we propagated an ephemeris, then converted it to Keplerian elements, to cover a period of 100 days. Next we compared the resulting with the JPL elements over the same period. From the comparison we obtained a good correspondence between the two set of elements as shown in Figure 4.2. The semi-major axis error δa turns out to be about 10^{-4} AU, or 10^4 km, with a corresponding error in mean motion δn of 10^{-4} deg/day. The errors in the eccentricity and inclinations were found to be $\delta e = 10^{-3}$ and $\delta i = 10^{-4}$ degrees.

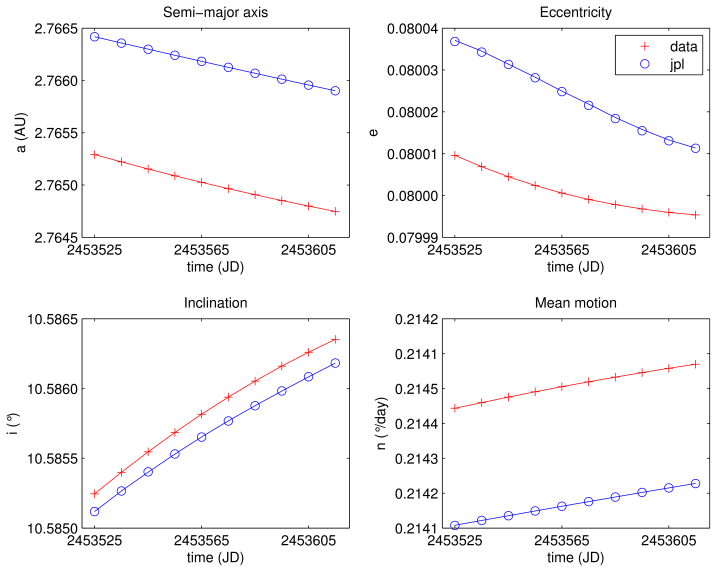

Figure 4.2: Ceres Keplerian elements obtained from preliminary determination methods, the red crosses, and the Keplerian elements of JPL, the blue circle.

We also plotted the residuals of the Cartesian state resulting from differencing our IOD orbits and those of JPL, as shown in Figure 4.3. The magnitude Δr of the residual of the position vector is 10^{-4} AU, which is compatible with that of the residuals in the semi-major axis. This is a further confirmation of the compatibility between the preliminary and the final orbits.

There exist some important relations between the variation of the Keplerian elements and the variations of position and velocity. The orbital elements are expressed in the inertial reference system but, if we consider the orbital reference system, we can write the radial component Δr of the

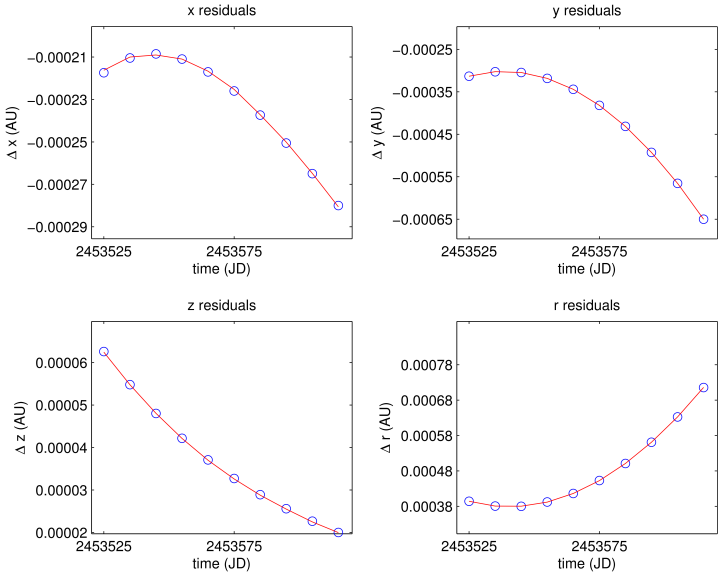

Figure 4.3: The residuals of position vector components for Ceres between the preliminary orbit and the final orbit.

position perturbation, the transverse $\Delta\tau$ and the normal $\Delta\chi$ [26] as:

$$\begin{aligned}
\Delta r &= \frac{r}{a}\Delta a + \frac{a^2}{r}(e - \cos E)\Delta e + \frac{\dot{r}}{n}\Delta M, \\
\Delta\tau &= a(\frac{a}{r} + \frac{1}{1-e^2})\sqrt{1-e^2}\sin E\Delta e + r\Delta\omega + r\cos i\Delta\Omega + \frac{h}{nr}\Delta M, \\
\Delta\chi &= r\sin u\Delta i - r\cos u\sin i\Delta\Omega. \qquad (4.5)
\end{aligned}$$

This formulation represents how the perturbations of the elements combine to first order generate a perturbation in the Cartesian state position. Vice-versa, there exist relations which indicate the variations of the Keplerian elements in terms of the variations of the Cartesian state vector.

4.3.1 An estimate of the sensitivity of the orbital elements to observational accuracy

The purpose of initial orbit computation is not to find the true orbit over a long period of time, but to provide a means to predict the position of the body and make it possible to track it day by day. For this reason a good estimate of errors and their implications becomes important.

A test utilized for this purpose is to map the variations of the orbital elements due to the observational errors. In the *Asteroids-Dynamic site* catalog

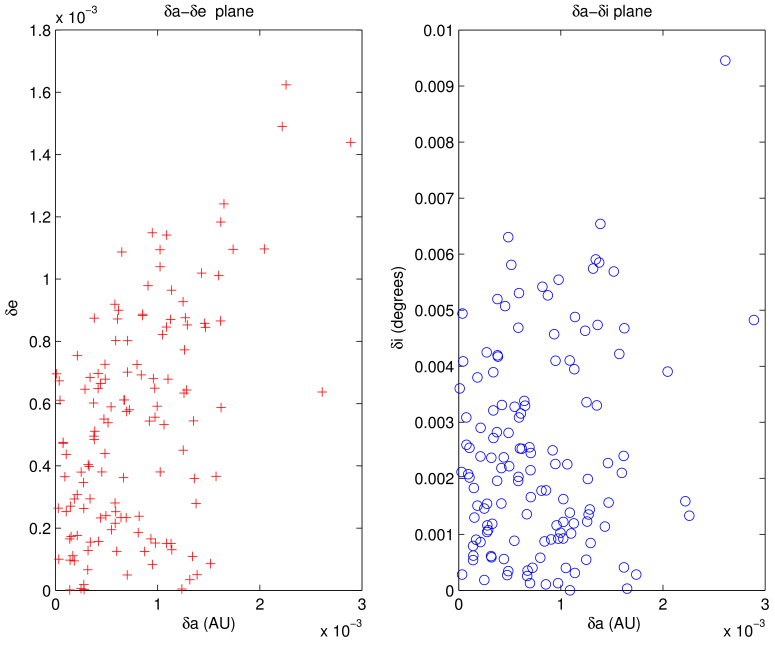

Figure 4.4: Residual of Ceres orbital elements derived from 150 random triads of fictitious observations. For each epoch a normal distribution of 400 synthetic observations was generated.

the right ascension (α) and declination (δ) values shown associated observational errors of respectively $0.15''$ and $0.10''$ for all of the observational data. We used these values as standard deviations in order to generate three populations of N normally distributed α and δ. All the possible combination of coordinates are chosen within the same population creating N^2 synthetic observations. Each group of data generated in this way represents a sort of cloud in the proximity of the three initial observations. Then we chose a sample of random combinations of three observations $(\alpha, \delta)_i$ $i = 1, 2, 3$, one from each group and we used them as input for the preliminary orbit determination methods. The orbits so obtained are compared with the one determined from the initial, real observations, obtaining the residuals in the orbital elements plane $\delta\alpha - \delta e$ and $\delta\alpha - \delta i$ as shown in Figure 4.4. The variation in semi-major axis due to these observational errors is of about the same order of magnitude of the variation mapped in Figure 4.2 and the variation of the other elements is even less of the ones provided in Figure 4.2. In fact from the tests made on a sample of asteroids we obtained: $\delta a \cong 10^{-3}$ AU , $\delta e \cong 10^{-3}$, $\delta i \cong 10^{-3}$ degrees, or few arcseconds. Therefore we conclude that the preliminary orbits computed are consistent within the errors expected from the accuracy of the observations.

In Figure 4.5 we show a variation of the previous analysis. The peculiar striped structure of the residuals distribution reflects the choice of the triads of synthetic observations. Starting from the same distributions of right ascension and declination variations we generated three clouds of observations. This time, in order to form the sets of three fictitious observations we selected one observation from each epoch in such a way to preserve the same distance from the nominal observation. This kind of procedure generates a bias, which is evident in the disposition of the elements and, because of that, it can be used to quantify the correspondences between the systematic errors due to the instruments and the orbital elements computed.

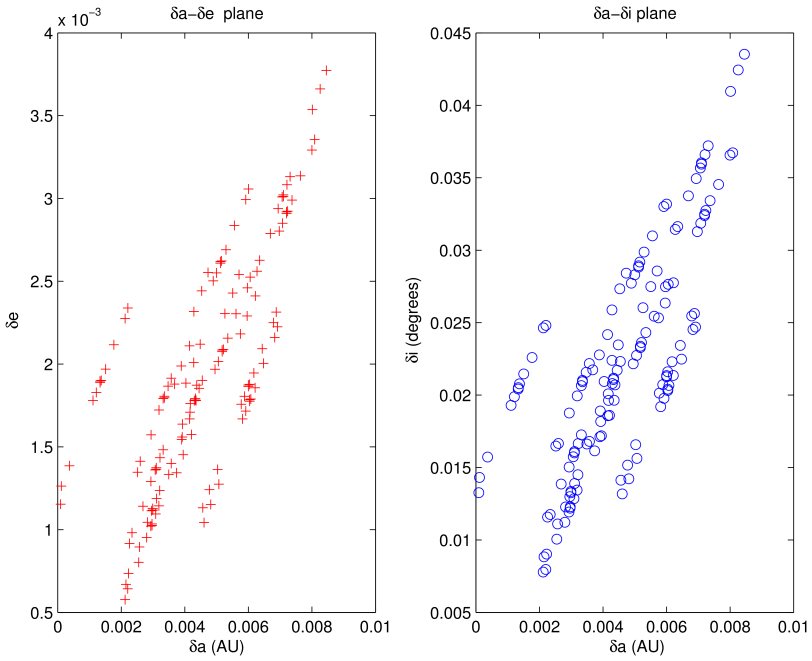

Figure 4.5: Residual of 392447 main belt asteroid derived from 144 triads of fictitious observations.

4.3.2 Tracking the object

Another test to evaluate the reliability of the orbits obtained from the methods consists on the computation of the angular position error, that is the angular distance between the preliminary orbit obtained with the methods and final orbits provided by JPL at a given epoch, as seen from the Earth. This error is then compared with the daily motion of the object in the sky.

We start from the computation of the main motion, the quantity which maps the angular path of the object with respect to the Sun in a day.

Then, in order to calculate it with respect to Earth, we made a change of coordinates passing from the heliocentric reference system to the geocentric. Next we calculated the relative velocity and relative position of the body:

$$\mathbf{v} = \mathbf{v}_A - \mathbf{v}_E, \tag{4.6}$$
$$\mathbf{r} = \mathbf{r}_A - \mathbf{r}_E, \tag{4.7}$$

where $\mathbf{v}_A$ is the velocity of the asteroid and $\mathbf{v}_E$ is the velocity of the Earth. Using the relation of scalar product we found the two components of the velocity:

$$\mathbf{v}_r = \frac{\mathbf{r} \cdot \mathbf{v}}{r^2}\mathbf{r}, \tag{4.8}$$
$$\mathbf{v}_t = \mathbf{v} - \mathbf{v}_r, \tag{4.9}$$

where v_r is the radial velocity and v_t the transverse component. At last the angular velocity n that correspond to the mean motion in the circular approximation for small angles is determined:

$$n = \frac{v_t}{r}. \tag{4.10}$$

The mean motion with respect to Earth changes significantly in time because of the relative motion between the asteroid and the Earth. It increases when the asteroid and the Earth are in the proximity of conjunction configuration and it decreases near the opposition, in quadratures it reaches the minimum values. We applied this analysis to some objects and we found that the angular position error is one order of magnitude smaller than the mean motion in degrees. This result allows to put some constraints to the field of view in which to research and it enables to track the object day by day. Therefore we can state that the prediction of the object's apparent position is efficient. The results obtained are shown in Table 4.8.

Object	Angular position error (°)	n w.r.t. Earth ($\frac{^\circ}{day}$)
Ceres	0.0025	0.1648
Apollo	0.1191	0.4867
Eros	0.1406	0.5619
393309	0.0516	0.1139
Chariklo	0.0126	0.0406
Quaoar	0.0116	0.0193

Table 4.8: Angular position errors and mean motion with respect to Earth.

Nowadays the surveys scan a wide part of sky so it is easier to recover the object in the sky also after several days. Catalina Sky Survey in Arizona,

for example, typically covers over 800 square degrees of sky in a single night of observing. The 76 cm f/1.9 Shmidt telescope, with a field of view of 8.2 squared degrees and a precision of 2.5″/pixel, in only one year, is able to submit about 330.000 astrometric observations to the Minor Planet Center resulting in a number of discoveries of new objects. We report in figure 4.6 an example of Catalina survey field of view. On the other hand, if

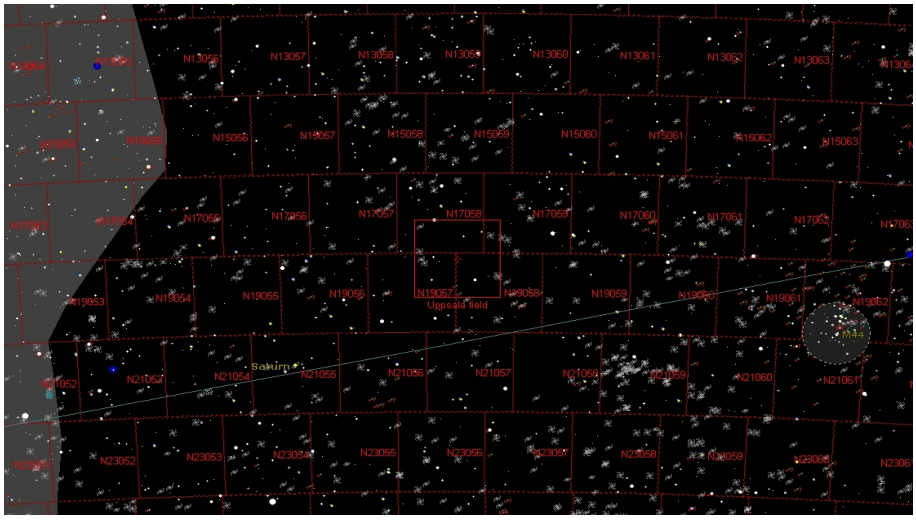

Figure 4.6: Catalina Sky Survey example of field of view. The survey covers a portion of sky of about 800 square degrees during a single night.

we wanted to take images with Asiago telescope we should settle of a field of view of $8.14' \times 8.14'$ with AFOSC instrument. This implies much more time of observation at the telescope and furthermore the impossibility to investigate a wide portion of the sky.

The values of mean motion with respect to Earth over a period of 100 days for Ceres are reported in figure 4.7. The values of main motion compute from the data provided by JPL are represented by the blue crosses, while the ones derived from the integrated preliminary orbits are the red points. We note a good agreement between the two sets.

Figure 4.8 shows the main motion with respect to Earth over a period of 2000 days that corresponds to about an orbital period of Ceres. It is possible to note a periodicity that corresponds to the Earth motion furthermore we can notice a lower peak fallowed by a higher peak, the first represents the opposition configuration and the second the conjunction one. The two minimums represent the quadrature configuration.

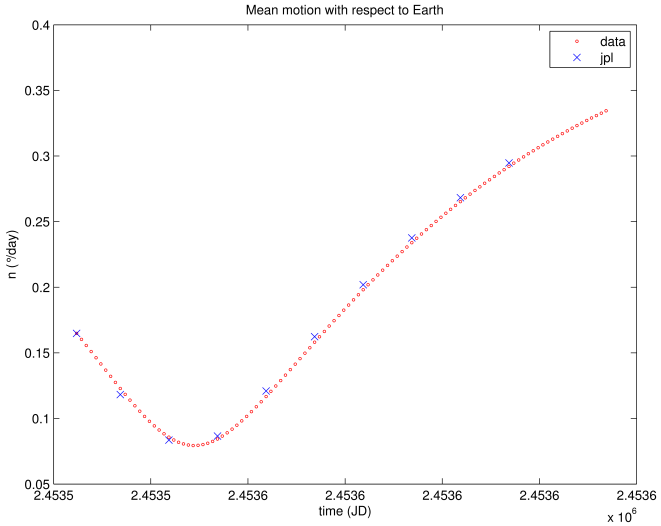

Figure 4.7: Mean motion with respect to Earth over a period of 100 days. Blue crosses are the JPL data while the red little circles are computed by preliminary orbit determination methods.

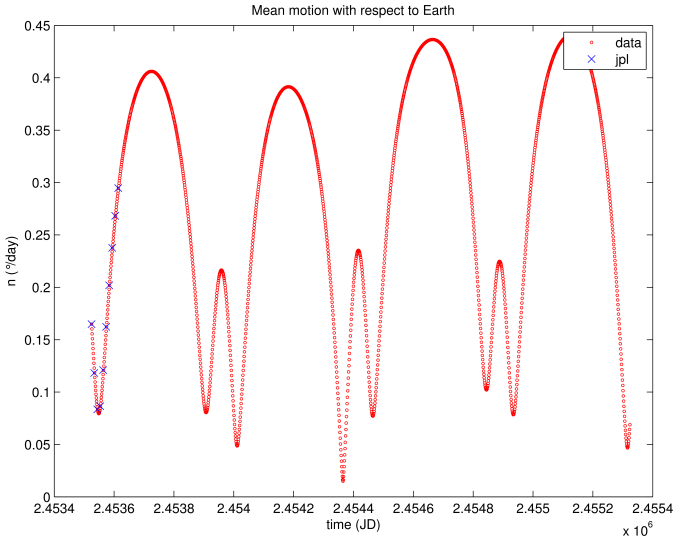

Figure 4.8: Mean motion with respect to Earth over a period of 2000 days which include an orbital period of Ceres.

4.3.3 IOD computation for other asteroids

The results of the analysis consist in the position vectors and the orbital elements, calculated for the epoch of the first observation. In Table 4.9 we provide the observations used to test the algorithms and the orbital elements obtained after the processing. All the observations are selected among those available in the *Asteroid-Dynamic site* of the University of Pisa, which in turn obtains the data from the *Minor Planet Center*. The site, as already noted in the first chapter, is one of the more complete for what concerns asteroids dynamics information. The choice of the asteroids was made so as to include members of different groups and families throughout the Solar System. In this way we could obtained an example of the efficiency of the algorithms in various representative cases. We distinguish between named and numbered objects, the latter having been discovered in the last ten years or less. To produce good results it was necessary to select different time intervals between the observations depending on the object distance from the observer. In fact, the greater the distance, the lower the observable arc traveled and the more difficult to observe the motion of the object in the sky. Therefore, for main belt asteroids or Near Earth object we chose non-equidistant time intervals of about ten days, whereas for objects at the edge of the Solar System we opted for intervals of about thirty days.

Tables 4.9 shows the orbital elements calculated for each triad of observations. The right ascension is measured in hours, minutes and seconds and the declination in degrees, arcminutes and arcseconds. Table 4.10 shows the corresponding orbital elements. The semi-major axis is measured in astronomical units (AU), the other elements in degrees, except for the eccentricity, which is dimensionless.

Asteroid	**Family**	**Date (UT)**	$\alpha(h)$	$\delta(^o)$
Apophis	Aten	2005 01 08.77227	02 39 16.820	-13 32 05.80
		2005 01 10.98870	02 51 25.100	-11 19 42.40
		2005 01 20.02240	03 31 52.590	-03 51 41.90
Eros	Amor	2005 05 16.51366	12 24 19.670	-35 06 51.80
		2005 06 05.51554	12 47 03.870	-30 01 38.60
		2005 07 03.43113	13 34 25.500	-26 24 04.70
Apollo	Apollo	2001 02 16.24162	08 29 26.780	+30 02 14.70
		2001 02 17.28412	08 27 47.300	+30 04 03.00
		2001 02 21.30950	08 21 47.500	+30 08 14.40
		2003 01 27.32107	10 48 45.290	+18 19 43.70
		2003 02 06.28381	10 35 19.400	+19 58 37.50
		2003 02 25.54599	10 02 30.390	+22 52 25.40
		2003 03 05.24123	09 49 16.540	+23 39 39.30

(Table 4.9: it continues on the next page)

Asteroid	**Family**	**Date (UT)**	$\alpha(h)$	$\delta(^o)$
		2003 03 13.18891	09 37 01.230	+24 10 22.00
		2003 03 26.18444	09 21 51.670	+24 22 48.20
		2014 04 20.37024	11 12 13.165	+11 28 58.03
		2014 04 24.16066	11 05 07.510	+11 42 32.60
		2014 05 01.22063	10 53 57.890	+11 52 08.90
		2006 06 21.21753	15 43 00.780	+21 29 54.76
		2006 07 13.15669	15 41 58.737	+17 27 14.78
		2006 07 24.17950	15 47 30.460	+14 41 14.80
		2007 09 21.41079	06 39 18.730	+00 47 33.20
		2007 10 13.43842	07 08 10.590	-03 35 04.60
		2007 10 30.51182	07 23 28.376	-07 19 53.78
		2009 06 12.47007	21 13 11.270	+17 20 25.27
		2009 06 22.96493	21 17 12.680	+18 44 31.90
		2009 07 01.00389	21 17 54.280	+19 24 00.20
Hungaria	434 Hungaria	2011 01 07.45629	10 35 42.568	-12 22 28.91
		2011 01 18.42577	10 34 56.945	-12 06 58.25
		2011 01 27.39879	10 31 28.727	-11 18 21.41
		2012 08 22.12426	02 10 25.200	+07 14 32.30
		2012 09 11.65076	02 19 48.930	+01 25 16.70
		2012 09 21.32058	02 18 57.060	-02 06 55.80
		2014 01 03.50944	13 14 37.860	-09 27 37.80
		2014 01 28.48214	13 50 27.620	-08 51 56.40
		2014 02 11.48710	14 06 14.980	-07 17 46.50
		2007 11 14.48891	07 49 31.756	-03 26 58.49
		2007 11 05.45791	07 48 07.755	-05 06 36.55
		2007 12 05.45147	07 44 17.747	-06 27 06.57
		2008 01 10.27077	07 14 53.531	-08 40 10.38
		2008 01 20.27532	07 05 15.710	-08 21 19.62
		2008 02 12.38950	06 48 16.019	-06 20 30.02
		2009 01 07.54525	12 46 14.129	-20 40 30.80
		2009 01 15.52732	12 52 20.147	-21 26 15.85
		2009 02 04.76926	13 02 34.940	-22 45 27.60
		2010 07 20.43166	02 35 12.390	+22 52 42.20
		2010 08 11.40460	03 06 58.730	+23 04 04.00
		2010 08 23.03744	03 19 55.080	+22 36 28.90
		2010 10 09.22673	03 32 07.260	+16 10 00.10
Phocaea	25 Phocaea	2010 10 19.37682	03 25 25.722	+13 51 27.82
		2010 10 29.34342	03 16 39.028	+11 26 44.64
		2011 11 12.54287	08 58 54.093	-06 46 00.87
		2011 11 24.51285	09 02 52.765	-08 38 40.45
		2011 12 01.49439	09 03 50.423	-09 40 56.76
		2012 01 18.37915	08 41 28.450	-13 39 18.20

(Table 4.9: it continues on the next page)

Asteroid	**Family**	**Date (UT)**	$\alpha(h)$	$\delta(^o)$
		2012 02 05.415181	08 24 33.828	-12 47 28.79
		2012 02 25.22149	08 08 48.888	-10 24 55.60
		2013 06 06.30091	15 28 44.610	+02 02 12.90
		2013 06 20.20534	15 21 42.075	+04 18 50.49
		2013 06 30.17704	15 20 17.243	+05 08 53.06
		2014 01 03.45391	09 46 14.610	+19 25 15.50
		2014 01 11.47344	09 41 23.100	+19 39 20.20
		2014 01 24.37922	09 29 43.938	+20 09 10.26
		2014 02 05.22772	09 16 31.610	+20 34 20.80
393309	4 Vesta	2014 02 18.27158	09 02 16.890	+20 47 53.80
		2014 02 23.26697	08 57 33.860	+20 47 46.32
		2014 02 23.27952	08 57 33.170	+20 47 46.27
		2014 03 06.41021	08 49 25.379	+20 36 22.21
		2014 04 02.13266	08 46 03.030	+19 16 05.90
		2014 01 09.16678	07 52 33.160	+18 04 11.20
393323	15 Eunomia	2014 01 21.33839	07 41 03.260	+19 54 19.70
		2014 01 27.16908	07 35 40.930	+20 46 31.50
		1999 01 06.17747	03 51 31.230	+18 37 42.80
		1999 01 25.80330	03 50 03.710	+19 44 50.80
		1999 02 01.10758	03 51 53.232	+20 10 39.23
		2003 09 20.49289	07 00 39.031	+23 08 40.55
Ceres	1272 Geofion	2003 09 29.45717	07 12 05.950	+23 14 24.30
		2003 10 22.54200	07 36 27.706	+23 38 46.82
		2005 06 03.23041	14 51 41.242	-08 51 06.86
		2005 06 15.19336	14 45 29.496	-09 25 07.67
		2005 06 30.15039	14 42 36.537	-10 27 52.33
		2005 10 08.33475	01 35 08.250	+05 45 42.00
		2005 10 12.30701	01 31 54.000	+05 29 14.30
		2005 10 26.15381	01 20 35.610	+04 35 59.10
		2008 02 28.39159	13 15 40.300	-03 51 35.90
263592	158 Koronis	2008 03 11.36803	13 10 02.090	-03 10 26.20
		2008 03 31.35029	12 55 53.470	-01 41 16.80
		2010 10 15.34666	02 11 51.876	+09 44 54.26
		2010 10 28.25215	02 01 00.910	+08 58 00.80
		2010 10 31.02251	01 58 40.710	+08 48 26.60
		2011 09 24.32170	23 59 36.450	-00 48 18.80
		2011 10 01.24966	23 54 07.380	-01 19 14.50
		2011 10 18.25742	23 42 34.990	-02 21 44.20
390797	158 Koronis	2014 04 01.30392	12 42 35.950	-04 27 24.00
		2014 04 20.25607	12 28 12.630	-03 07 28.50
		2014 04 29.34164	12 22 53.687	-02 38 37.73

(Table 4.9: it continues on the next page)

Asteroid	**Family**	**Date (UT)**	$\alpha(h)$	$\delta(^o)$
393067	221 Eos	2013 01 17.19169	08 02 53.940	+21 47 14.90
		2013 02 06.13695	07 45 30.460	+21 51 30.80
		2013 02 14.15155	07 39 55.170	+21 48 16.70
393301	221 Eos	2013 12 31.58189	07 51 29.285	+15 16 35.67
		2014 01 09.38398	07 44 02.300	+15 15 21.70
		2014 01 26.34633	07 29 22.801	+15 21 24.48
263013	10 Hygiea	2010 10 10.43271	03 49 59.078	+15 05 26.70
		2010 11 03.41893	03 36 36.900	+13 39 41.40
		2010 11 08.52784	03 32 49.799	+13 19 49.32
392447	24 Themis	2010 10 13.26359	02 13 14.410	+11 44 50.70
		2010 10 28.27470	02 01 28.200	+10 57 37.10
		2010 11 11.20876	01 51 00.500	+10 17 15.10
393136	24 Themis	2013 01 16.50314	08 16 23.792	+21 19 10.37
		2013 01 22.21601	08 11 21.660	+21 35 33.20
		2013 02 15.15379	07 53 10.890	+22 24 51.30
Hilda	153 Hilda	2005 03 17.25797	09 16 37.990	+05 43 29.90
		2005 03 25.25295	09 14 11.120	+06 10 18.30
		2005 04 14.45583	09 12 24.230	+07 02 31.50
		2006 01 31.49379	13 06 05.553	-13 29 16.65
		2006 02 22.53667	13 05 29.330	-13 37 09.60
		2006 03 08.31161	13 01 06.040	-13 12 14.80
		2009 11 17.21850	01 10 59.400	+11 10 04.80
		2009 11 24.12485	01 08 51.570	+10 45 01.20
		2009 12 28.09003	01 08 56.017	+09 47 10.88
		2013 04 22.11841	09 23 31.436	+06 27 00.08
		2013 05 02.18226	09 25 52.827	+06 38 42.42
		2013 05 30.16812	09 39 32.016	+06 28 53.97
Hidalgo	Centaurus	2003 07 18.70701	00 00 28.090	-9 25 33.30
		2003 08 10.20733	23 49 19.830	-51 46 19.10
		2003 12 06.07931	22 35 23.210	-41 42 35.30
		2004 07 24.06806	02 24 45.810	+05 16 37.50
		2004 08 09.07995	02 35 53.160	+08 51 01.40
		2004 08 27.49067	02 43 13.800	+13 33 56.20
		2004 09 09.29610	02 43 15.020	+17 24 41.30
		2004 09 25.42094	02 34 39.980	+23 03 31.40
		2004 10 14.44799	02 08 39.230	+30 32 07.70
		2004 11 03.35368	01 24 58.290	+37 30 54.40
		2004 12 01.00764	00 29 41.680	+42 50 51.20
		2004 12 29.69560	00 16 36.660	+46 05 52.80
		2005 01 08.80884	00 22 50.000	+47 28 43.70
		2005 02 01.81443	00 56 37.090	+51 35 30.70

(Table 4.9: it continues on the next page)

Asteroid	**Family**	**Date (UT)**	$\alpha(h)$	$\delta(^o)$
		2005 02 28.14795	02 03 41.560	+56 45 40.00
		2006 01 12.48338	13 39 17.830	+06 38 29.00
		2006 02 11.40819	13 36 51.610	+06 06 16.80
		2006 03 04.42354	13 25 08.180	+06 16 20.20
		2007 02 27.75457	14 08 55.820	-20 54 07.80
		2007 03 30.38411	13 54 04.260	-21 23 52.40
		2007 04 13.66944	13 44 56.970	-21 16 57.10
Chariklo	Centaurus	2004 02 07.44362	11 40 28.963	-21 45 40.43
		2004 03 18.52448	11 31 46.820	-21 35 00.20
		2004 04 14.25893	11 26 01.240	-20 56 58.90
Quaoar	Cubewnos	2002 06 04.23727	16 38 20.710	-14 51 18.20
		2002 07 03.26979	16 36 11.010	-14 47 52.10
		2002 07 30.32556	16 34 46.350	-14 47 43.50

Table 4.9: This table provides the data used for the computation of the preliminary orbits. The coordinates are the right ascension α measured in hours, minutes and seconds and the declination δ measured in degrees, arcminutes and arcseconds. All these data are provided from the Minor Planet Center service.

Name	Date (UT)	a	e	i
		ω	Ω	M
Apophis	2005 01 08.77227	0.9832	0.0152	0.2803
		57.5792	-51.3115	99.9610
Eros	2005 05 16.51366	1.4569	0.2226	11.0786
		-183.3750	-53.7365	75.9750
Apollo	2001 02 16.24162	1.4702	0.5727	6.6926
		-71.9306	35.1928	149.7885
	2003 01 27.32107	1.4712	0.5601	6.7160
		287.9645	33.6430	-172.5577
	2003 03 05.24123	1.4731	0.5586	6.7137
		287.6856	33.6408	-151.4338
	2014 04 20.37024	1.4686	0.5657	6.8535
		289.1957	33.0935	-66.2608
Hungaria	2006 06 21.21753	1.9449	0.0738	22.0713
		124.0190	175.2768	-41.5157
	2007 09 21.41079	1.9373	0.0756	22.0548
		-237.4526	175.1929	126.1590
	2009 06 12.47007	1.9112	0.0627	22.1402
		135.3822	174.5468	-15.9187
	2011 01 07.4562	1.9534	0.0625	21.8598
		132.5465	175.5966	-168.0767
	2012 08 22.122426	1.9369	0.0701	22.0535
		-237.6406	175.2684	59.7849
	2014 01 03.50944	1.9421	0.0741	22.0673
		124.7236	175.2433	-121.2987
Phocaea	2007 11 14.48891	2.4012	0.2556	21.2233
		-270.3606	214.9167	144.0893
	2008 01 10.27077	2.3995	0.2552	21.2136
		-270.5590	214.8802	159.5161
	2009 01 07.54525	2.5023	0.2060	20.8163
		82.7420	216.1443	-102.7051
	2010 07 20.43166	2.3521	0.2476	21.2564
		87.0757	214.7229	46.5154
	2010 10 09.22673	2.4000	0.2559	21.3232
		-270.7526	214.9025	65.5147
	2011 11 12.54287	2.3997	0.2558	21.2339
		-270.5150	214.8928	171.1874
	2012 01 18.37915	2.3981	0.2559	21.2290
		89.7075	214.9086	-171.4800
	20136 06 06.30091	2.3885	0.2491	21.3514
		88.9605	215.0149	-37.3763

(Table 4.10: it continues on the next page)

Name	Date (UT)	a	e	i
		ω	Ω	M
393309	2014 01 03.45391	2.3214	0.0442	7.5741
		35.9242	-21.6121	107.5808
	2014 02 05.22772	2.3734	0.1173	7.1316
		66.6527	-20.3171	75.7429
	2014 02 23.27952	2.3671	0.1088	7.1093
		67.5016	-20.2627	80.7247
393323	2014 01 09.16678	2.6813	0.1140	13.5254
		29.7552	118.6828	-28.1593
Ceres	1999 01 06.17747	2.7698	0.0807	10.6592
		75.9422	78.1987	-70.4435
	2003 09 20.49289	2.7816	0.0802	10.6619
		73.0283	78.2013	-59.8802
	2005 06 03.23041	2.7653	0.0800	10.6690
		75.4892	78.1033	70.9582
263592	2005 10 08.33475	2.8924	0.0841	3.2619
		-81.3778	65.3562	31.2874
	2008 02 28.39159	2.8884	0.0878	3.2586
		280.1459	65.2890	-154.3259
	2010 10 15.34666	2.8888	0.0989	3.1399
		-72.6057	66.1103	29.6574
390797	2011 09 24.32170	1.0012	0.0218	0.4399
		97.6101	0.0024	-94.3712
	2014 04 01.30392	2.8807	0.0400	2.3361
		-293.1759	11.1631	109.2128
393067	2013 01 17.19169	3.0480	0.0665	8.7248
		-2.0454	-53.5008	172.4718
393301	2013 12 31.58189	3.0688	0.0512	8.5462
		-301.2771	267.5705	142.2706
263013	2010 10 10.43271	3.1682	0.1079	5.2350
		20.0073	186.9766	5.3914
392447	2010 10 13.26359	3.1474	0.1918	2.6604
		-22.2191	45.3136	3.9853
393136	2013 01 16.50314	3.1913	0.1767	1.3868
		25.8354	33.4043	44.0168
Hilda	2005 03 17.25797	3.9306	0.1266	7.5561
		49.4838	230.7330	-120.9237
	2066 02 22.53667	3.9947	0.1107	7.4951
		30.0264	231.2023	-63.0847
	2009 11 17.21850	3.9747	0.1147	7.4964
		33.4334	230.7836	112.3967
		3.9804	0.1414	7.5419

(Table 4.10: it continues on the next page)

Name	Date (UT)	a	e	i
		ω	Ω	M
	2013 04 22.11841	35.3943	230.6583	-95.9329
Hidalgo	2009 07 18.70701	5.7494	0.6609	42.9723
		56.8150	21.3813	-39.5165
	2004 07 24.06806	5.7239	0.6594	42.9811
		56.8987	21.3677	-13.0780
	2004 09 09.29610	5.7424	0.6602	42.9855
		56.7913	21.3783	-9.6208
	2004 11 03.35368	5.7223	0.6594	42.9379
		56.9591	21.3574	-5.7266
	2005 01 08.80884	5.7992	0.6633	42.9773
		56.9371	21.3076	-0.9196
	2006 01 12.48338	5.7242	0.6589	42.9966
		56.7926	21.3678	25.6500
	2007 02 27.75457	5.8249	0.6639	42.5597
		-302.2661	21.2641	53.1919
Chariklo	2004 02 07.44362	5.8437	0.1746	23.5964
		-117.8886	-58.7114	-0.1172
Quaoar	2002 06 04.23727	43.7443	0.0952	7.5486
		152.1098	189.2952	-80.0593

Table 4.10:
Orbital elements obtained from the method for initial orbit determination. a is the semimajor axis measured in AU, e is the eccentricity, i is the inclination and is measured in degrees as the argument of the perihelion ω, the longitude of the ascending node Ω and the mean anomaly M.

From the data processing we obtained also some plots. From Figure 4.9 to 4.25 we represent the orbits propagated with the framework of the Three-Body Problem described in section 4.2.3, starting from the initial state vector obtained from the initial orbit determination methods. We represented the asteroid's orbits in red while the Earth's orbit in blue.

From Figure 4.26 to 4.30 we illustrate the differences between the Keplerian elements referred to the preliminary orbits and to the final orbit published by JPL. The elements were obtained from the integration of the state vector resulted from the IOD, over a period of time of 100 days.

In Figure 4.31 and 4.32 we plot the residuals of the position components of the Cartesian state obtained from the comparison of the preliminary value and the final value proposed by JPL in a span of time of 100 days.

The fourth set of images, referred to the figures from 4.33 to 4.36, represents the mean motion of the objects with respect to Earth. This is a significant result that allows to understand the effective shift of the asteroid in the sky night by night. As we said in section 4.3.2, the lower picks corre-

spond to the opposition configuration while the higher picks correspond to the conjunction configuration. It is interesting to note the particular trend of the mean motion's values in the case of Apollo. It does not correspond to the explanation just made because of the orbit of Apollo crosses the Earth orbit. This close encounter affects significantly its apparent motion, in fact in this period the value of the mean motion reaches its bigger value.

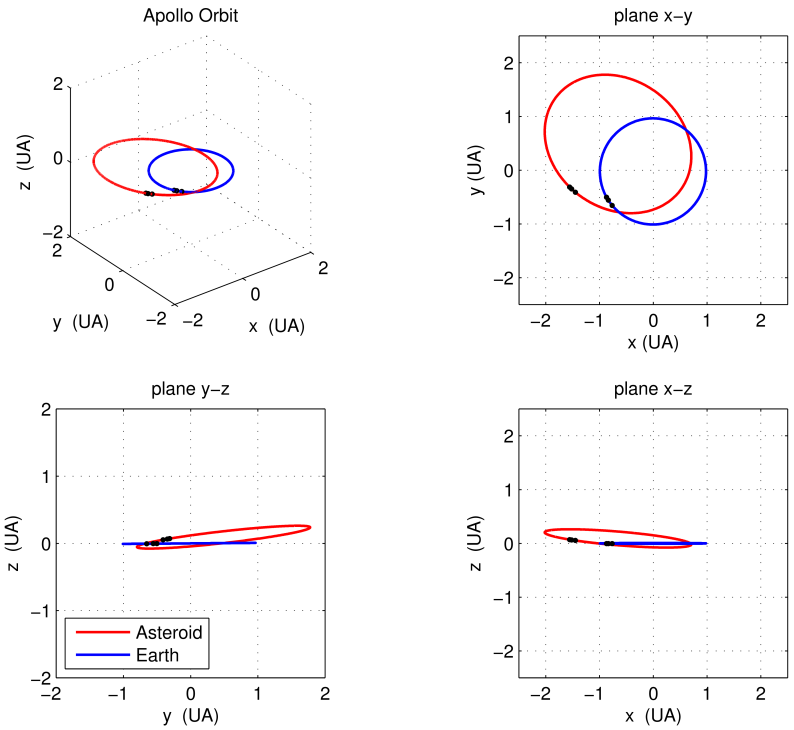

Figure 4.9: Preliminary orbit of Apollo near Earth asteroid. The orbits are obtained from the integration of the state vector resulted from the IOD within the framework of the Three-Body Problem.

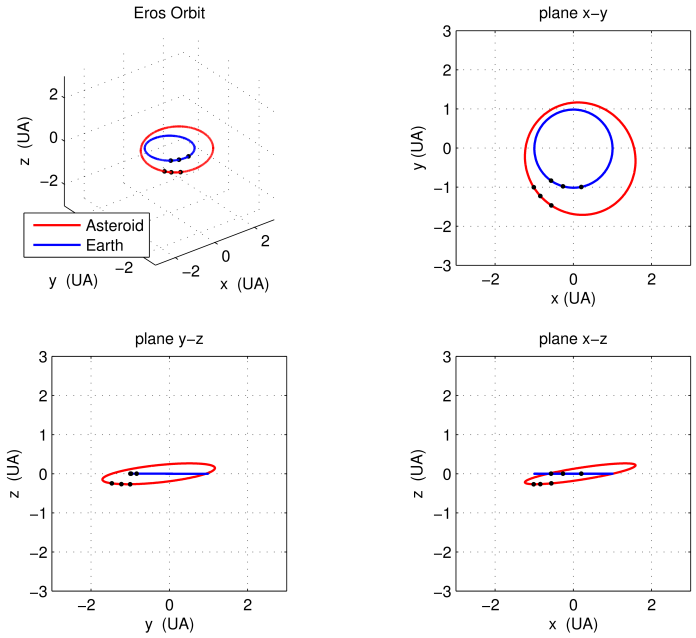

Figure 4.10: Preliminary orbit of Eros near Earth asteroid.

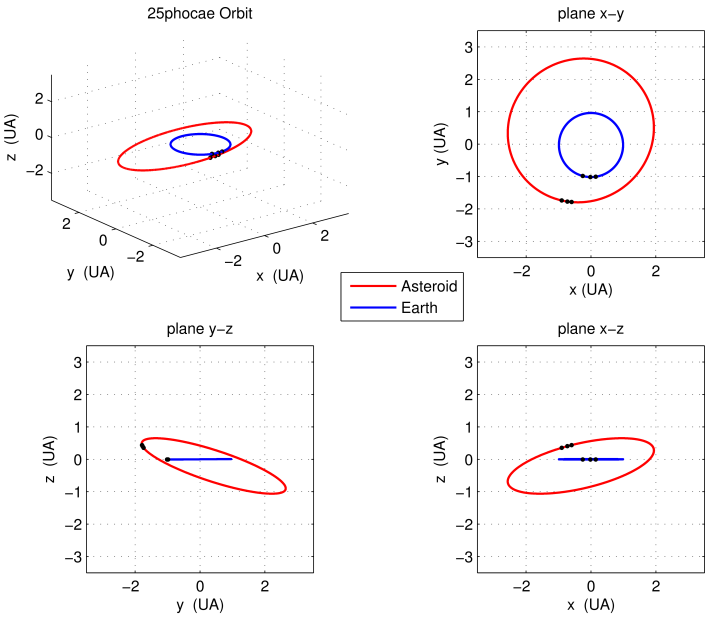

Figure 4.11: Preliminary orbit of 25 Phocaea main belt asteroid.

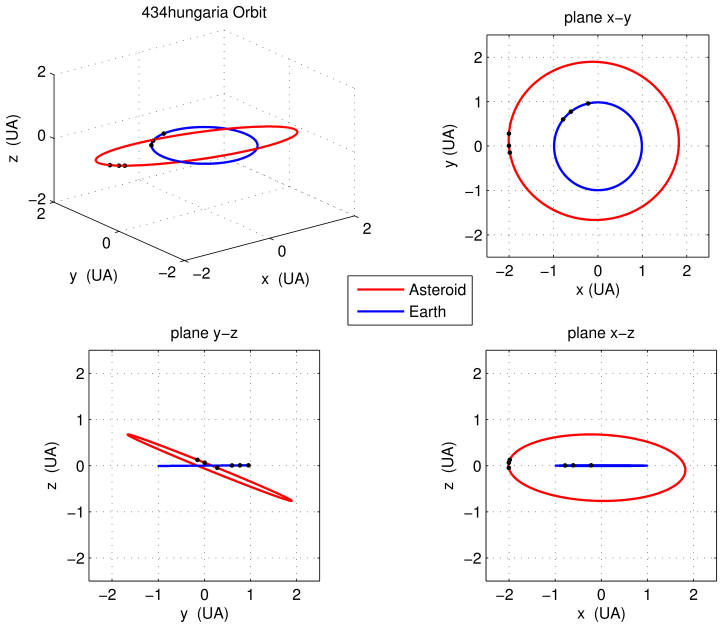

Figure 4.12: Preliminary orbit of 434 Hungaria main belt asteroid.

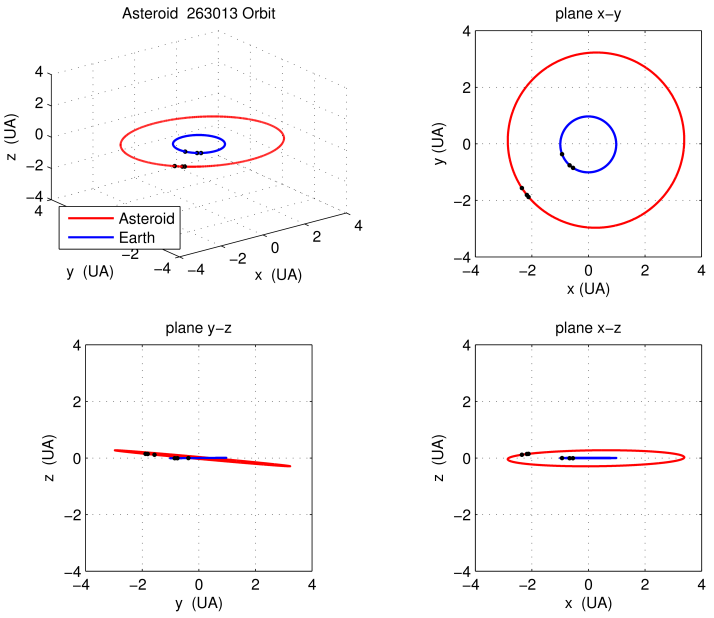

Figure 4.13: Preliminary orbit of 263013 main belt asteroid.

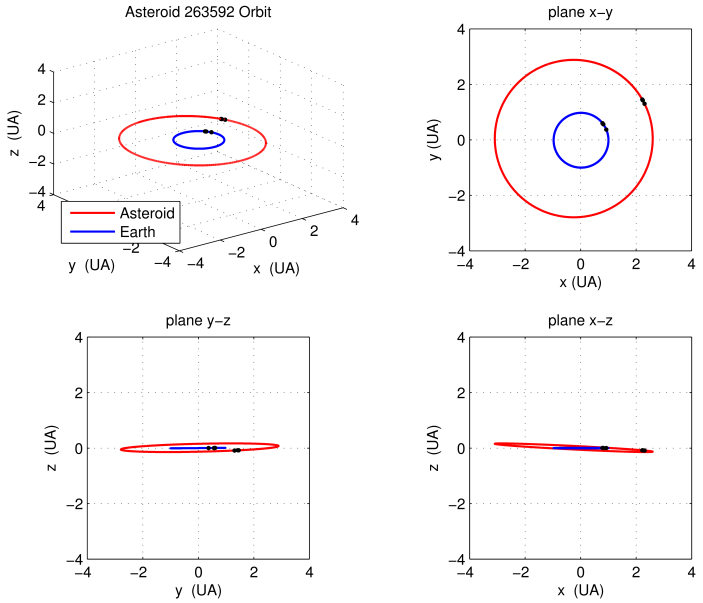

Figure 4.14: Preliminary orbit of 263592 main belt asteroid.

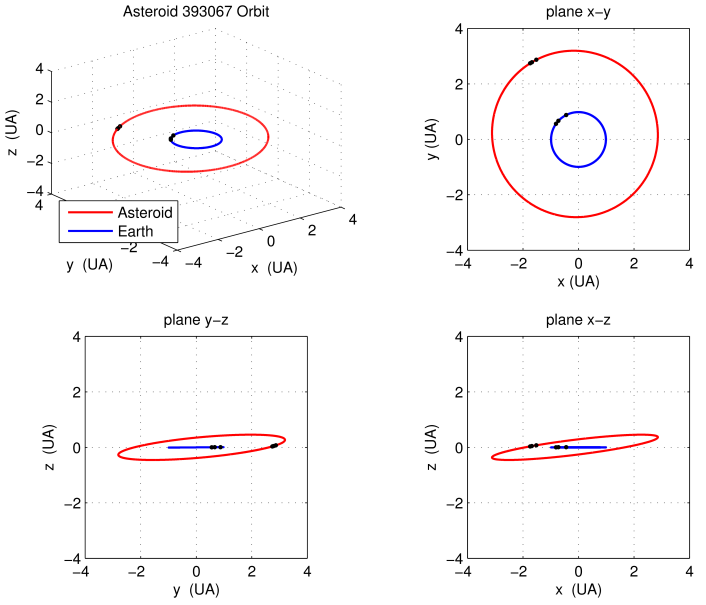

Figure 4.15: Preliminary orbit of 393067 main belt asteroid.

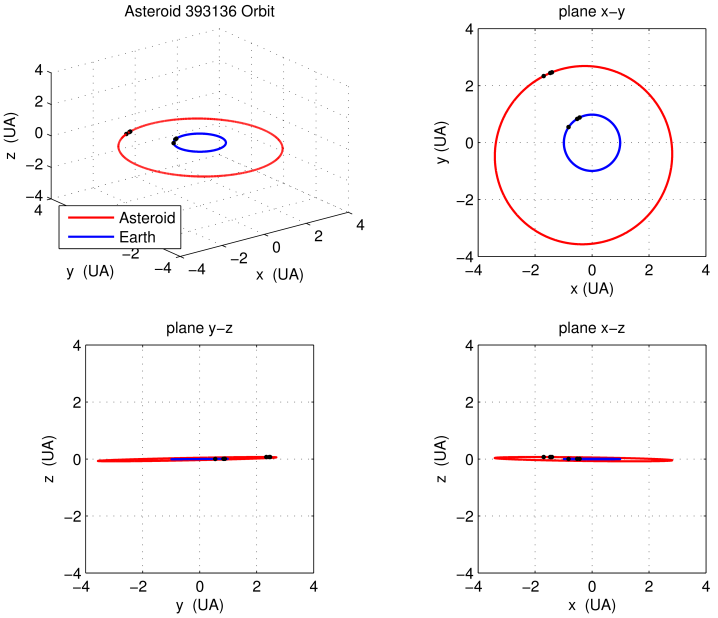

Figure 4.16: Preliminary orbit of 393136 main belt asteroid.

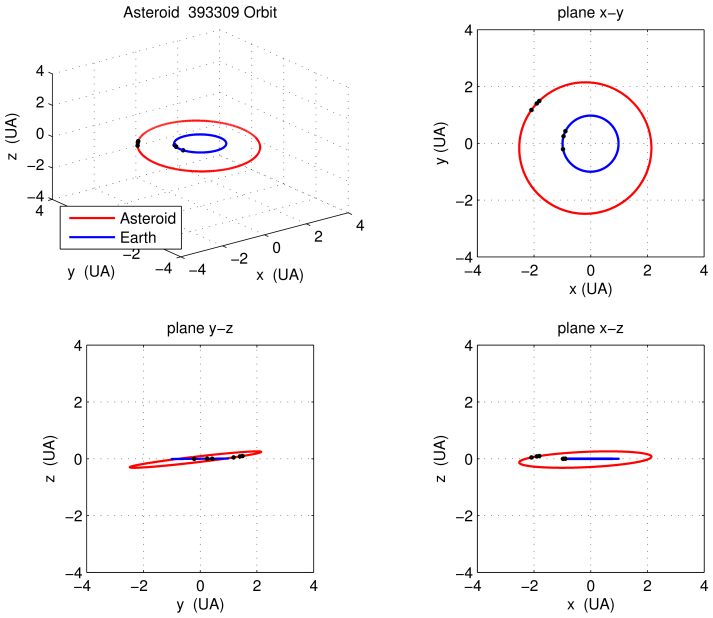

Figure 4.17: Preliminary orbit of 393309 main belt asteroid.

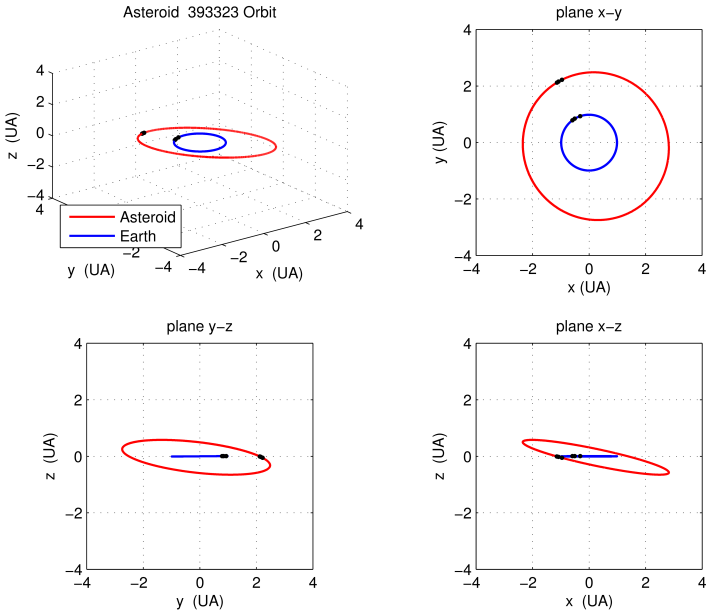

Figure 4.18: Preliminary orbit of 393323 main belt asteroid.

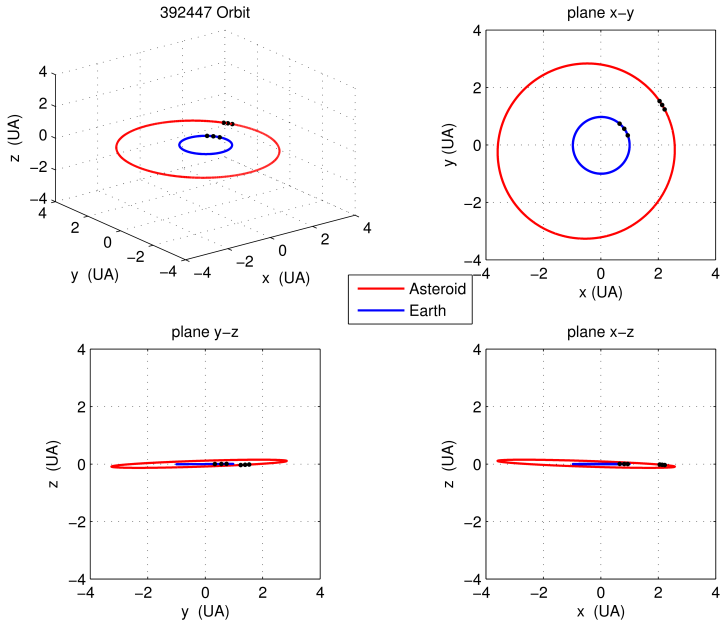

Figure 4.19: Preliminary orbit of 392447 main belt asteroid.

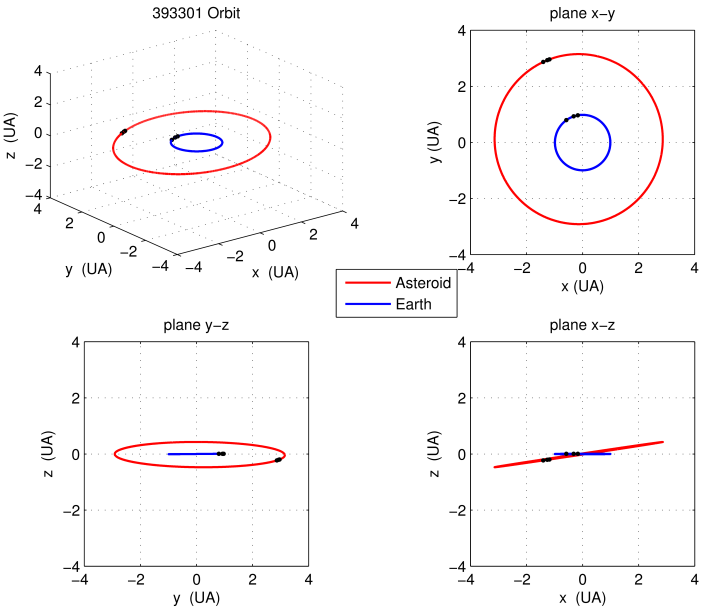

Figure 4.20: Preliminary orbit of 393301 main belt asteroid.

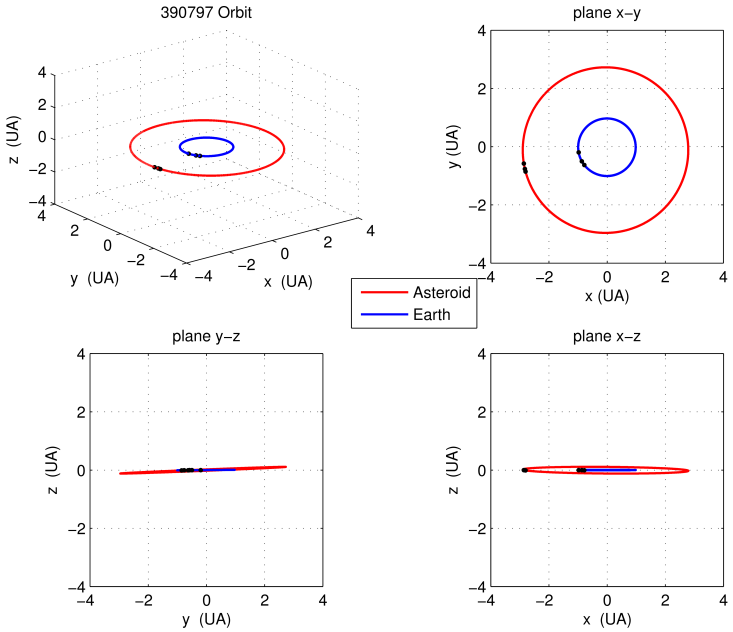

Figure 4.21: Preliminary orbit of 390797 main belt asteroid.

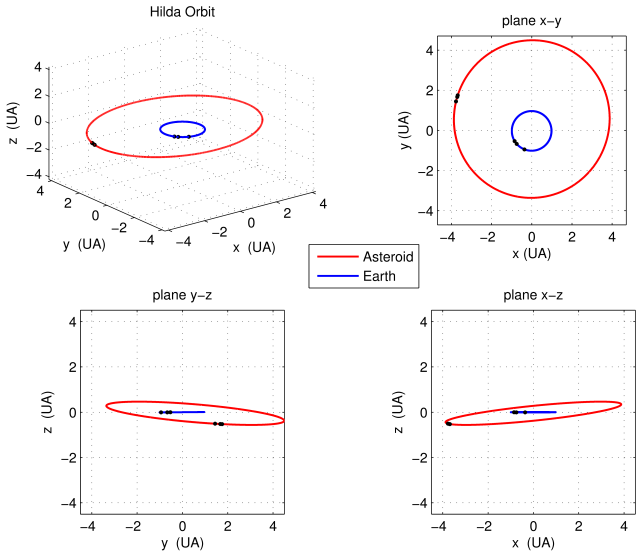

Figure 4.22: Preliminary orbit of 153 Hilda asteroid.

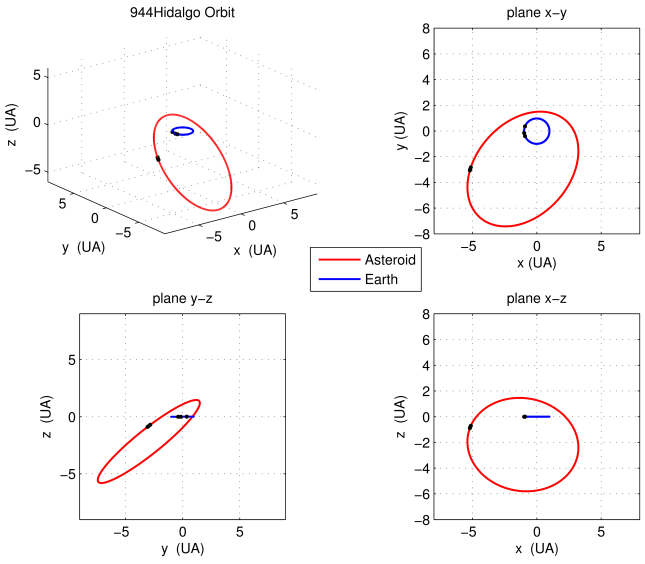

Figure 4.23: Preliminary orbit of the Centaurus 944 Hidalgo.

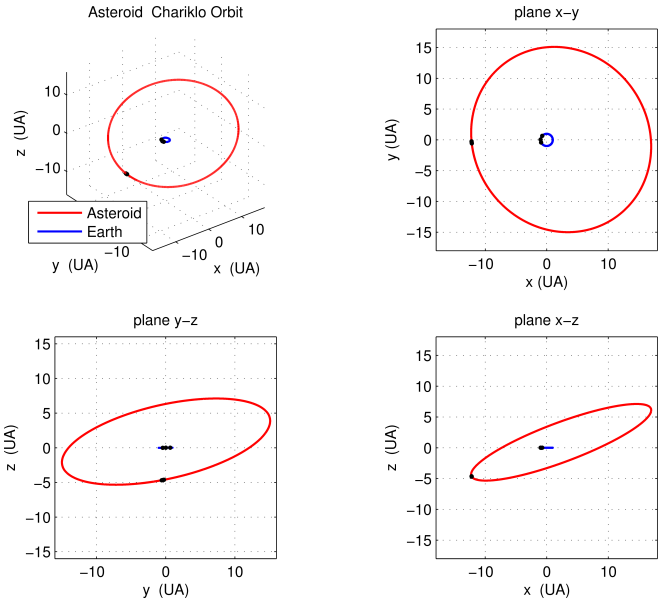

Figure 4.24: Preliminary orbit of the Centaurus Chariklo.

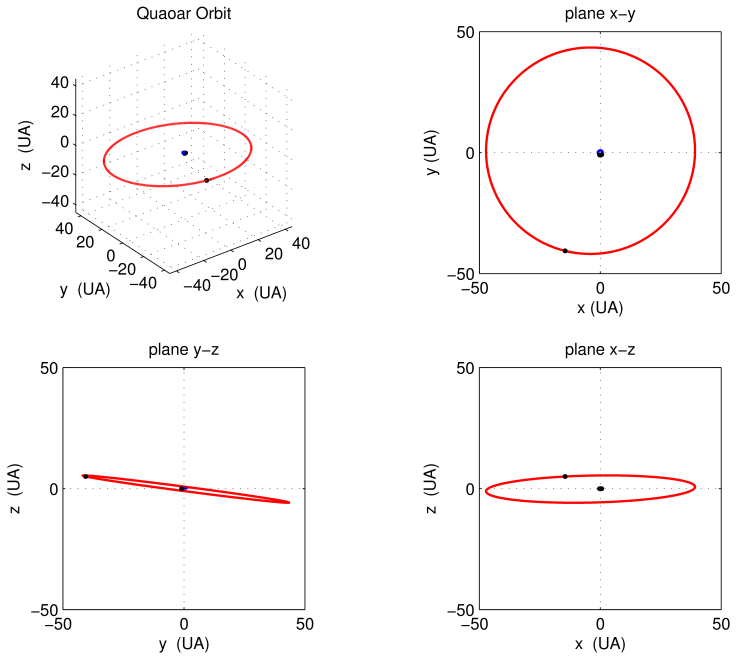

Figure 4.25: Preliminary orbit of Quaoar.

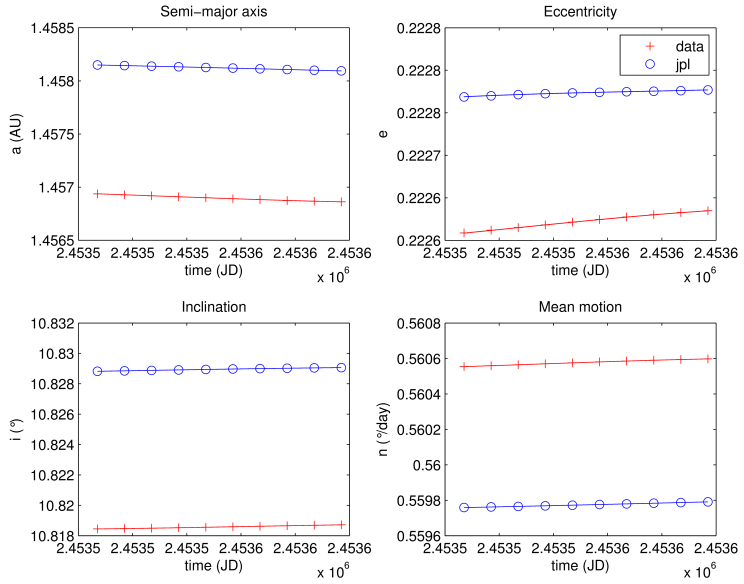

Figure 4.26: Orbital elements of Eros asteroid

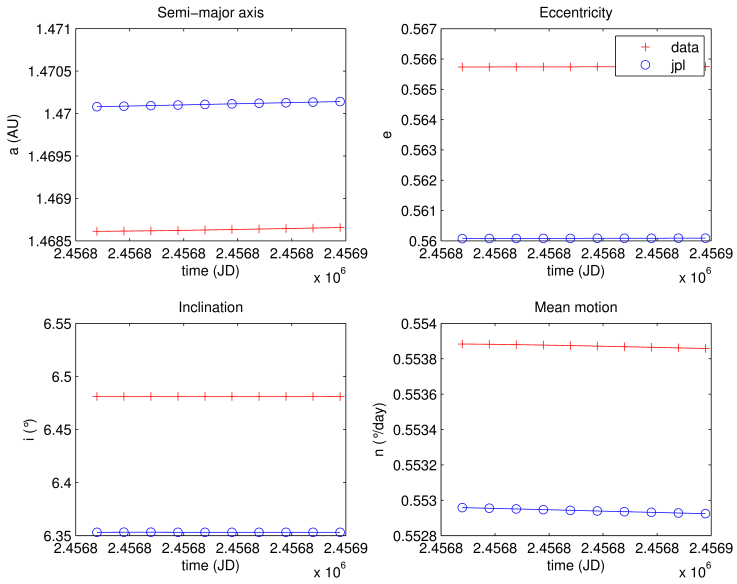

Figure 4.27: Orbital elements of Apollo asteroid.

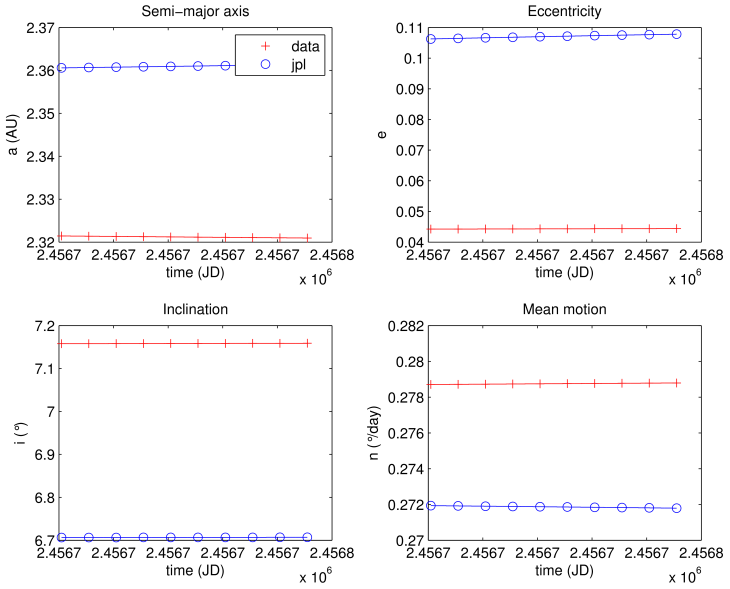

Figure 4.28: Orbital elements of 393309 main belt asteroid.

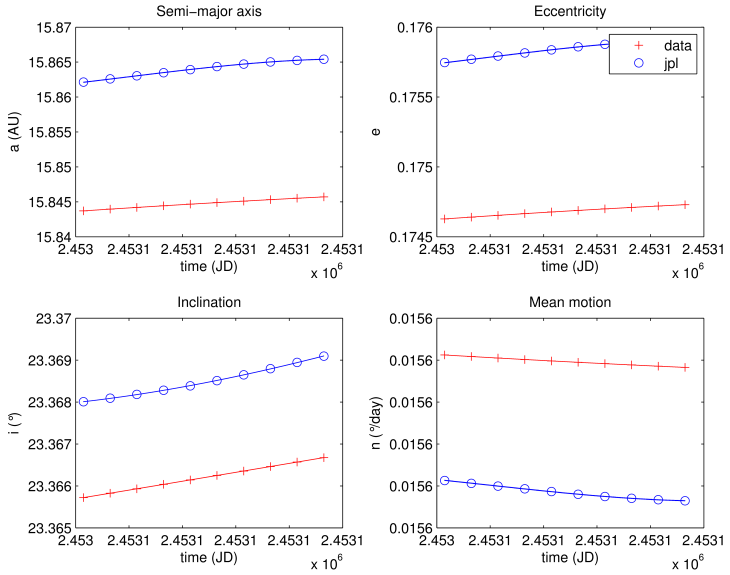

Figure 4.29: Orbital elements of Chariklo.

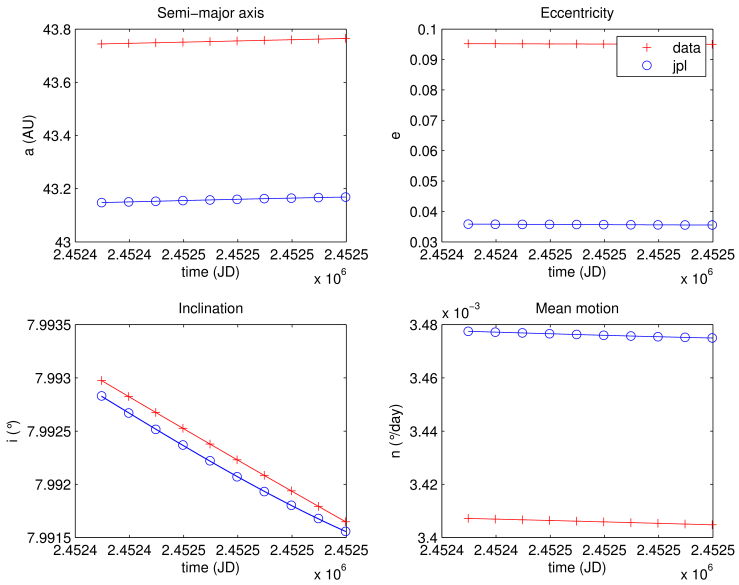

Figure 4.30: Orbital elements of Quaoar.

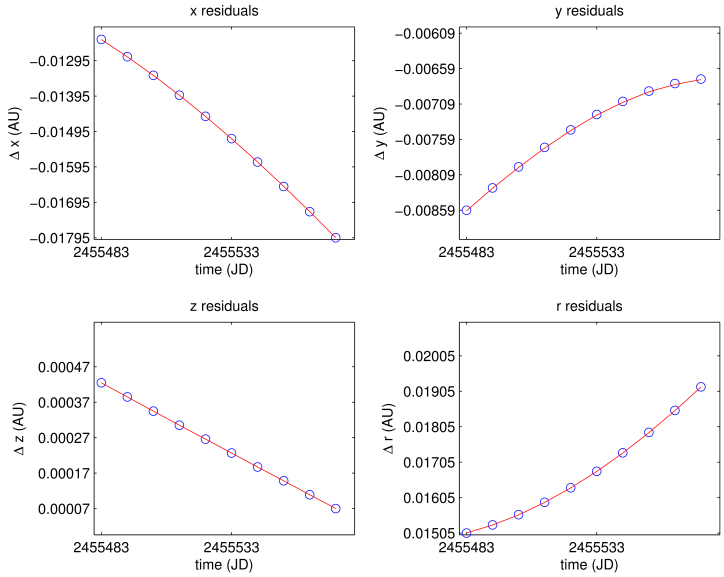

Figure 4.31: Residuals of the Cartesian position components of the 392447 main belt asteroid.

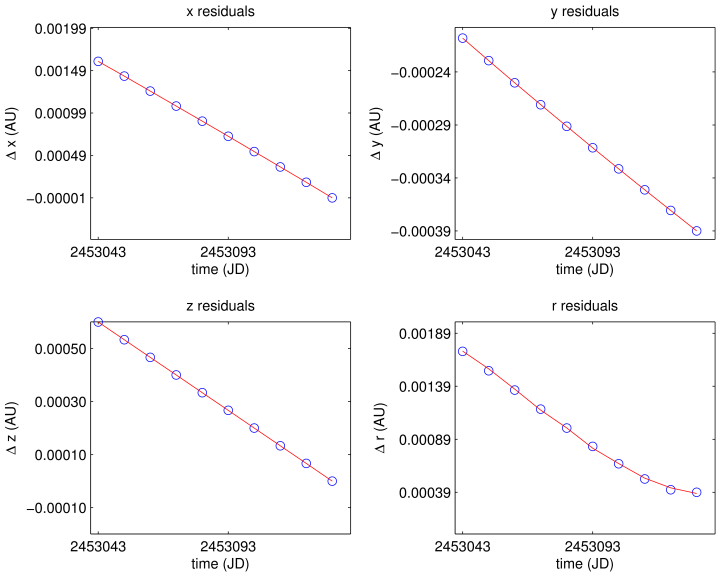

Figure 4.32: Residuals of the Cartesian position components of the Centaurus Chariklo.

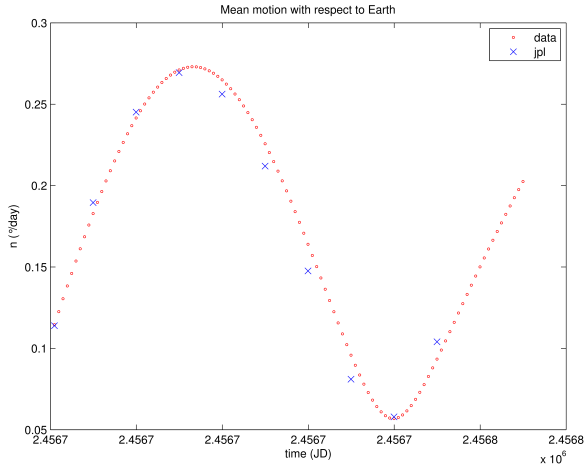

Figure 4.33: Mean motion with respect to Earth over a period of 100 days for the 393309 main belt asteroid.

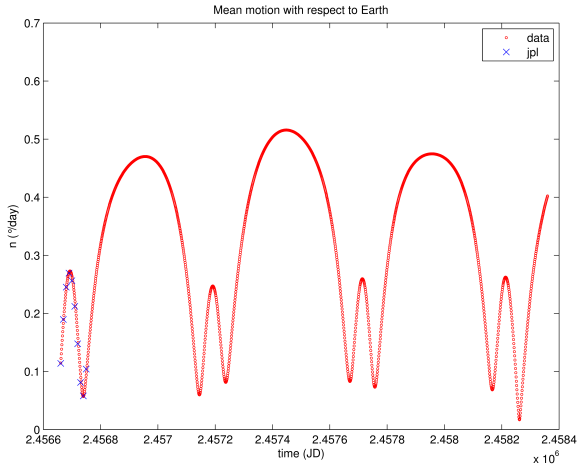

Figure 4.34: Mean motion with respect to Earth for 393309 asteroid over an orbital period.

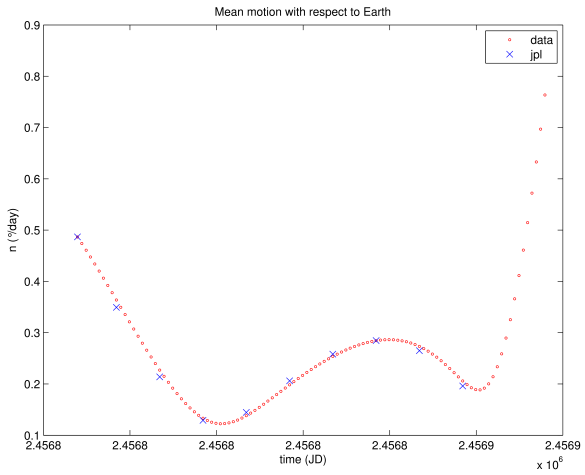

Figure 4.35: Mean motion with respect to Earth over a period of 100 days for the NEA Apollo.

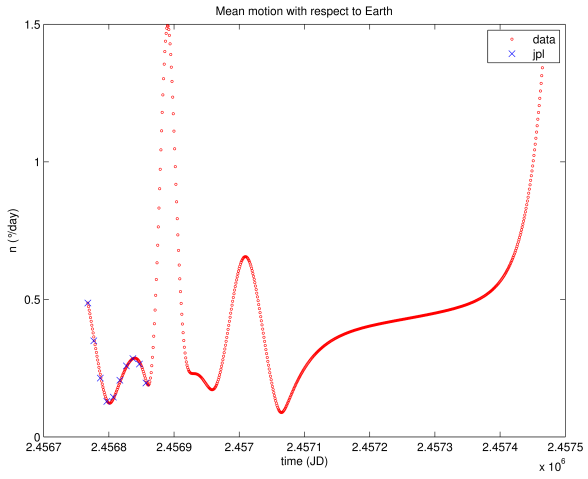

Figure 4.36: Mean motion with respect to Earth for NEA Apollo.

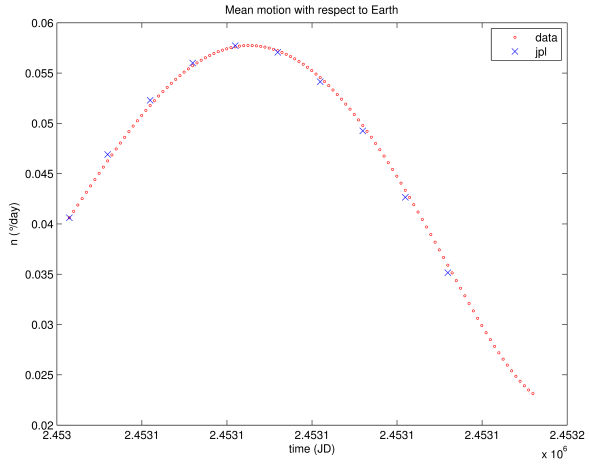

Figure 4.37: Mean motion with respect to Earth for Eros asteroid over a period of 100 days

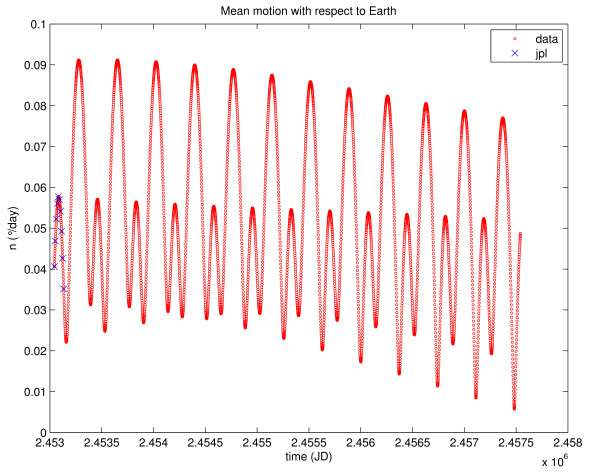

Figure 4.38: Mean motion with respect to Earth for Chariklo.

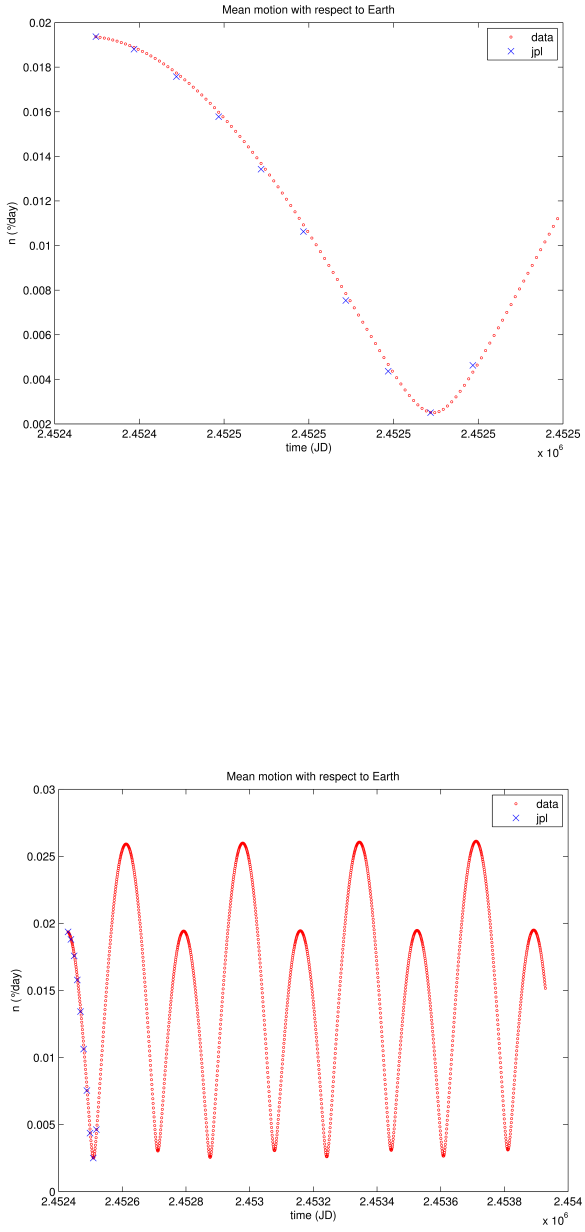

Figure 4.39: Mean motion with respect to Earth for Quaoar.

Chapter 5

Conclusions and future work

In this work three methods of initial orbit determination have been reviewed and software codes were developed for each of the three methods. The algorithms were tested first on synthetic data and then applied to real observations. These different approaches, using different procedures, yield the same results in terms of position vectors within a precision of 10^{-12} AU. Since it is more convenient to adopt a method with the lowest computational cost, we can conclude that the methods of Neutsch and Casotto are to be preferred over the more complex procedure of Gauss. It was found that the Neutsch method does not always converge. This problem is due to the choice of the orbit required to initialize the problem and we found that it occurs when the initial orbit is very different from the final one. The variation of the Gauss method proposed by Casotto is, unlike the method of Neutsch, an analytical technique which requires the solution of a non-linear system based on the same equations as the method of Gauss. We investigated the number of possible solutions of the non-linear system through the application of the Charlier theory, which was developed for the Gauss method. We found two or three solutions depending on the configuration of the object at the instants of observations, according to the theory. Our numerical investigation thus supports the validity of the Charlier's analysis also in the case of Casotto's method.

After the application of the three IOD methods to a number of real observational data from a wide set of representative objects we tested the reliability of the preliminary orbits with respect to the final orbits provided by JPL. We found that our preliminary orbits approach the final ones with an accuracy of 10^{-4} AU in the position components, which translates to a few arcseconds in the plane of the sky, if we consider main belt object.

We estimated how the observation uncertainty affects the determination of the preliminary orbits. A population of synthetic observations was created and preliminary orbits were determined choosing different combinations of three observations among the many created. A comparison between

synthetic orbits and the nominal one provided a difference, in terms of orbital elements and position components, of the same order of magnitude as between the preliminary orbits and the JPL orbits. Therefore we conclude that the results obtained from IOD methods are consistent within the error expected.

This work is a first step toward a more extensive investigation of the IOD methods in use. For what concerns the Neutsch method, for example, it will be interesting to determine how to constrain the initial orbit in order to ensure the convergence and to improve the algorithm. Moreover, it will be interesting to investigate the IOD methods based on the use of the two-body integrals and to compare their efficiency with the more classical techniques.

In the near future space missions like Gaia will provide accurate measurements of positions and velocities of main belt asteroids, NEOs and TNOs, which will make it possible to determine their orbits with unprecedented accuracy. Gaia will reach astrometric precisions of 10^{-5} arcseconds, 100 times more precise than Hipparcos. The huge number of data thus obtained will need to be processed with reliable and updated algorithms. For this reason it is of fundamental importance to introduce and test new procedures, both for preliminary and final orbit determination.

Bibliography

[1] K. F. Gauss, *Theoria Motus Corporum Coelestium*. Dover Publications Inc., New York, 1963.

[2] L. Euler, *Theoria Motuum Planetarum et Competarum*. Berlino, 1744.

[3] A. Milani and G. Gronchi, *Theory of Orbit Determination*. Cambrige, 2009.

[4] A. Milani et al. "Topocentric orbit determination: Algorithm for the next generation surveys," *Icarus*, Vol. 195, 2008, pp. 474-492.

[5] A. Milani G.F. Gronchi, M. De' Michieli Vitturi and Z. Knezevic, "Orbit Determination with Very Short Arcs. I Admissible Regions," *Celestial Mechanics and Dynamical Astronomy*, Vol. 90, 2004, pp. 59-87.

[6] O. Montenbruck and T. Pfleger, *Astronomy on the Personal Computer*. Springer, 2009.

[7] H. Bucerius, "Bahnbestimmung als Randwertproblem. I-II," *Astronomische Nachrichten*, Vol. 278, 1950.

[8] C.V.L. Charlier, "On multiple solutions in the determination of orbits from three observations," *Monthly Notices of the R.A.S.*, Vol. 71, 1910, pp. 120-122.

[9] S. Casotto, "A New Approach to Gaussian Initial Orbit Determination," *Advances in the Astronautical Sciences*, Vol.152, 2014, pp. 1313-1326 (paper AAS 14-290).

[10] W. Neutsch, "A simple Method of Orbit Determination," *Astronomy & Astrophysics,* Vol. 102, 1981, pp. 59-64.

[11] E. Goffin, "Orbit Determination without Gauss," in F. Baroli S. De Meis A. Panarino (Eds.), *Astronomical Amusements*, Milano, 2000 pp. 79-90.

[12] T. Mirtorabi, "A simple procedure to extend the Gauss method of determining orbital parameters from three to N points," *Astrophysics Space Sciences*, Vol. 349, 2014, pp. 137-141.

[13] R. R. Bate, D. D. Mueller and J. E. White, *Fundamentals of Astrodynamics*. Dover Publications, Inc., 1971.

[14] L. Rosino, *Lezioni di Astronomia*. Cedam-Padova, 1982.

[15] H. Eichhorn and Y. Xu, "An improved algorithm for the determination of the system parameters of a visual binary," *The Astrophysical Journal*, Vol. 385, 1990, pp. 575-587.

[16] D. Olevic and Z. Cvetkovic, "Orbits of 10 interferometric binary systems calculated by using the improved Koval'skij method" *Astronomy and Astrophysics*, Vol. 415, 2004, pp.259-264.

[17] H. Asada, T. Akasaka and K. Kudoh, "Simplified solution to determination of binary orbit," *The Astronomical Jurnal*, Vol. 133, 2007, pp. 1243-1246.

[18] G. H. Kaplan et al., "Mean and Apparent Place Computations in the new IAU System. III." *The Astronomical Jurnal*, Vol. 97, 1989, pp. 1197-1210.

[19] W. F. Folkner et al., "The Planetary and Lunar Ephemerides DE430 and DE431," *The Interplanetary Network Progress Report*, Jet Propulsion Laboratory, Pasadena, California, Vol. 42-196, 2014.

[20] G. Bernastein, B. Khushalani, "Orbit Fitting and Uncertainties for Kuiper Belt Objects," *The Astronomical Jurnal*, Vol. 120, 2000, pp. 3323-3332.

[21] J. Virtanen et al., "Orbit Computation for Transneptunian Objects," *Icarus*, Vol.161, 2003, pp.419-430.

[22] J. Virtanen et al., "Transneptunian Object Ephemeris Service (TNOEPH)," *Earth, Moon and Planets*, Vol. 92, 2003, pp. 73-78.

[23] M. E. Brown, C. Trujillo and D. Rabinowitz, "Discovery of a candidate Inner Oort Cloud Planetoid," *The Astrophysical Journal*, Vol. 617, 2004, pp. 645-649.

[24] R. Launhardt, "Exoplanet search with astrometry," *New Astronomy Reviews*, Vol. 53, 2009, pp. 294-300.

[25] S. T. Balan O. Lahav, "Exofit: orbital parameters of extrasolar planets from radial velocities," *Monthly Notices of the Royal Astronomical Society*, Vol. 394, 2009, pp. 1936-1944.

[26] S. Casotto, *Introduzione alla Meccanica Celeste*. Università degli studi di Padova, A.A. 2002-2003.

[27] G. F. Gronchi, L. Dimare and A. Milani, "Orbit determination with the two-body integrals," *Celestial Mechanics and Dynamical Astronomy*, Vol. 107, 2010, pp. 299-318.

[28] L. G. Taff and D. L. Hall, "The use of angles and angular rates. Initial orbit determination," *CMDA*, Vol. 16, 1977, pp. 481–488.